

STABILITY AND INTERACTION OF COHERENT
STRUCTURE IN SUPERSONIC REACTIVE WAKES

by
Suresh Menon

Dissertation submitted to the Faculty of the Graduate School
of the University of Maryland in partial fulfillment
of the requirements for the degree of
Doctor of Philosophy
1983

APPROVAL SHEET

Title of Thesis: Stability and Interaction of Coherent Structure in Supersonic Reactive Wakes

Name of Candidate: Suresh Menon
Doctor of Philosophy, 1983

Thesis and Abstract Approved:

John D. Anderson, Jr.
Dr. John D. Anderson, Jr.
Professor
Department of Aerospace Engineering

Date Approved:

December 9, 1983

ACKNOWLEDGEMENTS

I would like to express my sincere appreciation and gratitude to Professor John D. Anderson, Jr., for his constant support and encouragement during the course of this investigation. I would also like to express my wholehearted gratefulness to my co-advisor Professor Shih I Pai whose advise and guidance helped in overcoming many of the problems encountered during the theoretical formulation.

A major part of this work was supported by NASA Langley Research Center under Grant No. NCC1-41 with Mr. P.H. Drummond as contract monitor. I would like to thank Mr. Drummond and Dr. A. Kumar of NASA/LRC Computational Methods Branch for their assistance in understanding the NASA/LRC CYBER 203/STAR Computer where part of the computations were carried out. The majority of the calculations were done at the Computer Science Center of the University of Maryland which is also gratefully acknowledged.

This acknowledgement would not be complete without expressing my sincere thanks to my friend Vicki Brewer for her excellent typing of this work and to Kathy Matikas for her help in getting Chapter II in good shape.

CURRICULUM VITAE

Name: Suresh Menon.

Permanent address: 7700 Adelphi Rd., Apt. 1, Hyattsville, Maryland,
20783.

Degree and date to be conferred: Ph.D., 1983.

Secondary education: Delhi Public School, New Delhi, India, May 1971.

Collegiate institutions attended:	Dates	Degree	Date of Degree
Indian Institute of Technology Kanpur, India	July 71 July 76	B. Tech	July 1976
Indian Institute of Technology Kanpur, India	July 76 July 78	M. Tech	July 1978
University of Maryland College Park, Maryland	Aug. 78 Dec. 83	Ph.D.	Dec. 1983

Major: Aerodynamics and Propulsion.

Minor(s): Flight Mechanics and Applied Mathematics.

Professional publications:

1. Menon, S., "An Analysis of the Strong-Interaction Problem with Velocity-Slip and Temperature-Jump Effects," M. Tech. Thesis, Indian Institute of Technology, Kanpur, India, July 1978.
2. Pai, S.I., Menon, S., and Schultz, P.H., "Effects of Lift Forces on Ejecta Transport." Presented at the Tenth Lunar and Planetary Science Conference, Lunar and Planetary Institute, Houston, Texas. Also in Proc. Lunar Planet. Sci. Conf. 10th, p. 2779-2797, 1979.
3. Schultz, P.H., Srnka, L.J., Pai, S.I. and Menon, S., "Cometary Collisions on the Moon and Mercury." Presented at the Eleventh Lunar and Planetary Science Conference, Lunar and Planetary Institute, Houston, Texas, March 1980.
4. Gupta, R.N., Menon, S. and Rodkiewicz, C.M., "Analysis of the Strong Interaction Problem with Slip and Temperature-Jump Effects," AIAA Journal, Vol 18, No. 7, p. 844-846, July 1980.
5. Menon, S. and Anderson, J.D., Jr., "Computation of Particle Paths from Discrete Velocity Field Data in Fluid Flows," Technical Report AE 80-10, Department of Aerospace Engineering, University of Maryland, July 1980.

6. Pai, S.I., Menon, S. and Fan, Z.Q., "Strong Shock Wave Propagation in a Mixture of a Gas and Dusty Particles with Variable Initial Density." Presented at the APS Meeting, Washington, D.C., April-May 1980. Also in L'Aerotechnica Missile E Spazio, Italy, Vol. 59, No. 3, p. 228-234, Sept. 1980.
7. Pai, S.I., Menon, S. and Fan, Z.Q., "Similarity Solutions of a Strong Shock Wave Propagation in a Mixture of a Gas and Dusty Particles," International Journal of Engineering Sci., Vol. 18, No. 12, p. 1365-1373, December 1980.
8. Pai, S.I., Menon, S. and Fan, Z.Q., "Strong Shock Wave Propagation in a Mixture of a Gas and Dusty Particles with Gravitational Forces," ZAMM, West Germany, 61, p. 209-214, July 1981.
9. Pai, S.I., Menon, S. and Fan, Z.Q., "Strong Shock Wave Propagation in a Mixture of a Gas and Dusty Particles in a Moving Medium." Presented at the DGLR Conference, Aachen, West Germany, May 1981 (81-008). Also in the Conference Proceedings.
10. Pai, S.I., Menon, S. and Fan, Z.Q., "Strong Shock Wave Propagation in a Mixture of a Gas and Dusty Particles with Counter Pressure," ZAMM, 62, No. 4, p. 218-220, April 1982.
11. Pai, S.I., Sharma, V.D. and Menon, S., "Time Evolution of Discontinuities at the Wave-Head in a Non-Equilibrium Two-Phase Flow," Acta Mechanica, Vol. 46, No. 1-4, p. 1-13, 1983.
12. Menon, S., Pai, S.I. and Anderson, J.D., Jr., "On the Spatial Development of the Interaction Between Coherent Structure and Fine-Grained Turbulence in a Chemically Reacting Wake. I. Theoretical Formulation. Technical Report AE 83-1, Aerospace Engineering Department, University of Maryland, April 1983.
13. Menon, S., Anderson, J.D., Jr. and Pai, S.I., "Stability of a Laminar Premixed Supersonic Free Shear Layer with Chemical Reactions." To appear in International Journal of Engineering Sciences.

Professional positions held:

August 1979 to Present	Research Assistant, Department of Aerospace Engineering, University of Maryland, College Park, Maryland 20742.
Summers of 1980 and 1979	Visiting Graduate Fellow, Lunar and Planetary Institute, Houston, Texas.
August 1978 to May 1979	Research Assistant, Institute of Physical Science and Technology, University of Maryland, College Park, Maryland, 20742.
August 1976 to July 1978	Research Assistant, Department of Aeronautical Engineering, Indian Institute of Technology, Kanpur, India.

ABSTRACT

Title of Dissertation: Stability and Interaction of Coherent Structure in Supersonic Reactive Wakes

Suresh Menon, Doctor of Philosophy, 1983

Dissertation directed by: Dr. John D. Anderson, Jr.
Professor
Department of Aerospace Engineering

and

Dr. Shih I Pai
Professor Emeritus
Institute of Physical Science
and Technology

A theoretical formulation and analysis is presented for a study of the stability and interaction of coherent structure in reacting free shear layer. The physical problem under investigation is a premixed hydrogen-oxygen reacting shear layer in the wake of a thin flat plate. The coherent structure is modeled as a periodic disturbance and its stability is determined by the application of linearized hydrodynamic stability theory which results in a generalized eigenvalue problem for reactive flows. Detailed stability analysis of the reactive wake for neutral, symmetrical and antisymmetrical disturbance is presented. Reactive stability criteria is shown to be quite different from classical non-reactive stability. The interaction between the mean flow, coherent structure and fine-scale turbulence is theoretically formulated using von-Karman integral technique. Both time-averaging and conditional phase averaging are necessary to separate the three types of motion. The resulting integro-differential equations can then be solved subject to initial conditions with appropriate shape functions. In the laminar flow transition region of interest, the spatial interaction between the mean motion and coherent structure is

calculated for both non-reactive and reactive conditions and compared with experimental data wherever available. The fine-scale turbulent motion is determined by the application of integral analysis to the fluctuation equations. Since at present this turbulence model is still untested, turbulence is modeled in the interaction problem by a simple algebraic eddy viscosity model. The applicability of the integral turbulence model formulated here is studied parametrically by integrating these equations for the simple case of self-similar mean motion with assumed shape functions. The effect of the motion of the coherent structure is studied and very good agreement is obtained with previous experimental and theoretical works for non-reactive flow. For the reactive case, lack of experimental data made direct comparison difficult. It was determined that the growth rate of the disturbance amplitude is lower for reactive case. The results indicate that the reactive flow stability is in qualitative agreement with experimental observation.

TABLE OF CONTENTS

	Page
ACKNOWLEDGEMENTS	ii
LIST OF SYMBOLS	v
LIST OF FIGURES	xiii
I. INTRODUCTION	1
II. FORMULATION OF THE PROBLEM	7
2.1 The Governing Equation	7
2.2 Filtering Procedure	8
2.3 Conservation Equations for the Mean Flow	10
2.3.1 Specie Integral Equation	11
2.3.2 Streamwise Momentum Integral Equation	12
2.3.3 Normal Momentum Integral Equation	12
2.3.4 Energy Integral Equation	13
2.3.5 Equation of State	14
2.3.6 Mean Kinetic Energy Integral	14
2.4 Shape Assumptions for Mean Flow	16
2.5 Coherent Structure Closure	18
2.5.1 Shape Functions for Organized Structure	19
2.5.2 Coherent Structure Kinetic Energy Integral	21
2.6 Closure for the Fine-Scale Turbulence	23
2.6.1 Density Fluctuation Integral Equation	24
2.6.2 Specie Fluctuation Integral Equation	25
2.6.3 Turbulent Kinetic Energy Integral Equation	28
2.6.4 Total Enthalpy Fluctuation Integral Equation	32
2.6.5 Basis for Spectral Analysis	34
(a) Dissipation in the Production Zone	38
(b) Dissipation in the Transition Zone	39
2.6.6 Shape Functions for Fine-Scale Turbulence	43
2.7 Reaction Model	46
III. METHOD OF SOLUTION	50
3.1 Reactive Eigenvalue Problem	50
3.2 Interaction Between Coherent Structure and Mean Motion in Reactive Flow	51
3.3 Fine-Scale Turbulence in Reactive Flows	52
IV. RESULTS AND DISCUSSION	54
4.1 Stability of Reactive Laminar Wakes	56
4.2 Coherent Structure Interaction in Reactive Wakes	67
4.2.1 Effect of Initial Amplitude and Oscillation Frequency	75
4.2.2 Effect of Intermittency and Molecular Diffusion	79

TABLE OF CONTENTS (continued)

	Page
4.3 Fine-Scale Turbulence in Self-Similar Mean Flow	85
V. CONCLUDING REMARKS	88
APPENDIX A - The Eigenvalue Problem for Reactive Flows	90
APPENDIX B - Interaction Integrals for Coherent Structure Motion	101
APPENDIX C - Models for Turbulence, Intermittency and Diffusion	105
REFERENCES	108

LIST OF SYMBOLS

A	Complex amplitude of the coherent structure
$A_p, A_{Y_k}, A_H, A_q, A_{c_i}$	Normalizing constants for the fine-scale turbulent fluctuation, defined by equation (133)
$c(c_R, c_I)$	Complex phase velocity in the local coordinate system
$C(C_R, C_I)$	Complex phase velocity in the body fixed coordinate system
$C(x) = v_c^2 A ^2$	Averaged large-structure kinetic energy density defined by equation (160)
C_1	Constant defined by equation (32)
$C_k(x)$	Amplitude function for mass fraction fluctuation
C_D	Body drag coefficient
C_{D_k}	Constant appears in equation (86)
C_k^*	Constant defined by equation (35)
d	Characteristic body length (length of flat plate)
d_k	Diffusion term for k-th specie, equation (A3)
\bar{D}_k	Diffusion coefficient of the k-th specie
D_k	Constant defined by equation (32)
$D_i(x)$	Axial variation of the dissipation rates defined by equation (137)
$D(\kappa)$	Spectrum of the dissipation rates defined by equation (115)
$E(x)$	Averaged turbulent kinetic energy density defined by equation (135)
$E(\kappa)$	Turbulent kinetic energy spectrum
E_d	Energy dissipation term, equation (A5)
H	Total enthalpy
h_k	Static enthalpy of the k-th specie
I_{D_k}	Diffusion flux integral of the k-th specie, defined by equations (14) and (15)

I_M	x-momentum diffusion integral defined by equations (19)-(22)
I_E	Diffusion flux integral of mean flow total enthalpy defined by equations (25)-(27)
I_{KE}	Diffusion flux integral of mean flow kinetic energy defined by equations (37)-(39)
I_{RS}	Total stress production integral due to coherent structure and turbulence defined by equations (40)-(42)
I_{RS}^{cT}	Kinetic energy integral for the exchange between coherent structure and fine-scale turbulence, defined by equation (60)
I_{RS}^{TC}	Kinetic energy integral for the exchange between fine-scale turbulence and coherent structure, defined by equation (88)
I_p, I_p^c, I_p^T	Pressure work integrals contributing to mean flow, coherent structure and fine-scale turbulence respectively. Defined by equations (43), (62) and (94)
$I_\phi, I_\phi^c, I_\phi^T$	Viscous dissipation integrals contributing to the mean flow, coherent structure and fine-scale turbulent motion respectively. Defined by equations (46), (63) and (105)
$I_{\rho D}, I_{\rho s}, I_{\rho 3}$	Integrals appearing in the closure of turbulent density fluctuation $\overline{\rho''^2}$, defined by equations (67)-(70)
$I_{C_K}, I_{F_K}, I_{P_K}, I_{D_K}$	Integrals appearing in the closure of turbulent mass fraction fluctuation, $\overline{Y_k''^2}$, defined by equations (76)-(81)
$I_p^p, I_{H_p}^p$	Production integrals for turbulent kinetic energy and enthalpy dissipation rates in the production zone, defined by equation (119)
$I_p^s, I_{H_p}^s$	Production integrals for turbulent kinetic energy and enthalpy dissipation rates in the transfer zone, defined by equation (125)

$I_D^P, I_{H_D}^P$	Decay integrals for turbulent kinetic energy and enthalpy dissipation rates in the production zone, defined by equation (120)
$I_D^S, I_{H_D}^S$	Decay integrals for turbulent kinetic energy and enthalpy dissipation rates in the transfer zone, defined by equation (126)
$I_{D_i}^P, I_{H_{D_i}}^P$	Diffusion integrals for turbulent kinetic energy and enthalpy dissipation rates in the production zone, defined by equation (121)
$I_{D_i}^S, I_{H_{D_i}}^S$	Diffusion integrals for turbulent kinetic energy and enthalpy dissipation rates in the transfer zone, defined by equation (127)
$I_G^P, I_{G_H}^P$	Generation integrals for turbulent kinetic energy and enthalpy dissipation rates in the production zone, defined by equation (122)
k^C	Mean kinetic energy of the coherent structure defined by $\frac{1}{2}(\overline{u'^2} + \overline{v'^2})$
k^T	Mean kinetic energy of the fine-scale turbulence defined by $\frac{1}{2}(\overline{u''^2} + \overline{v''^2})$
k_{f_i}, k_{b_i}	Forward and backward reaction rate constants for the i-th reaction
L	Reference length
$L_{\phi\psi}$	Term defined by equation (31)
m_k	Total degrees of freedom of the k-th specie defined by equation (33)
$M_{\phi\psi\theta}$	Defined by equation (89)
M	Mach number
M_c	Wake centerline Mach number
M_r	Relative Mach number
M_k	Molecular weight of the k-th specie

N_k	Translational and rotational degrees of freedom of the k-th specie
$N(x)$	Average total turbulent enthalpy density defined by equation
$N(\kappa)$	Turbulent total enthalpy spectrum
$P(\theta)$	Clipped Gaussian probability density distribution, equation
p	Static pressure
q_i	Heat flux vector in the i-th direction defined by equation (8)
Q^2	Total mean kinetic energy given by $= \frac{1}{2} (\overline{u}^2 + \overline{u'}^2 + \overline{v'}^2 + \overline{u''^2} + \overline{v''^2})$
r_k^0	Volumetric production rate of the k-th specie
R_k^*	Integrated mean production rate of the k-th specie defined by equation (17)
R_k	Specific gas constant of the k-th specie
R	Universal gas constant
$R_{\phi\psi}$	Term defined by equation (31)
Re_L	Reynolds number based on reference length L
Re_T	Turbulent Reynolds number based on turbulent macroscale Λ
Re	Real part of a complex term
$r_{\phi\psi}$	Correlation coefficient for any two fluctuating quantities ϕ'' , ψ'' , defined by equation (138)
S	Term defined by equation (56)
$S_{\phi\psi\theta}$	Third order correlation term defined by equation (61)
S_ρ, S_{ρ_1}	Constants appearing in the closure for turbulent density fluctuation, $\overline{\rho''^2}$, equation (75)
S_{H_1}, S_{H_2}	Constants appearing in the closure for turbulent total enthalpy fluctuation, $\overline{H''^2}$, equations (110) and (111)

T	Static temperature of the mixture
T_c	Wake centerline temperature excess
t	Independent time coordinate
u	x-component of the velocity vector
u_{ki}	Diffusion flux velocity of the k-th specie in the i-th direction, defined by equation (9)
v	y-component of the velocity vector
V_c	Wake centerline velocity defect
$w = (\bar{u} - 1)/V_c$	x-component of the velocity vector in the local coordinate system
$x_i(x,y)$	Spatial coordinates
X_q	Partition coefficient for turbulent kinetic energy
X_H	Partition coefficient for turbulent total enthalpy
Y_k	Mass fraction of the k-th specie, normalized by their free stream values
Y_{kc}	Wake centerline mass fraction excess

Greek Symbols

α	Complex wave number
α_c	Neutral wave number
β	Spatial frequency of oscillation
$\bar{\beta}$	Complex term due to finite-rate kinetics in equation (55), defined in Appendix A
δ	Shear layer thickness defined by equation (51)
ϵ	Dissipation rate of turbulent kinetic energy
ϵ_H	Dissipation rate of turbulent total enthalpy
ϵ_p	Constant appearing in equation (71)

ϵ_{ijk}	Third order alternating tensor
ϵ_{k_f}	Heat of formation of the k-th specie
ϵ	Eddy momentum diffusivity
ϵ_H	Eddy enthalpy diffusivity
ϵ_ρ	Eddy mass diffusivity
γ	Ratio of specific heats
$(\hat{\alpha}, \hat{\beta}, \hat{\gamma})$	Constants appearing in the modeling turbulent pressure-strain rate, equation (98)
κ^*	Coefficient of thermal conductivity
κ	Wave number
λ	Taylor's microscale
μ	Coefficient of viscosity
ν^*	Complex term due to finite-rate kinetics in equation (55), defined in Appendix A
η_c	Critical point where $w = c$
Λ	Turbulent macroscale
ω	Specific dissipation rate, defined in equation (101)
$\phi_q = \tan^{-1} \left(\frac{\hat{q}_I}{\hat{q}_R} \right)$	The phase of any complex eigenfunction \hat{q}
ρ	Density of the mixture
ρ_k	Density of the k-th specie
$\sigma(x)$	Amplitude function for density fluctuation, $\overline{\rho'^2}$, defined in equation (133)
σ^2	Mean square fluctuation of normalized temperature, θ
ψ_q	Degree of spectral imbalance for turbulent kinetic energy, equation (130)
ψ_H	Degree of spectral imbalance for total enthalpy, equation (130)
θ	Nondimensional temperature, equation (144)

θ^*	Momentum thickness
θ_{k_i}	i-th vibrational degree of freedom of the k-th specie
(ξ, η, τ)	Local small scale coordinates defined by equation (52)
τ_{ij}	Shear stress tensor

Superscript

'	Fluctuation quantities for coherent structure; also for $\frac{d}{dn}$ where there is no confusion.
"	Fluctuation quantities for fine-scale turbulence
*	Dimensional quantity; also for complex conjugate in Appendix B
	Absolute value of a complex quantity
~	Complex Conjugate
-	Mean value
^	Complex eigenfunction of coherent structure fluctuation quantities
< >	Conditional phase average
c	Coherent structure contribution
T	Fine-scale turbulent contribution

Subscript

e	Edge values
I	Imaginary part of a complex quantity
k	k-th specie
o	Initial value at $x = x_0$
p	Production zone in the wave number space
s	Transfer zone in the wave number space

R Real part of a complex quantity
 ∞ Free stream values
 δ Shear layer edge

LIST OF FIGURES

<u>Figure</u>		<u>Page</u>
1	The geometry of the physical problem: Reacting free shear layer in the wake of a flat plate.	114
2	The path of numerical integration in the complex n -plane for the reactive eigenvalue problem.	115
3	Neutral stability characteristics for non-reacting flow: critical point, wave number and relative phase velocity as a function of temperature excess.	116
4	Variation of the neutral wave speed as a function of free stream Mach number and wake temperature excess.	117
5	Neutral wave numbers as a function of relative Mach number and wake temperature excess.	118
6	Spatial neutral wave frequency as a function of relative Mach number and wake temperature excess.	119
7	The eigenvalues for symmetrical oscillations as a function of wave frequency.	120
8	The eigenvalues for symmetrical oscillations as a function of free stream Mach number.	121
9	The eigenvalues for symmetrical oscillations as a function of wake velocity defect.	122
10	The eigenvalues for symmetrical oscillations as a function of wake temperature excess.	123
11	The eigenvalues for anti-symmetrical oscillations as a function of wave frequency.	124
12	The eigenvalues for anti-symmetrical oscillations as a function of free stream Mach number.	125
13	The eigenvalues for anti-symmetrical oscillations as a function of wake velocity defect.	126
14	The eigenvalues for anti-symmetrical oscillations as a function of wake temperature excess.	127
15	The characteristic variation of the pressure eigenfunction amplitude $ \hat{p} $ and phase ϕ_p across the shear layer. For symmetrical oscillation, $\hat{p}'(0) = 0$ and $M_\infty = 2$, $\beta = 0.1$, $T_\infty = 1500^\circ\text{K}$.	128

<u>Figure</u>		<u>Page</u>
16	The characteristic variation of the pressure eigenfunction amplitude $ \hat{p} $ and phase ϕ_p across the shear layer. For anti-symmetrical oscillation, $\hat{p}(0) = 0$ and $M_\infty = 2$, $\beta = 0.1$, $T_\infty = 1500^\circ\text{K}$.	129
17	The characteristic variation of the amplitudes of pressure eigenfunction $ \hat{p}(\eta) $ and vertical velocity eigenfunction $ \hat{v}(\eta) $ across a symmetric jet. For symmetrical oscillations, $M_\infty = 2.0$, $T_\infty = 1500^\circ\text{K}$, $T_c = 3.0$ and $\beta = 0.1$	130
18	Phase changes of the pressure eigenfunction ϕ_p and vertical velocity eigenfunction ϕ_v across a symmetric jet. Test conditions same as in Figure 17.	131
19	Variation of the centerline mean flow temperature excess for various initial amplitudes of the coherent structure. Laminar non reactive test case [39] for adiabatic flat plate wake at $M_\infty = 6$, $Re_L = 93,000$, $L = 2.54\text{cm}$, $x_0 = 1$, $V_{c_0} = 0.4$, $T_{c_0} = 4.0$, $(Y_{k_{c_0}} = 0.0; k = 1,4)$, $\beta_0 = 0.32$.	132
20	Variation of the centerline Mach number for various initial amplitudes of the coherent structure. Laminar non reactive case [39] for adiabatic flat plate wake at $M_\infty = 6$, $Re_L = 93,000$, $L = 2.54\text{cm}$, $x_0 = 1$, $V_{c_0} = 0.4$, $T_{c_0} = 4.0$, $(Y_{k_{c_0}} = 0.0, k = 1,4)$, $\beta_0 = 0.32$.	133
21	Mean flow specie mass fraction profiles across the wake at various axial locations for both non reactive and reactive cases. Laminar test case at $M_\infty = 2.0$, $T_\infty = 1200^\circ\text{K}$, $(Y_{k_\infty} = 0.05, 0.90, 0.025, 0.025$ $L = 2.54\text{cm}$, $Re_L = 93,000$, $x_0 = 1.0$, $V_{c_0} = 0.4$, $T_{c_0} = 4.0$ $Y_{k_{c_0}}^i = -0.25, -0.25, 3.0, 6.5)$, $ A _0^2 = 2 \times 10^{-5}$, $\beta = 0.3$, $C_D = 0.016$, $x = (x^* - x_0)/C_D L$.	
(a)	Hydrogen mass fraction profiles, \bar{Y}_{H_2}	134
(b)	Oxygen mass fraction profiles, \bar{Y}_{O_2}	135

<u>Figure</u>		<u>Page</u>
21	(c) Hydroxyl mass fraction profiles, \bar{Y}_{OH} (d) Water mass fraction profiles, \bar{Y}_{H_2O}	135 136
22	Decay of centerline mean flow temperature excess for non reactive turbulent wake behind flat plate at $M_\infty = 3.0$, $Re = 70,000/cm$, $\beta_0 = 0.3$, $C_D = 0.031$, $x_0 = 5.0$, $V_{C_0} = 0.23$, $T_{C_0} = 1.275$, $ A _0^2 = 4 \times 10^{-5}$. o: Experiment for heated flat plate [40] x: Experiment for an adiabatic flat plate [64]	137
23	Decay of centerline mean flow velocity defect for non reactive turbulent wake behind flat plate at $M_\infty = 3.0$, $Re = 70,000/cm$, $\beta_0 = 0.3$, $C_D = 0.031$, $x_0 = 5.0$, $V_{C_0} = 0.23$, $T_{C_0} = 1.275$, $ A _0^2 = 4 \times 10^{-5}$. o: Experiment for heated flat plate [40] x: Experiment for an adiabatic flat plate [64]	138
24	Development of the average coherent structure energy density, C , stress I_{RS}^C , dissipation I_ϕ^C and mean flow dissipation I_ϕ in the turbulent supersonic non reactive wake. Flat plate at $M_\infty = 3.0$, $Re = 70,000/cm$, $\beta_0 = 0.3$, $C_D = 0.031$, $x_0 = 5.0$, $V_{C_0} = 0.23$, $T_{C_0} = 1.275$, $ A _0^2 = 4 \times 10^{-5}$.	139
25	Growth of centerline mean flow temperature excess for various initial amplitudes of disturbance. Turbulent reactive test conditions: $M_\infty = 3.0$, $Re = 70,000/cm$, $T_\infty = 1500^\circ K$, $L_\infty = 0.3cm$, $\beta_0 = 0.2$, $x_0 = 5.0$, $V_{C_0} = 0.23$, $T_{C_0} = 1.275$, $(Y_{k_{C_0}} = 0.0, k = 1.4)$.	140
26	Decay of centerline mean flow velocity defect for various initial amplitudes of disturbance. Turbulent reactive test conditions as in Figure 25.	141
27	Development of the centerline mean flow specie mass fraction for various initial amplitudes of disturbance. Turbulent reactive test conditions as in Figure 25.	142

<u>Figure</u>		<u>Page</u>
27	(a) The centerline mean flow hydrogen and hydroxyl mass fractions defects. (b) The centerline mean flow water vapor mass fraction excess.	
28	Growth and decay characteristics of the amplitude of coherent structure for various initial values. Turbulent reactive test conditions as in Figure 25.	143
29	Growth and decay characteristics of the amplitude of coherent structure for various initial frequency of disturbance. Turbulent reactive test conditions: $M_\infty = 3.0$, $T_\infty = 1500^\circ\text{K}$, $L = 0.3\text{cm}$, $x_0 = 5.0$, $V_{C_0} = 0.25$, $T_{C_0}^\infty = 1.275$, $ A _0^2 = 4 \times 10^{-5}$.	144
30	Characteristic variation of the eigenvalues of the local stability problem for various initial frequency of disturbance. Turbulent reactive test conditions as in Figure 29.	145
31	Development of centerline mean flow specie mass fractions for various initial frequency of disturbance. Turbulent reactive test conditions as in Figure 29.	146
32	Development of the coherent structure energy transfer mechanism with and without intermittency. Turbulent reactive test conditions as in Figure 25.	147
33	Contribution of the mean flow kinetic energy diffusion, I_{KE} , the total enthalpy diffusion, I_E and specie diffusion, I_{D_K} , due to coherent structure motion. Intermittency effects in turbulent reactive wake with conditions as in Figure 25.	148
34	Variation across the shear layer of the intermittency factors for forward and backward rates at various streamwise locations in the reactive wake. Test conditions as in Figure 25.	149
35	Contributions to the Reynold stress energy transfer I_{RS}^C for reactive wake. Turbulent test conditions: $M_\infty = 3.0$, $T_\infty = 1500^\circ\text{K}$, $C_D = 0.031$, $Re = 70,000/\text{cm}$, $ A _0^2 = 4 \times 10^{-5}$, $R_0 = 0.2$, $x_0 = 5.0$, $V_{C_0} = 0.25$, $T_{C_0}^\infty = 1.275$, $(Y_{k_{C_0}} = 0.0, k = 1,4)$.	150

<u>Figure</u>		<u>Page</u>
36	Development of the centerline mean flow temperature excess in turbulent reactive and non reactive wakes. Comparison of the effects of intermittency and diffusion for $ A _0^2 = 0$ and 4×10^{-5} . Other conditions as in Figure 25.	151
37	Decay of the centerline mean flow velocity defect in turbulent reactive and non reactive wakes. Comparison of the effects of intermittency and diffusion for $ A _0^2 = 4 \times 10^{-5}$. Other conditions as in Figure 25.	152
38	Development of the centerline mean flow specie mass fractions in turbulent reactive wakes. Effects of intermittency and diffusion for $ A _0^2 = 4 \times 10^{-5}$. Test conditions as in Figure 25. (a) The hydrogen and hydroxyl mass fraction defects. (b) The water vapor mass fraction excess.	153
39	The streamwise development of the ratio between the reactive and non reactive disturbance amplitude growth rates for different initial frequency. Conditions as in Figure 25	154
40	The spectral dependence of the turbulent kinetic energy, $E(\kappa)$ and turbulent total enthalpy $N(\kappa)$.	155
41	(a) The variation across the shear layer of the mean flow temperature, \bar{T} normalized temperature θ and normalized temperature fluctuation θ'^2 . (b) The clipped Gaussian probability distribution for normalized temperature, $P(\theta)$.	156
42	The effect of temperature fluctuation on the mean production rate of hydrogen as a function of temperature.	157
43	The effect of variation of the correlation coefficients on the streamwise development turbulent kinetic energy and turbulent total enthalpy fluctuation.	158
44	The effect of variation of density strain rate constant on the streamwise development of turbulent mass density fluctuation, turbulent kinetic energy and turbulent total enthalpy fluctuation.	159

I. INTRODUCTION

The study of the interaction between turbulence and chemical reactions is a region of continued interest in fluid dynamics. A better understanding of the complexity involved will enhance design and predictive capability of advanced and more efficient propulsion systems. Of particular interest here is the combustion system of a Supersonic Combustion RAM Jet engine (SCRAMJET) being currently studied at NASA Langley Research Center [1]. In the combustor of a SCRAMJET, hydrogen fuel is injected at near sonic condition into a supersonic air stream and combustion occurs in the recirculatory zone inside the combustor. The analysis of such a high temperature, turbulent reactive flow is complicated by the ongoing interaction between fluid mechanical and chemical effects, whereby, the reactants first mix and then combine to release chemical energy which in turn significantly alters the flowfield. The analysis of such an interaction is so complicated that without some simplification the problem remains intractable. However, with some reasonable assumptions an understanding of the complex interaction can be obtained.

The application of the eddy-viscosity models developed for non-reactive flows in combustion studies has met with only limited success [2]. The use of gradient diffusion models have been shown to be incorrect in reactive and recirculatory flows where counter gradient diffusion is present [3, 4]. It became quite clear that new approaches were necessary to handle the complexity of reactive flows. This led to the counter gradient model [3] and probability distribution and functional formulations [5-8]. Though these models have been successful in predicting some of the phenomena inherent in reactive flows, there are still many unanswered questions concerning the interaction between chemical kinetics and flow

turbulence.

Ever since the existence of large scale coherent structures in turbulent shear flows became evident, the effect these coherent structures may have on combustion processes has been subject to speculations [9-12]. This has led to various new models, for example, Spalding's ESCIMO model [13,14] which accentuates a genuine property of turbulent flows that is evidently enhanced by large coherent structures: the stretching of local flame elements due to the straining motion of the flow. Another model by Marble and Broadwell [15] studies the diffusion flame structures as opposed to the premixed flame model of Spalding. The influence of fluid dynamics on combustion has been considered by Chorin [16] using a numerical method based on vortex dynamics which has been also extended by Ghoniem, Chorin and Oppenheim to non-constant density flows with the aim of modeling combustion in coherent structures [17].

There is now much experimental evidence of the existence of large scale coherent structures in free shear turbulent flows [9,10,18]. Through flow visualization, Moore [19] showed that a turbulent round jet also has a definite coherent structure that starts as an instability wave in the shear layer. Earlier experiments by Pai [20] had first pointed out the existence of secondary flow inside rotating cylinders. More recently, Ganji and Sawyer [21] observed large structures dominating mixing layer that develops behind a step under non-reacting and reacting conditions. In comparing reacting and non-reacting flows, they found that the reacting eddies have a lower growth rate, and more closely distributed in space and have a slightly smaller ratio of coalescence than non-reacting eddies. In turbulent flames Yule et. al [22,23] found that combustion driven instabilities effect the coherent structure growth and decay. In fact, they found

at least two combustion driven instabilities, an inner high frequency and an outer low frequency phenomena. These instabilities are genuine properties of flames and do not occur in non-reactive flows, leading to the term 'combustion driven coherent structures' [24]. Such experimental evidence supports Roshko's [25] conclusion that coherent structures play a central role in the development of many turbulent shear flows such as mixing layers, boundary layers, and the early regions of jets and wakes.

It has also been noted that combustion in non-premixed flames seems to conserve coherent structures in the flow by delaying transition to turbulence [26]. All available data seems to indicate that coherent structures are potentially more important in combustion systems than any other flow systems due to the strong influence they have on the turbulent mixing of reactants and to the stabilization of existing structures by combustion.

The transport processes across the mixing layer is considerably under-predicted by all theoretical models leading to the point of view that the effect of large scale coherent structures on scalar mixing processes cannot be predicted by methods that use scalar flux approximations. Therefore, it seems clear that a different closure model is necessary to handle the combustion problem in turbulent flow.

The present investigation considers the theoretical analysis of the laminar-turbulent transition of compressible reactive wakes. Experimental measurements in non-reactive wakes behind flat plates and slender wedges [27,28] have shown remarkable similarity with the low-speed wake transition analysis by Sato and Kuriki [29]. Due to their inherent dynamic instability, wakes sustain travelling wave disturbances. The development of these instability waves and their consequent interaction with the mean

velocity, thermal and concentration fields and the fine-scale turbulent fields constitutes the interaction problem considered here. The coherent structure discussed above is modelled as an instability wave which develops from a linear growth region into a nonlinear growth and finally into three dimensionality. The disturbance amplitude is very small in the linear region and the mean field is uncoupled from the disturbance field. However, in the nonlinear region, the amplitude becomes large and there is a strong interaction between the mean field and disturbance field causing the mean field to decay more rapidly than in the linear region. Beyond the nonlinear region, the disturbance becomes three dimensional and for high enough Reynolds number the flow becomes turbulent. This is the general picture of wake transition although the actual extent of each region depends upon flow field parameters like the Reynolds number and Mach number.

This analysis considers the motion of the turbulent fluid as a combination of three distinct motions: the mean motion, the large-scale coherent structure motion and the fine-scale turbulence. Such a splitting procedure was first used by Reynolds and Hussain [30] and has been used extensively by Liu et. al [31-34] in their study of coherent structures. More specifically, Liu and Merkin [33], Liu and Alper [34], Alper and Liu [35] and Gatski and Liu [36] have studied the interaction between a monochromatic component of the large-scale coherent structure and the fine-grained turbulence in developing mean flows with inflexional profiles. There, the nonlinear interactions between the three components of flow are depicted in terms of the non-equilibrium adjustments between the mean shear layer growth rate and the integrated energy densities of the large-scale structure and the fine-grained turbulence. Their analysis was limited to

incompressible non-reactive flow, however, they found reasonable agreement with experiments for the spatial spreading rate of the shear layer.

The present theoretical study is an analysis of the nonlinear interaction between the three motions in a compressible multicomponent reactive flow. Two averaging procedures are necessary to consider the interaction among the three components of flow: conditional phase averaging which explicitly filters the coherent structure from the total fluctuations containing both random and coherent components; and the conventional Reynolds averaging which separates the mean flow from the fluctuations. Due to the complexity of the resultant equations, finite-difference computations of the interaction is very complicated. Stuart [37] and Ko, Kubota and Lees [38] analysed the development of finite amplitude disturbances in incompressible shear flows using von Karman integral formulation. Integral considerations were also used by Liu and Gururaj [39] to study compressible wake transition and they obtained good agreement with experimental data for hypersonic wakes [27, 40]. Accordingly, the present study incorporates von Karman integral method to obtain the conservation equations for the mean flow. The mean flow is then characterized by the wake width, the wake centerline values of the mean velocity defect, the mean temperature excess and the mean specie mass fraction defects. The disturbance is characterized by its amplitude and its variation across the shear layer is determined by the application of hydrodynamic stability theory to the disturbance equations. The integral technique is also applied to the fine-scale turbulence equations to achieve closure. Though the present formulation is simplified by various assumptions (to be discussed later), it is expected that this formulation can be used to obtain a better understanding of the

interaction between the three components of flow during combustion, an area of research that has not been studied so far.

The physical problem studied at present is the growth of a multi-component free shear layer in the wake of a flat plate (Figure 1). For simplicity we consider a supersonic premixed stream of hydrogen, oxygen, hydroxyl radical and water vapor in the shear layer. The interaction problem for both non-reactive and reactive flow conditions is studied and the changes in the organized motion due to reaction is discussed. In Chapter II the governing conservation equations of the interaction problem is formulated and the various assumptions used are discussed. Chapter III describes the numerical methods used to solve reactive stability problem and the integral equations of motion. In Chapter IV the results of the numerical calculations are presented and compared with other theoretical studies and experimental data wherever possible.

II. FORMULATION OF THE PROBLEM

2.1 The Governing Equation

The general conservation equations for a multicomponent mixture in a cartesian coordinate system can be written in dimensional form as

a) Mass conservation

$$\frac{\partial \rho}{\partial t} + \frac{\partial \rho u_i}{\partial x_i} = 0 \quad (1)$$

b) Species Conservation

$$\frac{\partial \rho Y_k}{\partial t} + \frac{\partial}{\partial x_i} \rho Y_k (u_i + u_{ki}) = r_k^0 \quad k = 1 \dots v \quad (2)$$

c) Momentum Conservation

$$\frac{\partial \rho u_i}{\partial t} + \frac{\partial}{\partial x_j} (\rho u_i u_j + p \delta_{ij}) = \frac{\partial}{\partial x_j} \tau_{ij} \quad (3)$$

d) Energy Conservation

$$\frac{\partial}{\partial t} (\rho H - p) + \frac{\partial}{\partial x_i} (\rho u_i H - u_j \tau_{ji} + q_i) = 0 \quad (4)$$

e) Equation of State

$$p = \rho T \sum_k R_k Y_k \quad (5)$$

Here τ_{ij} is the shear stress tensor given as

$$\tau_{ij} = -\frac{2}{3} \mu \frac{\partial u_k}{\partial x_k} \delta_{ij} + \mu \left(\frac{\partial u_i}{\partial x_j} + \frac{\partial u_j}{\partial x_i} \right) \quad (6)$$

H is the total enthalpy defined as

$$H = \frac{1}{2} (u^2 + v^2) + \sum_k (m_k^* T + \epsilon_{k_f}^*) Y_k \quad (7)$$

where $m_k^* = (n_k^* + \frac{\theta_{i_k}^*/T}{\theta_{i_k}^*/T - 1}) R_k$ gives the translational and rotational degrees of freedom (by n_k^*) and $\theta_{i_k}^*$ gives the i -th vibrational degree of

freedom for the k-th specie and $\epsilon_{k_f}^*$ is the heat of formation for k-th specie.

q_i is the heat flux defined as

$$q_i = -\kappa^* \frac{\partial T}{\partial x_i} + \sum_k \rho Y_k h_k u_{k_i} \quad (8)$$

where $h_k = e_k + R_k T$ is the static enthalpy for the k-th specie; e_k and R_k are the specific internal energy and specific gas constant for the k-th specie. u_{k_i} is the diffusion flux velocity for the k-th species given by

$$u_{k_i} = -\frac{D_k}{Y_k} \frac{\partial Y_k}{\partial x_i}, \quad k=1, \dots, v \quad (9)$$

where D_k is the molecular diffusivity of the k-th specie and κ^* is the thermal conductivity.

2.2 Filtering Procedure

The above equations (1 - 9) are now reduced to the integral form to be used in this analysis. Though turbulence is essentially three-dimensional, for numerical simplicity, we consider two-dimensional flow. Extension to three-dimensional flow will not change the governing equations appreciably. In wake type flows, it has been shown that the detailed distribution of the disturbances is not very sensitive to the viscous terms leading to the 'inviscid' considerations [39,41]. Though molecular transport phenomena is important in turbulent reactive flows, it is smaller in comparison to the transport due to turbulent stresses and may be neglected in comparison. We include only a simplified form of the dissipation terms in the governing equations and neglect the fluctuations in the transport properties.

Any instantaneous flow variable, $q(x,y,t)$ is then decomposed as follows:

$$q(x,y,t) = \overline{q(x,y)} + q'(x,y,t) + q''(x,y,t) \quad (10)$$

Here \overline{q} is the mean flow component, q' and q'' the corresponding coherent structure and fine-scale turbulent components respectively.

On using (10) in the Navier-Stokes equations and time averaging we get the equations governing the mean motion. Subtracting the mean motion equations from the original equations and then taking phase averaging we extract the equations governing organized motion. When we subtract the equations for organized motion from the total fluctuation equation we obtain the equations governing fine-grained turbulence (see Appendix B). The two averaging processes as discussed above are defined as follows:

Time average is

$$\overline{q(x,y)} = \lim_{T \rightarrow \infty} \frac{1}{T} \int_0^T q(x,y,t) dt \quad (11)$$

where T is greater than the period τ of the large-scale structure at least. The conditional phase average is

$$\langle q(x,y,t) \rangle = \lim_{N \rightarrow \infty} \frac{1}{N} \sum_{n=0}^N q(x,y,t + n\tau) \quad (12)$$

The conditional and time average of a turbulent quantity, $q''(x,y,t)$, are zero by definition. The conditional average of a large scale structure quantity, $q'(x,y,t)$ reproduces itself and its time average is zero. We assume that the two components of the fluctuations are not correlated. Furthermore, the conditional average of two fine-scale turbulent quantities after subtracting the steady part, $\langle q''q'' \rangle - \overline{q''q''}$, is periodic and oscillates at the same frequency as the large-scale structure [31].

Though the large-structure may have many frequency components, at present we consider the propagation of only the fundamental component.

This is a reasonable approximation because it has been shown experimentally that through proper control it is possible to get a single mode propagation in the flow [42]. Furthermore, as a first approximation, the energy this fundamental mode exchanges with other frequency components can be neglected with respect to the energy it exchanges with the mean flow or the fine grained turbulence.

2.3 Conservation Equations for the Mean Flow

To derive the mean flow equation we nondimensionalize all variables with respect to the free stream conditions which are assumed to be constant. Thus, velocity and coordinates are nondimensionalized by the free stream velocity, u_∞ , and reference length, L respectively; the pressure, temperature and density are made dimensionless by their corresponding free stream values p_∞ , T_∞ and ρ_∞ .

The time averaged equations obtained are complicated and contain many unknown correlations of the fluctuations. To reduce the complexity, we make some approximations which have been shown to be reasonable by past analysis of wake flows. Since we are considering free shear flows at present, we can apply the boundary layer approximations without losing significant accuracy. We further use von Karman integral technique to integrate the governing equations across the shear layer (normal direction) and obtain a set of integro-differential equations. In deriving these equations we assume that all fluctuation correlations vanish far away from the flat plate and shear layer region. The problem then reduces to determining the shape functions for the mean flow variables associated with the von Karman integral formulation.

After some manipulation we get the following integral equations:

2.3.1 Specie Integral Equation

$$\frac{d}{dx} \int_{-\infty}^{\infty} \bar{\rho} \bar{u} (\bar{Y}_k - 1) dy = - \frac{dI_{D_k}}{dx} + R_k^*; \quad k = 1 \dots v \text{ species} \quad (13)$$

Here, $\bar{\rho}$ and \bar{u} are the dimensionless mean density and streamwise velocity respectively. \bar{Y}_k is the normalized mean mass fraction of the k th specie defined as $\bar{Y}_k = \bar{Y}_k^*/Y_{k\infty}$, where \bar{Y}_k^* is the mean mass fraction and $Y_{k\infty}$ is the freestream value of mass fraction of the k th specie.

I_{D_k} is the species diffusion flux integral for the k th specie made up of contributions from the organized structure motion, $I_{D_k}^c$ and the fine-scale turbulence, $I_{D_k}^T$. They are given as

$$I_{D_k}^c = \int_{-\infty}^{\infty} [\bar{\rho}' u' (\bar{Y}_k - 1) + \bar{\rho} \bar{u}' Y_k' + \bar{u} \bar{\rho}' Y_k'] dy \quad (14)$$

and

$$I_{D_k}^T = \int_{-\infty}^{\infty} [\bar{\rho}'' u'' (\bar{Y}_k - 1) + \bar{\rho} \bar{u}'' Y_k'' + \bar{u} \bar{\rho}'' Y_k'' + \bar{\rho}'' u'' Y_k''] dy \quad (15)$$

so that

$$I_{D_k} = I_{D_k}^c + I_{D_k}^T \quad (16)$$

R_k^* is the integrated mean rate of production of the k th specie given as

$$R_k^* = \int_{-\infty}^{\infty} \bar{r}_k^{\circ} dy \quad (17)$$

Here \bar{r}_k° is the dimensionless mean rate of production of the k th specie and is defined in Appendix B.

2.3.2 Streamwise Momentum Integral Equation

$$\frac{d}{dx} \int_{-\infty}^{\infty} \bar{\rho} \bar{u} (\bar{u} - 1) dy = - \frac{dI_M}{dx} \quad (18)$$

The momentum diffusion integral, I_M is defined as

$$I_M = I_M^C + I_M^T + I_{M_p} \quad (19)$$

where

$$I_M^C = \int_{-\infty}^{\infty} [\bar{\rho}' u' (2\bar{u} - 1) + \bar{\rho} \overline{u'^2}] dy \quad (20)$$

$$I_M^T = \int_{-\infty}^{\infty} [\bar{\rho}'' u'' (2\bar{u} - 1) + \bar{\rho} \overline{u''^2} + \overline{\rho'' u''^2}] dy \quad (21)$$

$$I_{M_p} = C_1 \int_{-\infty}^{\infty} \bar{p} dy \quad (22)$$

In the free shear layer, pressure is nearly constant and so the term $\frac{dI_{M_p}}{dx}$ is negligible in equation (18) and $C_1 = p_\infty / \rho_\infty u_\infty^2$.

2.3.3 Normal Momentum Integral Equation

$$\begin{aligned} \bar{p} = 1 - \frac{1}{C_1} [& \bar{\rho} (\overline{v'^2} + \overline{v''^2}) + \frac{d}{dx} \int_{-\infty}^y \{ \bar{\rho} (\overline{u'v'} + \overline{u''v''}) \\ & + \bar{u} (\overline{\rho'v'} + \overline{\rho''v''}) + \overline{\rho''u''v''} \} dy] \end{aligned} \quad (23)$$

It has been shown by Liu and Gururaj [39] that for wake flows the last term on the right side of equation (23) is negligible relative to the others and pressure \bar{p} can be determined from the reduced equation.

2.3.4 Energy Integral Equation

$$\frac{d}{dx} \int_{-\infty}^{\infty} \bar{\rho} \bar{u} (\bar{H} - 1) dy = - \frac{dI_E}{dx} \quad (24)$$

The total enthalpy integral, I_E is defined as

$$I_E = I_E^C + I_E^T \quad (25)$$

where

$$I_E^C = \int_{-\infty}^{\infty} [\bar{\rho} \overline{u'H'} + \bar{u} \overline{\rho'H'} + (\bar{H} - 1) \overline{\rho'u'}] dy \quad (26)$$

$$I_E^T = \int_{-\infty}^{\infty} [\bar{\rho} \overline{u''H''} + \bar{u} \overline{\rho''H''} + (\bar{H} - 1) \overline{\rho''u''} + \overline{\rho''u''H''}] dy \quad (27)$$

and the mean total enthalpy, \bar{H} is given as

$$\bar{H} = Q^2 + \sum_{k=1}^v m_k D_k (\bar{T} \bar{Y}_k + \overline{T'Y_k'} + \overline{T''Y_k''}) + \sum_{k=1}^v \epsilon_{k_f} \bar{Y}_k \quad (28)$$

where $Q^2 = \frac{1}{2} (\bar{u}^2 + \overline{u'^2} + \overline{v'^2} + \overline{u''^2} + \overline{v''^2})$ is the total mean kinetic energy. The fluctuation contribution to the total enthalpy are

$$\begin{aligned} H' = & \bar{u} u' + \frac{1}{2} (R_{uu} + R_{vv}) + \sum_{k=1}^v m_k D_k (\overline{T'Y_k'} + \overline{T'Y_k'} + R_{TY_k}) \\ & + \sum_{k=1}^v \epsilon_{k_f} Y_k' \end{aligned} \quad (29)$$

$$\begin{aligned} H'' = & \bar{u} u'' + \frac{1}{2} (L_{uu} + L_{vv}) + \sum_{k=1}^v m_k D_k (\overline{T''Y_k''} + \overline{T''Y_k''} + L_{TY_k}) \\ & + \sum_{k=1}^v \epsilon_{k_f} Y_k'' \end{aligned} \quad (30)$$

The term $R_{\phi\psi}$ and $L_{\phi\psi}$ appearing in equations (29) and (30) are defined explicitly for any variable ϕ and ψ as

$$R_{\phi\psi} = \langle \phi' \psi' \rangle - \overline{\phi' \psi'} + \langle \phi'' \psi'' \rangle - \overline{\phi'' \psi''}$$

(31)

and

$$L_{\phi\psi} = \phi' \psi' - \langle \phi' \psi' \rangle + \phi'' \psi'' - \langle \phi'' \psi'' \rangle$$

C_1 , D_k and ϵ_{k_f} are constants given as

$$C_1 = \frac{p_\infty}{\rho_\infty u_\infty^2}, \quad D_k = \frac{RT_\infty Y_{k_\infty}}{M_k u_\infty^2} \text{ and } \epsilon_{k_f} = \frac{\epsilon_{k_f}^\circ Y_{k_\infty}}{u_\infty^2}$$

(32)

Here, R is the universal gas constant and M_k and $\epsilon_{k_f}^\circ$ are the molecular weight and heat of formation of the k -th species. Also

$$m_k = \left[N_k + \sum_{i=1}^N \frac{\theta_{k_i}/\bar{T}}{(e^{\theta_{k_i}/\bar{T}} - 1)} \right]$$

(33)

gives the translational, rotational (by N_k) and vibrational degrees of freedom with θ_{k_i} as the characteristic dimensionless temperature for the i -th vibrational frequency of k -species.

2.3.5 Equation of State

$$\bar{p} = \sum_{k=1}^v C_k^* \left[\bar{\rho} \bar{T} Y_k + \overline{\rho (T' Y_k)} + \overline{T'' Y_k''} \right] + \overline{T (\rho' Y_k' + \rho'' Y_k'')} + \overline{Y_k (\rho' T' + \rho'' T'')} + \overline{\rho'' T'' Y_k''}$$

(34)

where

$$C_k^* = \frac{\rho_\infty RT_\infty}{M_k p_\infty} Y_{k_\infty}$$

(35)

2.3.6 Mean Kinetic Energy Integral

It is also necessary to derive the integral equation governing the

total mean kinetic energy and can be written as

$$\frac{1}{2} \frac{d}{dx} \int_{-\infty}^{\infty} \bar{\rho} \bar{u} (\overline{u^2} - 1) dy = -\frac{d I_{KE}}{dx} - I_{RS} + I_p - I_\phi \quad (36)$$

Here, I_{KE} represents the mean flow kinetic energy diffusion flux integral and is defined as

$$I_{KE} = I_{KE}^c + I_{KE}^T \quad (37)$$

where I_{KE}^c and I_{KE}^T are the diffusion flux integrals due to organized structure motion and fine-scale turbulence respectively. They are given as

$$I_{KE}^c = \int_{-\infty}^{\infty} \left[\frac{1}{2} (3\bar{u}^2 - 1) \overline{\rho' u'} + \bar{\rho} \bar{u} \overline{u'^2} \right] dy \quad (38)$$

and

$$I_{KE}^T = \int_{-\infty}^{\infty} \left[\frac{1}{2} (3\bar{u}^2 - 1) \overline{\rho'' u''} + \bar{\rho} \bar{u} \overline{u''^2} + \overline{\rho'' u''^2} \right] dy \quad (39)$$

I_{RS} represents the total turbulent stress production integral contributing to the mean flow. It is defined as

$$I_{RS} = I_{RS}^c + I_{RS}^T \quad (40)$$

where I_{RS}^c is the Reynold stress production due to organized structure motion

$$I_{RS}^c = - \int_{-\infty}^{\infty} \left[(\bar{u} \overline{\rho' u'} + \bar{\rho} \overline{u'^2}) \frac{\partial \bar{u}}{\partial x} + (\bar{\rho} \overline{u' v'} + \bar{v} \overline{\rho' u'}) \frac{\partial \bar{u}}{\partial y} + \bar{\rho} \overline{v'^2} \frac{\partial \bar{v}}{\partial y} \right] dy \quad (41)$$

and I_{RS}^T the corresponding stress production integral due to fine scale turbulence

$$I_{RS}^T = - \int_{-\infty}^{\infty} [(\bar{u} \overline{\rho'' u''} + \bar{\rho} \overline{u''^2} + \overline{\rho'' u''^2}) \frac{\partial \bar{u}}{\partial x} + (\bar{\rho} \overline{u'' v''} + \bar{v} \overline{\rho'' u''} + \overline{\rho'' u'' v''}) \frac{\partial \bar{u}}{\partial y} + (\bar{\rho} \overline{v''^2} + \overline{\rho'' v''^2}) \frac{\partial \bar{v}}{\partial y}] dy \quad (42)$$

I_p denotes the pressure integral given as

$$I_p = I_{p_1} + I_{p_2} \quad (43)$$

where

$$I_{p_1} = -C_1 \frac{d}{dx} \int_{-\infty}^{\infty} (\bar{p} - 1) \bar{u} dy \quad (44)$$

and

$$I_{p_2} = C_1 \int_{-\infty}^{\infty} (\bar{p} - 1) \left(\frac{\partial \bar{u}}{\partial x} + \frac{\partial \bar{v}}{\partial y} \right) dy \quad (45)$$

Here, I_{p_1} is the pressure diffusion integral and I_{p_2} gives the work done due to expansion. The mean flow viscous dissipation integral is simply taken to be

$$I_{\phi} = \frac{1}{Re_L} \int_{-\infty}^{\infty} \bar{\mu} \left(\frac{\partial \bar{u}}{\partial y} \right)^2 dy \quad (46)$$

where $\bar{\mu}$ is the dimensionless viscosity coefficient and $Re_L = \rho_{\infty} u_{\infty} L / \mu_{\infty}$ is the Reynolds number based on freestream conditions.

2.4 Shape Assumptions for Mean Flow

Experimental investigation indicates that in a wake the momentum thickness θ^* , is very nearly constant. Equation (18) may then be rewritten as

$$\int_{-\infty}^{\infty} \bar{\rho} \bar{u} (\bar{u} - 1) dy = \text{Constant} \quad (47)$$

by neglecting the integral I_M .

On using the definition of momentum thickness

$$\theta^* = \int_0^{\infty} \bar{\rho} \bar{u} (1 - \bar{u}) dy = \frac{C_D}{4} = \text{constant} \quad (48)$$

where, C_D is the body drag coefficient, along with equation (47) a relation between the wake width and the centerline velocity defect can be obtained as shown later.

The solution of the governing integral equations for the mean motion depends upon the proper choice of the shape functions characterizing the variation of the mean flowfield in the wake. It is well known that the Von Karman integral method allows quite accurate calculations of the gross features while remaining quite insensitive to the finer-details, provided of course, that the shape function representation is physically reasonable. The distribution of the mean flow variables across the wake has been experimentally shown to be nearly Gaussian [27,65]. Therefore, the the mean flow is represented by

$$\begin{aligned} \bar{u}(x, \eta) &= 1 - V_c(x) \exp(-\eta^2) \\ \bar{T}(x, \eta) &= 1 + T_c(x) \exp(-\eta^2) \end{aligned} \quad (49)$$

$$\bar{Y}_k(x, \eta) = 1 + Y_{k_c}(x) \exp(-\eta^2), \quad \alpha = 1, \dots, v$$

where all variables are non-dimensionalized with respect to their edge values. Here, $V_c(x)$, $T_c(x)$ and $Y_{k_c}(x)$ are the mean horizontal velocity defect, temperature and k-specie mass fraction excesses at the centerline of the wake. The coordinate η , is defined as the Howarth transformed variable given by

$$\eta = \int \frac{y}{\bar{\rho}} dy / \delta(x) \quad (50)$$

where $\delta(x)$ is the dimensionless shear layer thickness which can be shown to be related to the centerline velocity defect $V_c(x)$ by equation (48) to give

$$\delta(x) = \frac{C_D/2}{V_c(C_1 - C_2 V_c)} \quad (51)$$

where $C_1 = \int_{-\infty}^{\infty} e^{-\eta^2} d\eta$ and, $C_2 = \int_{-\infty}^{\infty} e^{-2\eta^2} d\eta$

Therefore, the mean flow can then be characterized by $V_c(x)$, $T_c(x)$, and $Y_{k_c}(x)$. The variation of mean density $\bar{\rho}(x, \eta)$ and pressure, $\bar{p}(x, \eta)$ can be represented in terms of $V_c(x)$, $Y_{k_c}(x)$ and $T_c(x)$ in the governing equations with the help of normal momentum equation (23) and the equation of state (34). The mean flow field can then be completely defined in terms of the variable $V_c(x)$, $T_c(x)$ and $Y_{k_c}(x)$.

2.5 Coherent Structure Closure

The equations described in Section 2.3 govern the mean flow. However, they contain correlations due to the fluctuations of the coherent structure variables and also fine-grained turbulence. Here, we discuss the closure of the coherent structure correlations. As mentioned before, the equations governing the coherent structure motion are derived using the hydrodynamic stability theory. The coherent structure is assumed to have a wave-like periodicity as is defined by its amplitude $A(x)$ and its frequency of oscillation β . By choosing appropriate shape functions for the coherent structure variables we derive the local eigenvalue equation which is solved using local linear stability analysis.

To facilitate numerical solution we define local coordinates given as

$$\xi \equiv \frac{x - x_0}{\delta(x)}$$

$$\eta = \int \frac{\bar{\rho} dy}{\delta(x)} \quad (52)$$

$$\tau = \frac{t}{\delta(x)}$$

where for the eigenvalue problem the dimensionless shear layer thickness $\delta(x)$ is considered locally a constant and x_0 is a location close to x such that the mean flow streamwise gradients are negligible.

2.5.1 Shape functions for Organized Structures

The shape functions assumed for the coherent structure in their dimensionless form can be written in the local coordinates as

$$\begin{pmatrix} u'(\xi, \eta, \tau)/V_c \\ v'(\xi, \eta, \tau)/V_c \\ \rho'(\xi, \eta, \tau) \\ p'(\xi, \eta, \tau) \\ T'(\xi, \eta, \tau) \\ Y_k'(\xi, \eta, \tau), k=1, \nu \end{pmatrix} = A(x) \begin{pmatrix} \hat{u}(\eta) \\ \alpha \hat{v}(\eta) \\ \hat{\rho}(\eta) \\ \hat{p}(\eta) \\ \hat{T}(\eta) \\ \hat{Y}_k(\eta), k=1, \nu \end{pmatrix} e^{-i\beta\tau + c \cdot c + O(|A|^2)} \quad (53)$$

Here, $c \cdot c$ denotes the complex conjugate and the complex eigenfunctions of the fundamental component \hat{u} , \hat{v} , $\hat{\rho}$, \hat{p} , \hat{T} and \hat{Y}_k correspond to the wave streamwise velocity, normal velocity, density, pressure, temperature and k th species mass fraction, respectively. Furthermore, $\beta = \beta^* \frac{\delta(x)L}{u_\infty}$ is the real dimensionless frequency, β^* the physical frequency; and $\alpha = \alpha^* \delta(x)L$ is the dimensionless complex wavenumber and α^* its dimensional value. The local streamwise derivatives of the disturbances

are evaluated by the local relation [31].

$$\frac{dA}{d\xi} = i\alpha A \quad (54)$$

On using (53) and (54) in the linearized inviscid equations for the organized motion and on some algebraic manipulation (see Appendix A), the governing equation in terms of the pressure perturbation $\hat{p}(\eta)$ can be written as

$$\begin{aligned} \hat{p}'' + \hat{p}' \left[-\frac{2w'}{(w-c)} + \frac{\bar{T}'}{\bar{T}} (v^*-1) - \frac{S'}{S} - \bar{\beta} \right] \\ + \hat{p} \left[\frac{(w-c)^2 v_c^2}{\bar{T}} v^* \left(\frac{1}{C_1 S} - \frac{1}{M} \right) - 1 \right] \alpha^2 S^2 \bar{T}^2 = 0 \end{aligned} \quad (55)$$

where $w = (\bar{u}-1)/V_c$ and c is the dimensionless complex phase velocity defined as $c = (\beta/\alpha - 1)/V_c$. Here, prime denotes differentiation with respect to η , and

$$S = \sum_{k=1}^{\nu} C_k^* Y_k, \quad S' = \sum_{k=1}^{\nu} C_k^* Y_k', \quad \text{and} \quad M = \sum_{k=1}^{\nu} m_k D_k Y_k \quad (56)$$

Also, $v^* (= v_R^* + i v_I^*)$ and $\bar{\beta} (= \bar{\beta}_R + i \bar{\beta}_I)$ are complex terms appearing due to the presence of finite rate kinetics and are described in Appendix A. We note here that this eigenvalue problem eq. (55) reduces to the classical Lees and Lin [43] problem when the flow is non-reactive and single specie. For multi-component non-reactive flow

$$\begin{aligned} v_R^* = 1, \quad v_I^* = 0 \\ \bar{\beta}_R = -\frac{S'}{S}, \quad \bar{\beta}_I = 0 \end{aligned} \quad (57)$$

The eigenvalue equation (55) is solved for the assumed mean flow profiles and appropriate boundary conditions for a given frequency $\bar{\beta}$

and complex wave number α . All other eigenfunctions \hat{u} , \hat{v} , $\hat{\rho}$, \hat{T} and \hat{Y}_k are subsequently determined from the local solution for $\hat{p}(\eta)$. Inherent in such a consideration described above is the assumptions of 'local similarity' which implies that the eigenfunction $\hat{p}(\eta)$ adjusts instantaneously to the mean flow. To complete the closure of the coherent structure we need to determine the amplitude $A(x)$ appearing in equation (53). This is given by the equation governing the time-averaged kinetic energy production associated with wavelike motion of the organized structure.

2.5.2 Coherent Structure Kinetic Energy Integral

$$\frac{d}{dx} \int_{-\infty}^{\infty} \bar{\rho} \bar{u} k^c dy = I_{RS}^c - I_{RS}^{cT} + I_p^c - I_\phi^c \quad (58)$$

where $k^c = \frac{1}{2} (\overline{u'^2} + \overline{v'^2})$ is the organized structure mean kinetic energy. The eigenfunctions are normalized such that $|A|^2$ is the dimensionless kinetic energy per unit length, of the instability wave across a slice of the shear flow [39]:

$$|A|^2 = \frac{1}{V_c^2} \int_{-\infty}^{\infty} k^c d\eta = \frac{1}{2V_c^2} \int_{-\infty}^{\infty} (\overline{u'^2} + \overline{v'^2}) d\eta \quad (59)$$

and may be considered as the energy density in terms of the transformed coordinate η .

I_{RS}^c is the Reynolds stress production integral defined in equation (41). I_{RS}^{cT} is the kinetic energy integral for the exchange between the organized structure and the fine scale turbulence and is given as

$$\begin{aligned}
I_{RS}^{cT} &= \int_{-\infty}^{\infty} \bar{\rho} \left[-R_{uu} \frac{\partial u'}{\partial x} - R_{uv} \left(\frac{\partial u'}{\partial y} + \frac{\partial v'}{\partial x} \right) - R_{vv} \frac{\partial v'}{\partial y} \right] dy \\
&+ \int_{-\infty}^{\infty} \bar{u} \left[-R_{\rho u} \frac{\partial u'}{\partial x} - R_{\rho v} \frac{\partial v'}{\partial x} \right] dy \\
&+ \int_{-\infty}^{\infty} \left[-S_{\rho uu} \frac{\partial u'}{\partial x} - S_{\rho uv} \left(\frac{\partial u'}{\partial y} + \frac{\partial v'}{\partial x} \right) - S_{\rho vv} \frac{\partial v'}{\partial y} \right] dy
\end{aligned} \tag{60}$$

where

$$S_{\phi \psi \theta} = \langle \phi'' \psi'' \theta'' \rangle - \phi'' \psi'' \theta'' \tag{61}$$

I_p^c is the pressure gradient work integral of the disturbance and is given as

$$I_p^c = -C_1 \int_{-\infty}^{\infty} \left[u' \frac{\partial p'}{\partial x} + v' \frac{\partial p'}{\partial y} \right] dy \tag{62}$$

and the viscous dissipation integral for the disturbance is simply taken to be [41]:

$$\begin{aligned}
I_\phi^c &= \frac{1}{Re_L} \int_{-\infty}^{\infty} \bar{\mu} \left[\frac{4}{3} \left\{ \left(\frac{\partial u'}{\partial x} \right)^2 + \left(\frac{\partial v'}{\partial y} \right)^2 - \left(\frac{\partial u'}{\partial x} \frac{\partial v'}{\partial y} \right) \right\} \right. \\
&\left. + \left(\frac{\partial u'}{\partial y} + \frac{\partial v'}{\partial x} \right)^2 \right] dy.
\end{aligned} \tag{63}$$

I_ϕ^c generates mean flow thermal energy at the expense of disturbance kinetic energy.

The energy exchange integral I_{RS}^{cT} which describes the interaction between the coherent structure and fine-scale turbulence is in a form that requires closure. The terms $R_{\phi\psi}$ are specified in terms of an eddy viscosity and disturbance strain rate model similar to Liu [31] such that

$$\begin{aligned}
-R_{uu} &\approx \overline{u''^2} - \langle u''^2 \rangle = 2\epsilon \frac{\partial u'}{\partial x} \\
-R_{vv} &\approx \overline{v''^2} - \langle v''^2 \rangle = 2\epsilon \frac{\partial v'}{\partial y} \\
-R_{uv} &= \overline{u''v''} - \langle u''v'' \rangle = 2\epsilon \left(\frac{\partial u'}{\partial y} + \frac{\partial v'}{\partial x} \right)
\end{aligned} \tag{64}$$

and

$$\begin{aligned}
-R_{\rho u} &= \overline{\rho''u''} - \langle \rho''u'' \rangle = \sigma_\rho^* \epsilon_\rho \frac{\partial \rho'}{\partial x} \\
-R_{\rho v} &= \overline{\rho''v''} - \langle \rho''v'' \rangle = \sigma_\rho^* \epsilon_\rho \frac{\partial \rho'}{\partial y}
\end{aligned} \tag{65}$$

On neglecting the terms larger than $O(|A|^2)$, I_{RS}^{CT} can be written as

$$\begin{aligned}
I_{RS}^{CT} &= 2 \int_{-\infty}^{\infty} \bar{\rho} \epsilon \left[\left(\frac{\partial u'}{\partial x} \right)^2 + \left(\frac{\partial u'}{\partial y} + \frac{\partial v'}{\partial x} \right)^2 + \left(\frac{\partial v'}{\partial y} \right)^2 \right] dy \\
&\quad + \sigma_\rho^* \int_{-\infty}^{\infty} \bar{u} \epsilon_\rho \left[\frac{\partial \rho'}{\partial x} \frac{\partial u'}{\partial x} + \frac{\partial \rho'}{\partial y} \frac{\partial v'}{\partial y} \right] dy
\end{aligned} \tag{66}$$

The eddy viscosity ϵ, ϵ_ρ used in this closure is obtained in terms of the turbulent kinetic energy and dissipation determined in the next section, and σ_ρ^* is a constant. To first approximation, $\epsilon_\rho \approx \epsilon$.

2.6 Closure for the Fine-Scale Turbulence

The equations governing the fine-scale turbulent quantities can be obtained by subtracting the contributions to the mean and organized structure motion from the instantaneous equations. These equations are quite complex and will not be shown here. Here we present a closure model for the turbulent fluctuation correlations. Since the mean motion and the organized structure motion have been formulated using integral technique, we follow similar steps to develop the turbulent equations. Essentially, we manipulate the turbulent fluctuation equations and write equations for turbulent-density correlation $\overline{\rho''^2}$, turbulent-specie mass fraction correlation $\overline{Y_k''^2}$, turbulent-total enthalpy correlation $\overline{H''^2}$

and turbulent kinetic energy $\overline{q''^2}$. On integrating the resultant equations across the shear layer and assuming that all fluctuation correlations vanish far away from the shear layer we get the following integral equations.

2.6.1 Density Fluctuation Integral Equation

$$\frac{1}{2} \frac{d}{dx} \int_{-\infty}^{\infty} \overline{u \rho''^2} dy = - I_{\rho D} + I_{\rho S} - I_{\rho 3} \quad (67)$$

where $I_{\rho D}$ is the production of $\overline{\rho''^2}$ due to mean strain rate and is given by

$$I_{\rho D} = \int_{-\infty}^{\infty} \overline{\rho''^2} \left[\frac{1}{2} \frac{\partial \overline{u}}{\partial x} + \frac{\partial \overline{v}}{\partial y} \right] dy \quad (68)$$

$I_{\rho S}$ is the diffusion flux integral given as

$$I_{\rho S} = - \int_{-\infty}^{\infty} \overline{\rho \rho'' \left(\frac{\partial u''}{\partial x} + \frac{\partial v''}{\partial y} \right)} dy - \int_{-\infty}^{\infty} \left[\overline{\rho'' u''} \frac{\partial \overline{\rho}}{\partial x} + \overline{\rho'' v''} \frac{\partial \overline{\rho}}{\partial y} \right] dy \quad (69)$$

and $I_{\rho 3}$ is the diffusion integral for higher order correlation.

$$I_{\rho 3} = \frac{d}{dx} \int_{-\infty}^{\infty} \overline{\rho'' L_{\rho J}} dy - \int_{-\infty}^{\infty} \left[L_{\rho u} \frac{\partial \overline{\rho''}}{\partial x} + L_{\rho v} \frac{\partial \overline{\rho''}}{\partial y} \right] dy \quad (70)$$

We observe that there are terms given above that require closure assumptions. Hence we make the following assumptions. The turbulent density strain rate is given as

$$\overline{\rho'' \left(\frac{\partial u''}{\partial x} + \frac{\partial v''}{\partial y} \right)} = \frac{\epsilon_{\rho}}{\lambda} (\overline{\rho'' u''} + \overline{\rho'' v''}) \quad (71)$$

where ϵ_{ρ} is a constant and λ is the Taylor's microscale characteristic of this problem to be defined later.

We further use a simplified gradient formulation to model terms like $L_{\phi\psi}$. Thus

$$-L_{\rho u} = \epsilon_{\rho} \frac{\partial \rho''}{\partial x} \quad (72)$$

$$-L_{\rho v} = \epsilon_{\rho} \frac{\partial \rho''}{\partial y}$$

and

$$\overline{\left(\frac{\partial \rho''}{\partial x}\right)^2} - \overline{\left(\frac{\partial \rho''}{\partial y}\right)^2} = S_{\rho} \frac{\overline{\rho''^2}}{\lambda^2} \quad (73)$$

The integrals I_{ρ_5} and I_{ρ_3} in equations (53) and (54) then become

$$I_{\rho_5} = - \int_{-\infty}^{\infty} \overline{\rho'' u''} \left[\frac{\partial \bar{\rho}}{\partial x} + \frac{\bar{\rho} \epsilon_{\rho}}{\lambda} \right] dy \quad (74)$$

$$- \int_{-\infty}^{\infty} \overline{\rho'' v''} \left[\frac{\partial \bar{\rho}}{\partial y} + \frac{\bar{\rho} \epsilon_{\rho}}{\lambda} \right] dy$$

and

$$I_{\rho_3} = - S_{\rho_1} \frac{d}{dx} \int_{-\infty}^{\infty} \epsilon_{\rho} \frac{d}{dx} \overline{\rho''^2} dy + S_{\rho} \int_{-\infty}^{\infty} \epsilon_{\rho} \frac{\overline{\rho''^2}}{\lambda^2} dy \quad (75)$$

where S_{ρ} and S_{ρ_1} are constants that have to be adjusted with the help of experimental data and ϵ_{ρ} is the eddy mass diffusivity.

2.6.2 Specie Fluctuation Integral Equation

$$\frac{1}{2} \frac{d}{dx} \int_{-\infty}^{\infty} \overline{\rho \bar{u} \gamma_k''^2} dy = I_{c_k} - I_{F_k} - I_{k_3} + I_{p_k} + I_{D_k}, \quad k=1, \dots, v \quad (76)$$

where I_{c_k} is the convective flux integral given as

$$I_{c_k} = \frac{1}{2} \int_{-\infty}^{\infty} \overline{\gamma_k''^2} \left[\frac{\partial \bar{\rho}}{\partial x} \bar{\sigma} + \frac{\partial \bar{\rho}}{\partial y} \bar{\nu} \right] dy \quad (77)$$

I_{F_k} is the diffusion flux integral due to mean concentration gradient.

$$I_{F_k} = \int_{-\infty}^{\infty} \left[\left\{ \overline{\rho u'' Y_k''} + \bar{u} \overline{\rho'' Y_k''} + \overline{Y_k'' L_{\rho u}} \right\} \frac{\partial \bar{Y}_k}{\partial x} \right. \\ \left. + \left\{ \overline{\rho v'' Y_k''} + \overline{Y_k'' L_{\rho v}} \right\} \frac{\partial \bar{Y}_k}{\partial y} \right] dy \quad (78)$$

I_{k_3} is the turbulent diffusion of species and is given by

$$I_{k_3} = \frac{d}{dx} \int_{-\infty}^{\infty} \left[\overline{\rho Y_k'' L_{u Y_k}} + \bar{u} \overline{Y_k'' L_{\rho Y_k}} \right] dy \\ - \int_{-\infty}^{\infty} \left[\overline{\rho \left\{ L_{u Y_k} \frac{\partial Y_k''}{\partial x} + L_{v Y_k} \frac{\partial Y_k''}{\partial y} \right\}} + \bar{u} \overline{L_{\rho Y_k} \frac{\partial Y_k''}{\partial x}} \right] dy \quad (79)$$

I_{ρ_k} is the production integral for the k-th species due to chemical reaction

$$I_{\rho_k} = \int_{-\infty}^{\infty} \overline{Y_k'' r_k^{\circ''}} dy \quad (80)$$

where $r_k^{\circ''}$ is the turbulent production rate of the k-th specie due to finite-rate kinetics and is obtained from the total species production rate. I_{D_k} is the diffusion flux integral due to species diffusivity.

$$I_{D_k} = \int_{-\infty}^{\infty} \overline{\rho \bar{D}_k Y_k'' \nabla^2 Y_k''} dy \quad (81)$$

Here, \bar{D}_k is the mean molecular diffusivity of the k-th specie and is defined later. We neglect any fluctuations in \bar{D}_k at present.

To model the unknown correlations we follow similar approximation steps. For example,

$$\overline{Y_k'' L_{\rho u}} = - \epsilon_{\rho} \overline{Y_k'' \frac{\partial \rho''}{\partial x}} = - \epsilon_{\rho} \epsilon_{\rho} \frac{\overline{\rho'' Y_k''}}{\lambda}$$

$$\overline{Y_k'' L_{\rho v}} = \overline{Y_k'' L_{\rho u}} \quad (82)$$

$$\overline{Y_k'' L_{u Y_k}} = - \frac{\overline{D}_k}{2} \frac{\partial}{\partial x} \overline{Y_k''^2}$$

$$\overline{Y_k'' L_{v Y_k}} = - \frac{\overline{D}_k}{2} \frac{\partial}{\partial y} \overline{Y_k''^2}$$

and

$$L_{u Y_k} \frac{\partial Y_k''}{\partial x} = - \overline{D}_k \left(\frac{\partial Y_k''}{\partial x} \right)^2 = - \overline{D}_k \frac{Y_k''^2}{\lambda^2} \quad (83)$$

$$L_{v Y_k} \frac{\partial Y_k''}{\partial y} = - \overline{D}_k \left(\frac{\partial Y_k''}{\partial y} \right)^2 = - \overline{D}_k \frac{Y_k''^2}{\lambda^2}$$

On replacing these approximations in the integrals in Equations (61), (62), (63) and (64) we get

$$I_{F_k} = \int_{-\infty}^{\infty} \left[\left\{ \overline{\rho} \overline{u'' Y_k''} + (\overline{u} - \epsilon_{\rho} \frac{\epsilon_{\rho}}{\lambda}) \overline{\rho'' Y_k''} \right\} \frac{\partial \overline{Y}_k}{\partial x} + \left\{ \overline{v'' Y_k''} - \epsilon_{\rho} \frac{\epsilon_{\rho}}{\lambda} \overline{\rho'' Y_k''} \right\} \frac{\partial \overline{Y}_k}{\partial y} \right] dy \quad (84)$$

$$I_{k_3} = - \frac{1}{2} \frac{d}{dx} \int_{-\infty}^{\infty} \overline{\rho} \overline{D}_k \frac{d}{dx} \overline{Y_k''^2} dy + S_k \int_{-\infty}^{\infty} \left[\overline{\rho} \overline{D}_k \frac{Y_k''^2}{\lambda^2} - (\overline{Y_k''^2})^{1/2} \overline{\rho'' Y_k''} \left(\frac{\overline{u}}{\lambda} + \frac{\partial \overline{u}}{\partial x} \right) \right] dy \quad (85)$$

and

$$I_{D_k} = C_{D_k} \int_{-\infty}^{\infty} \overline{\rho} \overline{D}_k \frac{Y_k''^2}{\lambda^2} dy \quad (86)$$

where S_k and C_{D_k} are constants that are adjusted with available experimental data.

2.6.3 Turbulent Kinetic Energy Integral Equation

$$\frac{1}{2} \frac{d}{dx} \int_{-\infty}^{\infty} \bar{\rho} \bar{u} \overline{q''^2} dy = I_{RS}^T - I_{RS}^{TC} + I_p^T - I_\phi^T \quad (87)$$

where $\frac{1}{2} \overline{q''^2} = \frac{1}{2} (\overline{u''^2} + \overline{v''^2})$ is the turbulent kinetic energy and I_{RS}^T is the Reynold stress integral associated with the fine-scale turbulence interaction with mean flow and is given in Equation (33).

I_{RS}^{TC} is the Reynold stress production integral associated with the interaction of fine scale turbulence with itself and is given as

$$\begin{aligned} I_{RS}^{TC} = & \int_{-\infty}^{\infty} \bar{\rho} \left[-L_{uu} \frac{\partial u''}{\partial x} - L_{uv} \left(\frac{\partial u''}{\partial y} + \frac{\partial v''}{\partial x} \right) - L_{vv} \frac{\partial v''}{\partial y} \right] dy \\ & + \int_{-\infty}^{\infty} \bar{u} \left[-L_{\rho u} \frac{\partial u''}{\partial x} - L_{\rho v} \frac{\partial v''}{\partial y} \right] dy \\ & + \int_{-\infty}^{\infty} \left[-M_{\rho uu} \frac{\partial u''}{\partial x} - M_{\rho uv} \left(\frac{\partial u''}{\partial y} + \frac{\partial v''}{\partial x} \right) - M_{\rho vv} \frac{\partial v''}{\partial y} \right] dy \end{aligned} \quad (88)$$

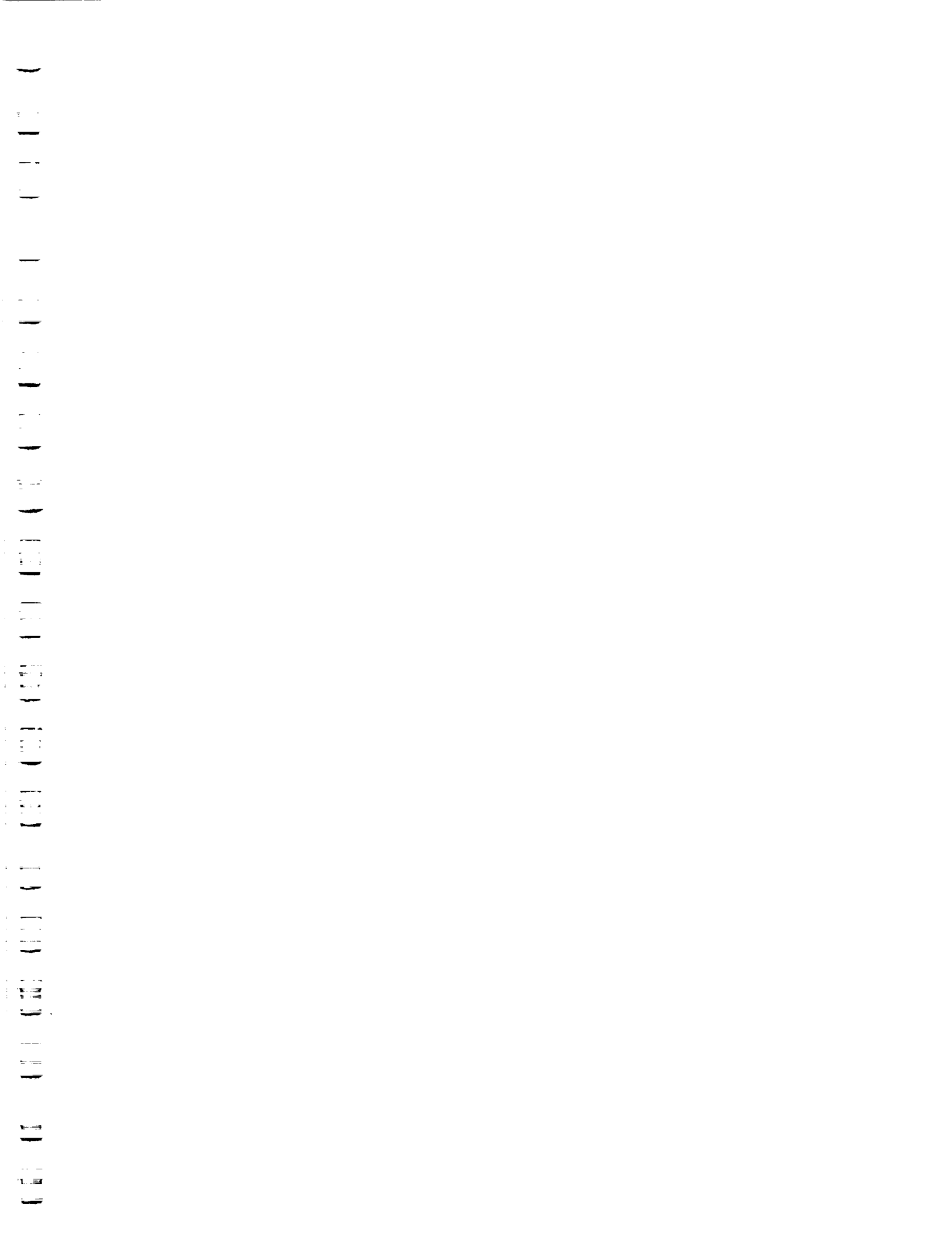
where

$$M_{\phi\psi\theta} = \overline{\phi''\psi''\theta''} - \langle \phi''\psi''\theta'' \rangle \quad (89)$$

On neglecting fourth order terms at present and following the previous closure approximation we get

$$\begin{aligned} I_{RS}^{TC} = & 2 \int_{-\infty}^{\infty} -\bar{\rho} \epsilon \left[\overline{\left(\frac{\partial u''}{\partial x} \right)^2} + \overline{\left(\frac{\partial u''}{\partial y} + \frac{\partial v''}{\partial x} \right)^2} + \overline{\left(\frac{\partial v''}{\partial y} \right)^2} \right] dy \\ & + k_3^* \int_{-\infty}^{\infty} \bar{u} \epsilon_\rho \left[\overline{\left(\frac{\partial \rho''}{\partial x} \frac{\partial u''}{\partial x} \right)} + k_4^* \overline{\frac{\partial \rho''}{\partial y} \frac{\partial v''}{\partial y}} \right] dy \end{aligned} \quad (90)$$

where k_3^* and k_4^* are adjustable constants.



The terms appearing in (90) measure the effect of viscous decay on the second order correlations. We follow here Varma et. al. [44] approach which is an anisotropic dissipation model and is shown to have correct expression in the limits of small and large Reynolds number. In general we write

$$\delta^{ij} \overline{(u''_{k,i} u''_{l,j})} = \delta_{kl} \frac{\overline{q''^2}}{3\lambda^2} + \frac{a}{\Lambda^2} (\overline{u''_k u''_l} - \delta_{kl} \frac{\overline{q''^2}}{3}) \quad (91)$$

where λ is the Taylors microscale length and is related to the macro-scale Λ by the Rotta's form

$$\lambda^2 = \frac{\Lambda^2}{a + \frac{b(\overline{q''^2})^{1/2} \Lambda}{\nu}} \quad (92)$$

where

$$\Lambda \approx 0.5 \delta \text{ and } \nu = \bar{\mu} / \bar{\rho}$$

The study of incompressible boundary layer led to values of constants a and b as $a = 3.25$ and $b = 0.125$. However, for compressible flows they may have to be readjusted [44].

The dissipation correlations involving scalar fluctuations are modeled in the following form

$$\delta^{ij} \overline{u''_{k,i} \rho''_{,j}} = S_{\rho_2} \frac{\overline{u''_k \rho''}}{\lambda^2} \quad (93)$$

where

$$S_{\rho_2} \approx 1.0.$$

I_p^T is the pressure work integral due to fine scale turbulence and can be split into two parts.

$$I_p^T = I_{p_1}^T + I_{p_2}^T \quad (94)$$

where $I_{p_1}^T$ is the pressure work due to expansion and is given as

$$I_{p_1}^T = -c_1 \frac{d}{dx} \int_{-\infty}^{\infty} \overline{p''u''} dy \quad (95)$$

and $I_{p_2}^T$ is the pressure-strain rate

$$I_{p_2}^T = c_1 \int_{-\infty}^{\infty} \overline{p'' \left(\frac{\partial u''}{\partial x} + \frac{\partial v''}{\partial y} \right)} dy \quad (96)$$

To determine these terms we follow Varma et. al [44] approach to model the pressure diffusion term as follows

$$\overline{p''u''} = \bar{\rho} \Lambda \frac{\partial \overline{u''^2}}{\partial x} \left[p_2 (\overline{q''^2})^{1/2} + p_1 \Lambda \frac{\partial \bar{u}}{\partial x} \right] \quad (97)$$

where p_1 and p_2 are constants. We take $p_2 = 0.1$ and p_1 which is associated with the mean strain, needs to be adjusted with available data. The pressure-strain rate is given by the form developed by Launder et. al. [45] which includes the tendency towards isotropy terms.

$$\begin{aligned} \frac{p''}{\bar{\rho}} \left(\frac{\partial u_i''}{\partial x_j} + \frac{\partial u_j''}{\partial x_i} \right) = & C_1^* \beta^* \omega \left[\tau_{ij} + \delta_{ij} \frac{2}{3} \overline{q''^2} \right] \\ & - \hat{\alpha} \left[P_{ij} - \frac{2}{3} \delta_{ij} P \right] \\ & - \hat{\beta} \left[D_{ij} - \frac{2}{3} \delta_{ij} P \right] \\ & - \hat{\gamma} [S_{ij}] \overline{q''^2} \end{aligned} \quad (98)$$

where the first-term is proportional to the anisotropy of the turbulence. The other terms are due to the interaction between turbulence and mean flow and is given by production terms

depends upon the size of eddy we apply the knowledge from simple spectral analysis to find the variation of dissipation rate in the shear layer. We shall return to the determination of ϵ later on.

Finally, I_{ϕ}^T is the turbulent viscous dissipation integral due to fine scale turbulence. We model this term in a form similar to the viscous dissipation due to organized structure motion. It is then given as

$$I_{\phi}^T = \frac{1}{Re_d} \int_{-\infty}^{\infty} \bar{\mu} \left[\frac{4}{3} \left\{ \left(\frac{\partial u''}{\partial x} \right)^2 + \left(\frac{\partial v''}{\partial y} \right)^2 - \frac{\partial u''}{\partial x} \frac{\partial v''}{\partial y} \right\} + \left(\frac{\partial u''}{\partial y} + \frac{\partial v''}{\partial x} \right)^2 \right] dy \quad (105)$$

where $\bar{\mu}$ is the mean molecular viscosity and we neglect any fluctuation in transport properties. I_{ϕ}^T generates mean flow thermal energy at the expense of fine-scale turbulent kinetic energy.

Since the energy conservation requires balance of the kinetic energy in the three modes of motion, Mankbadi and Liu [48] determined equations where the stress term I_{RS}^{cT} in equation (58) appeared with an opposite sign in equation (87). Since at present, equation (87) does not contain any term defining the interaction between the turbulent and disturbance field, to the first approximation we replace $I_{RS}^{TC} = -I_{RS}^{cT}$ in equation (87).

2.6.2 Total Enthalpy Fluctuation Integral Equation

$$\frac{1}{2} \frac{d}{dx} \int_{-\infty}^{\infty} \bar{\rho} \bar{u} \overline{H''^2} dy = -I_{H_C} + I_{H_{C_x}} - I_{H_3} - I_{H_{\phi}} \quad (106)$$

where I_{H_C} is the convective flux integral due to mean strain rate and is given by

$$I_{H_C} = \frac{1}{2} \int_{-\infty}^{\infty} \overline{H''^2} \left[\frac{\partial \bar{\rho} \bar{u}}{\partial x} + \frac{\partial \bar{\rho} \bar{v}}{\partial y} \right] dy \quad (107)$$

I_{H_C} is the diffusive flux integral due to mean total enthalpy gradients.

$$I_{H_C} = - \int_{-\infty}^{\infty} \left[\bar{\rho} \overline{u''H''} + \bar{u} \overline{\rho''H''} + \overline{H''L_{\rho u}} \right] \frac{\partial \bar{H}}{\partial x} dy$$

$$- \int_{-\infty}^{\infty} \left[\bar{\rho} \overline{v''H''} + \overline{H''L_{\rho v}} \right] \frac{\partial \bar{H}}{\partial y} dy \quad (108)$$

and I_{H_3} is the turbulent enthalpy diffusion integral

$$I_{H_3} = \frac{d}{dx} \int_{-\infty}^{\infty} \bar{\rho} \overline{H''L_{uH}} dy + \int_{-\infty}^{\infty} \left[\bar{u} \overline{H'' \frac{\partial L_{\rho H}}{\partial x}} + \overline{H''L_{\rho H}} \frac{\partial \bar{u}}{\partial x} \right] dy \quad (109)$$

I_{H_ϕ} is the dissipation integral which we neglect at present.

Following the same closure approximations we get the following integrals

$$I_{H_C} = - \int_{-\infty}^{\infty} \left[\bar{\rho} \overline{u''H''} + (\bar{u} - S_{H_1} \frac{\epsilon_\rho}{\lambda}) \overline{\rho''H''} \right] \frac{\partial \bar{H}}{\partial x} dy$$

$$- \int_{-\infty}^{\infty} \left[\bar{\rho} \overline{v''H''} - S_{H_1} \frac{\epsilon_\rho}{\lambda} \overline{\rho''H''} \right] \frac{\partial \bar{H}}{\partial y} dy \quad (110)$$

and

$$I_{H_3} = - \frac{1}{2} \frac{d}{dx} \int_{-\infty}^{\infty} \bar{\rho} \epsilon_H \frac{d}{dx} \overline{H''^2} dy - S_{H_2} \int_{-\infty}^{\infty} (\overline{H''^2})^{1/2}$$

$$\cdot \overline{\rho''H''} \left\{ \frac{\bar{u}}{\lambda} + \frac{\partial \bar{u}}{\partial x} \right\} dy \quad (111)$$

where S_{H_1} and S_{H_2} are constants.

Here, ϵ_H is the turbulent total enthalpy diffusivity and is defined by the relation

$$\epsilon_H = C_H k^3 / \epsilon_H = C_H^* (\overline{q''^2})^3 / \epsilon_H$$

where C_H is a constant and ϵ_H is the dissipation rate for total enthalpy fluctuation correlation $\overline{H''^2}$.

It should be noted here that the closure form used here in terms of $\overline{H''^2}$ contains implicitly the combined effect of turbulent kinetic energy, the turbulent thermal energy and the turbulent chemical energy. Therefore, the turbulent total enthalpy diffusivity ϵ_H can be used instead of D_K in the equation for $\overline{Y_k''^2}$. Since, momentum dissipation ϵ and enthalpy dissipation ϵ_H are very important in the turbulent field development, we determine them by using a simplified spectral analysis using the multiple scale approach of Hanjalic et al [49]. The underlying physical mechanism of energy transfer in turbulent flows is complicated further due to the presence of finite rate kinetics and therefore a multiple scale process of energy transfer seem more appropriate for the present problem.

2.6.5 Basis for Spectral Analysis

It is well known that turbulent energy transport occurs due to the motion of turbulent eddies in the flow. Besides kinetic energy of the motion, thermal energy and chemical energy due to reactions is also being transported when different species mix and react at the molecular level within these eddies.

The complex interaction of the turbulence and chemical reaction leads to growth and decay of turbulent eddies in a manner significantly different from non reactive flows. Previous analysis of energy cascade

phenomena in turbulent flows assumes that energy is extracted from the mean flow and transferred in proportion, from the largest eddies to the smallest eddies where it is dissipated. Recent developments bring to light the complex nature of energy exchange even in homogeneous flows and it seems that the concept of one-sided energy cascade has to be reexamined [50]. Typically, in some experiments extended areas of 'negative' turbulent production has been revealed [51]. This is very pertinent to reactive flows where due to reactions, energy is absorbed and released in a manner that could possibly enhance the reverse cascade phenomena.

The fine grained turbulence derives energy from the mean and organized motion and dissipates some of it but returns some of the energy to support the generation of the larger structures. The turbulent kinetic energy is contained mainly in the larger eddies and only a small amount resides in the smaller eddies where viscous dissipation is important. On the other hand, for chemical reactions the species must first mix at the molecular level which is more likely to occur in smaller eddies. Therefore spectral variation of turbulent total enthalpy fluctuation, $\overline{H''^2}$, may be different from the variation of kinetic energy, $\overline{q''^2}$. However, at present we disregard this difference for the sake of simplicity.

In the determination of the dissipation rates ϵ and ϵ_H , we therefore assume that there are two distinct ranges of wave numbers. There exists a range of smaller wave numbers (large eddies) in which viscous dissipation is negligible. In the other end of the wave number spectrum there is a range of large wave number (small eddies) in which viscous dissipation is important. Between these two is the inertial subrange

which contains most of the turbulent kinetic energy $\overline{q''^2}$ and turbulent total enthalpy $\overline{H''^2}$.

In the past, investigators studied turbulent energy transfer by approximating Reynold stresses in terms of turbulent kinetic energy, k and viscous dissipation $\epsilon = \nu \overline{\left(\frac{\partial u_i''}{\partial x_k}\right)^2}$ such that the characteristic time scale for the turbulent field was (k/ϵ) . However, it is generally recognized that turbulent interaction time scales vary in different parts of the energy spectrum and single scale model accounts for only the energy containing large eddies. Based on physical arguments and simple closure model Hanjalic et al. [49] developed a multiple-scale model which showed striking improvement in the level of agreement with experiment over that obtained with single scale models [49]. Essentially, they partition the turbulent kinetic energy spectrum $E(\kappa)$ between the production region ($\kappa < \kappa_1$) and transfer region ($\kappa_1 < \kappa < \kappa_2$) with negligible energy in the viscous dissipation region ($\kappa > \kappa_2$) such that the total turbulent kinetic energy is given by Figure 40.

$$k = \frac{1}{2} (\overline{u''^2} + \overline{v''^2}) = \int_0^{\kappa_1} E(\kappa) d\kappa + \int_{\kappa_1}^{\infty} E(\kappa) d\kappa = k_p + k_T \quad (113)$$

where κ_1 is the wave number at which partitioning takes place.

Energy is transported from the production (low wave number) region at a rate ϵ_p and enters the dissipation region (high wave number) at a rate ϵ . The energy transfer rate in the transition region is ϵ_s [49]. In terms of the energy spectrum these dissipation terms may be written as

$$\epsilon = 2\nu \int_0^{\infty} \kappa^2 E(\kappa) d\kappa \quad (114)$$

and

$$\epsilon_p + \epsilon_s = \int_0^{k_1} D(\kappa) d\kappa + \int_{k_1}^{\infty} D(\kappa) d\kappa \quad (115)$$

where $D(\kappa)$ would then represent the partitioned energy spectrum in terms of k_p and k_T . Balance equations were modeled for the kinetic energy and dissipation rates in the production and transition regions and for spectral equilibrium in very small eddies, the rate ϵ becomes identically equal to ϵ_s . The various improvements possible with such a multiple scale modeling was discussed in reference [49], and specially for reactive flows this model's ability to account for different time scales of interaction seems promising. Beside characteristic time scales of kinetic energy transfer, in chemically reacting flows, the model must also allow for the characteristic time scale of chemical production rate. In the present formulation, this is attempted by considering a turbulent total enthalpy fluctuation spectrum $N(\kappa)$ such that

$$\begin{aligned} \overline{H''^2} &= \int_0^{\infty} N(\kappa) d\kappa = \int_0^{k_1} N(\kappa) d\kappa + \int_{k_1}^{\infty} N(\kappa) d\kappa \\ &= (\overline{H''^2})_p + (\overline{H''^2})_s. \end{aligned} \quad (116)$$

This spectrum is also partitioned in a manner similar to the kinetic energy spectrum (Figure 40). The spectral transfer rate of enthalpy is then ϵ_{H_p} in the production region, ϵ_{H_s} in the transition region and ϵ_H in the dissipation region. Balance equations are then written for these rates along with the equations for energy dissipation rates. The basic modeling formulation follows Hanjalic et.al.[49] and the effect of the density fluctuation is modeled in a very simple manner. Since the present formulation is basically an integral one, the differential balance equations are integrated across the shear layer which results in the following integral equations.

a) Dissipation in the Production zone:

$$\frac{d}{dx} \int_{-\infty}^{\infty} \bar{\rho} \bar{u} \epsilon_p dy = I_{p}^P - I_{D}^P + I_{Di}^P + I_{G}^P \quad (117)$$

and

$$\frac{d}{dx} \int_{-\infty}^{\infty} \bar{\rho} \bar{u} \epsilon_{H_p} dy = I_{H_p}^P - I_{H_D}^P + I_{H_Di}^P + I_{G_H}^P \quad (118)$$

where I_{p}^P and $I_{H_p}^P$ are the production integrals for the turbulent kinetic energy and turbulent total enthalpy respectively and are given as:

$$I_{p}^P = C_{p_1} \int_{-\infty}^{\infty} \frac{\epsilon_p}{(q''^2)_p} \{ \bar{\rho} \overline{u_i'' u_j''} + \bar{u}_i \overline{\rho'' u_j''} + \bar{u}_j \overline{\rho'' u_i''} \} \frac{\partial \bar{u}_i}{\partial x_j} dy \quad (119)$$

$$I_{H_p}^P = C_{H_1} \int_{-\infty}^{\infty} \frac{\epsilon_{H_p}}{(H''^2)_p} \{ \bar{\rho} \overline{H''^2} + 2 \bar{H} \overline{\rho'' H''} \} \frac{\partial \bar{u}_i}{\partial x_i} dy$$

I_{D}^P and $I_{H_D}^P$ are the decay integrals for ϵ_p and ϵ_{H_p} respectively. They are given by

$$I_{D}^P = C_{p_2} \int_{-\infty}^{\infty} \bar{\rho} \frac{\epsilon_p^2}{(q''^2)_p} dy \quad (120)$$

and

$$I_{H_D}^P = C_{H_2} \int_{-\infty}^{\infty} \bar{\rho} \frac{\epsilon_{H_p}^2}{(H''^2)_p} dy$$

I_{Di}^P and $I_{H_Di}^P$ are diffusion integrals and are written as

$$I_{Di}^P = C_{\epsilon_p} \frac{d}{dx} \int_{-\infty}^{\infty} \bar{\rho} \frac{(\overline{q''^2})_p}{\epsilon_p} \left[\overline{u''^2} \frac{\partial \epsilon_p}{\partial x} + \overline{u''v''} \frac{\partial \epsilon_p}{\partial y} \right] dy \quad (121)$$

and

$$I_{Di}^P = C_{\epsilon_{H_p}} \frac{d}{dx} \int_{-\infty}^{\infty} \bar{\rho} \frac{(\overline{H''^2})_p}{\epsilon_{H_p}} \left[\overline{u''^2} \frac{\partial \epsilon_{H_p}}{\partial x} + \overline{u''v''} \frac{\partial \epsilon_{H_p}}{\partial y} \right] dy$$

Here, C_{p_1} , C_{p_2} , C_{H_1} , C_{H_2} , C_{ϵ_p} and $C_{\epsilon_{H_p}}$ are constants defined later.

I_G^P and $I_{G_H}^P$ are the generation terms due to mean vorticity.

$$I_G^P = \alpha_q \int_{-\infty}^{\infty} (\overline{q''^2})_p \frac{\partial \bar{u}_\ell}{\partial x_m} \frac{\partial \bar{u}_\ell}{\partial x_j} \epsilon_{\ell mk} \epsilon_{ijk} \rho dy \quad (122)$$

and

$$I_{G_H}^P = \alpha_H \int_{-\infty}^{\infty} (\overline{H''^2})_p \frac{\partial \bar{u}_\ell}{\partial x_m} \frac{\partial \bar{u}_i}{\partial x_j} \epsilon_{\ell mk} \epsilon_{ijk} \rho dy$$

where $\epsilon_{\ell mk}$ is the alternating third order tensor and $\alpha_q = \alpha_H = 0.1$.

This term vanishes for an irrotational flow and was found necessary to include for rotational flows [49].

b) Dissipation in the Transition zone:

$$\frac{d}{dx} \int_{-\infty}^{\infty} \bar{\rho} \bar{u} \epsilon_s dy = I_p^S - I_D^S + I_{Di}^S \quad (123)$$

and

$$\frac{d}{dx} \int_{-\infty}^{\infty} \bar{\rho} \bar{u} \epsilon_{H_s} dy = I_{H_p}^S - I_{H_D}^S - I_{H_{Di}}^S \quad (124)$$

here I_p^S and $I_{H_p}^S$ are the production integrals for the dissipation rates ϵ_s and ϵ_{H_s} in the subrange. They are

$$I_{p}^S = C_{S1} \int_{-\infty}^{\infty} \bar{\rho} \frac{\epsilon_p \epsilon_s}{(q''^2)_s} dy$$

and

$$I_{H_p}^S = C_{H3} \int_{-\infty}^{\infty} \bar{\rho} \frac{\epsilon_{H_p} \epsilon_{H_s}}{(H''^2)_s} dy$$

(125)

I_D^S and $I_{H_D}^S$ are the decay integrals and are given as

$$I_D^S = C_{S2} \int_{-\infty}^{\infty} \bar{\rho} \frac{\epsilon_s^2}{(q''^2)_s} dy$$

(126)

$$I_{H_D}^S = C_{H4} \int_{-\infty}^{\infty} \bar{\rho} \frac{\epsilon_{H_s}^2}{(H''^2)_s} dy$$

And finally, I_{Di}^S and $I_{H_{Di}}^S$ are the diffusion flux integrals in the subrange.

$$I_{Di}^S = C_{\epsilon_p} \frac{d}{dx} \int_{-\infty}^{\infty} \bar{\rho} \frac{(q''^2)_p}{\epsilon_p} \left[\overline{u''^2} \frac{\partial \epsilon_s}{\partial x} + \overline{u''v''} \frac{\partial \epsilon_s}{\partial y} \right] dy$$

and

$$I_{H_{Di}}^S = C_{\epsilon_{H_p}} \frac{d}{dx} \int_{-\infty}^{\infty} \bar{\rho} \frac{(H''^2)_p}{\epsilon_{H_p}} \left[\overline{u''^2} \frac{\partial \epsilon_{H_s}}{\partial x} + \overline{u''v''} \frac{\partial \epsilon_{H_s}}{\partial y} \right] dy$$

(127)

The constants appearing in Equations (117) to (127) are defined, at present, using the data available from Hanjalic et. al. [49]. They are given as

$$\begin{aligned}
C_{p_1} &= C_{H_1} = 2.2 \\
C_{p_2} &= 1.8 - 0.3 \frac{(X_q - 1)}{(X_q + 1)} \\
C_{s_1} &= 1.08 \psi_q \\
C_{s_2} &= C_{H_4} = 1.15 \\
C_{H_2} &= 1.8 - 0.3 \frac{(X_H - 1)}{(X_H + 1)} \\
C_{H_3} &= 1.08 \psi_H
\end{aligned}
\tag{128}$$

where

$$X_q = \frac{\overline{(q''^2)}_p}{\overline{(q''^2)}_s}
\tag{129}$$

$$X_H = \frac{\overline{(H''^2)}_p}{\overline{(H''^2)}_s}$$

and

$$\begin{aligned}
\psi_q &= \frac{\epsilon_p}{\epsilon_s} \\
\psi_H &= \frac{\epsilon_{H_p}}{\epsilon_{H_s}}
\end{aligned}
\tag{130}$$

The X_q and X_H are partition coefficients which define the amount of turbulent kinetic energy and turbulent total enthalpy present in the production zone and transition zone. Since we assumed negligible energy in the dissipation zone ($\kappa > \kappa_2$) we may thus write in terms of $\overline{q''^2}$ and $\overline{H''^2}$

$$(\overline{q''^2})_p = \left(\frac{\chi_q}{1+\chi_q}\right) \overline{q''^2}$$

$$(\overline{q''^2})_s = \left(\frac{1}{1+\chi_q}\right) \overline{q''^2}$$

and

$$(\overline{H''^2})_p = \left(\frac{\chi_H}{1+\chi_H}\right) \overline{H''^2}$$

$$(\overline{H''^2})_s = \left(\frac{1}{1+\chi_H}\right) \overline{H''^2}$$

(131)

The coefficients χ_q and χ_H are given inputs to the problem whereas ψ_q and ψ_H are obtained as a part of the solution.

Here χ_q and χ_H characterizes the shape of energy and total enthalpy spectrums respectively and ψ_q and ψ_H gives their degrees of spectral imbalance.

The solution to the above integrals requires appropriate choices of shape functions. However, once the shape functions are defined, we can solve the complete interaction problem. Although the dissipation rates in the dissipation zone, ϵ and ϵ_H , are different from the rates in the production and transition zones, at present, we assume spectral equilibrium between the transition and dissipation zones and take

$$\epsilon \equiv \epsilon_s$$

$$\epsilon_H \equiv \epsilon_{H_s}$$

(132)

With the assumption we can then determine the eddy diffivities ϵ and ϵ_H defined in equations (104) and (112).

The solution of equations (117), (118), (123) and (124) along with the mean motion equations and turbulent fluctuation equations gives the

complete interaction problem. The problem will be completely defined once we can specify the shape functions for the unknown variables. Here we are guided by available experimental data wherever possible. However, there is a lack of well defined experiments specifically for reactive flows and so the choice of shape functions here have to be modified depending upon the results of numerical experiments.

2.6.6 Shape Functions for Fine-Scale Turbulence

The governing integral equations (67), (76), (87) and (106) for the turbulent correlations are solved by assuming appropriate shape functions for the correlations. Though it would be more accurate to use strip-wise shape functions, i.e., to do a strip-wise integration, at present, to keep the problem tractable and consistent with the mean flow formulation a single shape function is assumed for the whole shear layer. Furthermore, since we are assuming that all fluctuation correlations vanish as $\eta \rightarrow \pm \infty$, we take the following shape functions

$$\begin{aligned} \frac{\overline{\rho''^2}}{\bar{\rho}} &= A_\rho \sigma(x) e^{-\eta^2} ; \quad A_\rho = 1.0 \\ \overline{Y_k''^2} &= A_{Y_k} C_k(x) e^{-\eta^2} ; \quad A_{Y_k} = 1.0, k = 1 \dots v \\ \overline{H''^2} &= A_H N(x) e^{-\eta^2} \end{aligned} \tag{133}$$

and

$$\overline{q''^2} = A_q E(x) e^{-\eta^2}$$

Thus $\sigma(x)$, $C_k(x)$, $N(x)$ and $E(x)$ are the amplitude functions which are the basic unknowns of the problem. $\sigma(x)$ is the centerline magnitude of the density fluctuation $\overline{\rho''^2}$ and similarly $C_k(x)$ are the centerline magnitude of the species mass fraction $\overline{Y_k''^2}$, $N(x)$ is the total turbulent

enthalpy density across the shear layer normalized by

$$N(x) = \int_{-\infty}^{\infty} \overline{H''^2} d\eta \quad (134)$$

so that $A_H = 1/\sqrt{\pi}$

Similarly, $E(x)$ is defined as the turbulent kinetic energy per unit length across the shear layer and is normalized as follows

$$E(x) = \frac{1}{2} \int_{-\infty}^{\infty} \overline{q''^2} d\eta \quad (135)$$

so that $A_q = 2/\sqrt{\pi}$.

We use experimental data to approximate velocity fluctuation correlations [52] such that

$$\frac{-\overline{u''v''}}{\frac{1}{2} \overline{q''^2}} = a_1, \quad a_1 = 0.3 \quad (136)$$

and

$$\frac{\overline{v''^2}}{\overline{u''v''}} = c, \quad c = 2.0$$

The shape functions for the dissipation rates are given by

$$\epsilon_i = A_{\epsilon_i} D_i(x) e^{-\eta^2} \quad (137)$$

where $i = 1, 4$ denotes p, s, H_p and H_s respectively. Again we use shape functions similar to the ones used for other unknown quantities. If we identify ϵ_i as the dissipation rate per unit length across the shear layer we can normalize equation (137) to get $A_{\epsilon_i} = 1/\sqrt{\pi}$

The interaction problem then is basically completed by the definition of the various shape functions and its use in the governing integral equations. The reactive flow can then be solved by numerically integrating

the mean motion equations and the turbulent correlation equations simultaneously along with the eigenvalue solution. The various constants that appear in the equations have to be adjusted to get the best fit with experimental data.

The above closure method requires determination of the cross correlations of turbulent fluctuation. From existing data, for example, [6, 53] we see that one form of correlating data is to use correlation coefficients. This if ϕ'' and ψ'' are two turbulent fluctuations we define correlation coefficient $r_{\phi\psi}$ as

$$r_{\phi\psi} = \frac{\overline{\phi''\psi''}}{(\overline{\phi''^2} \overline{\psi''^2})^{1/2}} = r_{\phi\psi}(x, \eta); -1 \leq r_{\phi\psi} \leq 1 \quad (138)$$

Experiments indicate that $r_{\phi\psi}$ is well defined in a shear layer and some guidance is available from available data [6, 46]. Furthermore, except for the near wake area, where the interaction is highly nonlinear, we may consider nearly self similar profiles for $r_{\phi\psi}$ across the shear layer. Therefore, to the first approximation we consider $r_{\phi\psi} = r_{\phi\psi}(\eta)$ specified as a known input to the problem. With the specification of $r_{\phi\psi}$ we then can determine all cross correlations of the form $\overline{\phi''\psi''}$ in terms of known variables $\overline{\phi''^2}$ and $\overline{\psi''^2}$. Numerical experiments with reacting flows [6] indicate that as the flow proceeds far downstream the mean flow approaches self similarity and the correlation coefficients, $r_{\phi\psi}$ tend to either +1 or -1. For self similar conditions, therefore, $r_{\phi\psi}$ can be taken to be a given input to the problem. For turbulent fluctuation correlations of $O(3)$ we follow gradient formulation similar to Varma, et. al. [44] to achieve closure. All higher order terms are at present neglected for simplicity.

2.7 Reaction Model

The reaction model used in this analysis is the quasi-global two-reaction, four-specie model due to Rogers and Chinitz [54]. This model is simple enough to handle numerically and has been shown to have reasonable agreement with experimental data. At present, this model is sufficient to show the effect of finite-rate kinetics on multi-component flow. The reactions are given by



where k_{f_i} and k_{b_i} are the forward and backward rate constants and are given in reference [54] and will not be repeated here.

The instantaneous volume rate of production of each specie is then determined from the reaction model (139) and are given in their non-dimensional form as

$$\begin{aligned} r_{\text{O}_2}^{\circ} &= x_{\text{O}_2} \rho^2 [B k_{b_1} Y_{\text{OH}}^2 - A k_{f_1} Y_{\text{H}_2} Y_{\text{O}_2}] \\ r_{\text{H}_2\text{O}}^{\circ} &= x_{\text{H}_2\text{O}} \rho^2 [C \rho k_{f_2} Y_{\text{OH}}^2 Y_{\text{H}_2} - D k_{b_2} Y_{\text{H}_2\text{O}}^2] \\ r_{\text{H}_2}^{\circ} &= E r_{\text{O}_2}^{\circ} - \frac{1}{2} F r_{\text{H}_2\text{O}}^{\circ} \\ r_{\text{OH}}^{\circ} &= -2 G r_{\text{O}_2}^{\circ} - H r_{\text{H}_2\text{O}}^{\circ} \end{aligned} \tag{140}$$

where

$$X_{O_2} = \frac{\rho_\infty L M_{O_2}}{u_\infty Y_{O_2e}} \quad \text{and} \quad X_{H_2O} = 2 \frac{\rho_\infty L M_{H_2O}}{u_\infty Y_{H_2Oe}} \quad (141)$$

and

$$\begin{aligned} A &= \frac{Y_{H_2e} Y_{O_2e}}{M_{H_2} M_{O_2}} & B &= \frac{Y_{OH_e}^2}{M_{OH}^2} \\ C &= \frac{Y_{H_2e}^2 Y_{H_2e}}{M_{OH}^2 M_{H_2}} & D &= \frac{Y_{H_2Oe}^2}{M_{H_2O}^2} \\ E &= \frac{M_{H_2} Y_{O_2e}}{M_{O_2} Y_{H_2e}} & F &= \frac{M_{H_2} Y_{H_2Oe}}{M_{H_2O} Y_{H_2e}} \\ G &= \frac{M_{OH} Y_{O_2e}}{M_{O_2} Y_{OH_e}} & H &= \frac{M_{OH} Y_{H_2Oe}}{M_{H_2O} Y_{OH_e}} \end{aligned} \quad (142)$$

On time averaging equation (140) we get the mean rate of production of the i -th species, $\overline{r_i^\circ}$ appearing in equation (17). Following the filtering procedure we can separate out the contribution $r_i^{\circ'}$ and $r_i^{\circ''}$ corresponding to the organized structure motion and fine scale turbulent motion respectively.

To the first approximation, any fluctuation in k_{f_i} and k_{b_i} due to the coherent structure and turbulence fluctuations can be neglected. However, when turbulence is included, the rate constants based on mean temperature $k(\overline{T})$ has been shown to be significantly in error when compared to the actual mean rate constant $\overline{k(\overline{T})}$ [6]. The time averaged rate constants \overline{k}_{f_i} and \overline{k}_{b_i} can be determined by using a probability density distribution approach first suggested by Chinitz [55].

In essence, a probability distribution function $P(\theta; x, y)$ is considered at any given point (x, y) to define the temperature between θ and $\theta + d\theta$ so that

$$\overline{k_{f_1}} = \int_0^1 k_{f_1}(\theta) P(\theta) d\theta \quad (143)$$

$$\text{where } \theta = \frac{T - T_{\min}}{T_{\max} - T_{\min}} ; 0 \leq \theta \leq 1 \quad (144)$$

To solve (143) $P(\theta)$ must be prescribed a priori. Chinitz [55] used a clipped Gaussian distribution for $P(\theta)$. In free shear flows, such a distribution seems reasonable [56] and therefore was used here also. Here, T_{\max} is the maximum temperature attainable in the reaction model and T_{\min} is the temperature in the shear layer for no reactions. A clipped Gaussian distribution for $P(\theta)$ can be written as

$$P(\theta) = \psi_1 \delta(0) + \psi_2 \delta(1) + (H(1) - H(0)) \frac{1}{\sigma\sqrt{\pi}} \exp\left[-\frac{(\theta-\mu)^2}{2\sigma^2}\right] \quad (145)$$

where $(H(1) - H(0))$ is the Heavyside function given as unity in the range $0 \leq \theta \leq 1$ and zero elsewhere. Furthermore,

$$\psi_1 = \frac{1}{2} \operatorname{erfc}\left[\frac{\mu}{(2\sigma^2)^{1/2}}\right] \quad (146)$$

$$\psi_2 = \frac{1}{2} \operatorname{erfc}\left[\frac{1-\mu}{(2\sigma^2)^{1/2}}\right]$$

Using equation (145) in the definition of $\bar{\theta}$ and $\overline{\theta^2}$ we get [56]

$$\bar{\theta} = \psi_2 + \mu(1 - \psi_1 - \psi_2) + \left(\frac{\sigma^2}{2\pi}\right)^{1/2} \left[\exp\left(\frac{-\mu^2}{2\sigma^2}\right) - \exp\left(\frac{-[1-\mu]^2}{2\sigma^2}\right)\right] \quad (147)$$

and

$$\begin{aligned} \overline{\theta^2} = \overline{\theta'^2} + \overline{\theta''^2} = \psi_2 + (\mu^2 + \sigma^2)(1 - \psi_1 - \psi_2) + \left(\frac{\sigma^2}{2\pi}\right)^{1/2} \exp\left(\frac{-\mu^2}{2\sigma^2}\right) \\ - (1 + \mu)\left(\frac{\sigma^2}{2\pi}\right)^{1/2} \exp\left[-\frac{(1 - \mu)^2}{2\sigma^2}\right] - \overline{\theta}^2 \end{aligned} \quad (148)$$

$\overline{\theta}$ and $\overline{\theta^2}$ ($= \overline{\theta'^2} + \overline{\theta''^2}$) are related to \overline{T} and $(\overline{T'^2} + \overline{T''^2})$ and equations (147) and (148) can be inverted to obtain μ and σ^2 which can be used in equation (145) and hence finally determine $\overline{k_{f_i}}$ by equation (143).

Solution of equation (24) gives $\overline{T}(x, \eta)$ in the shear layer. $\overline{T'^2}$ ($= 2|A|^2|\overline{T}|^2$) can be obtained from the eigenvalue problem (55) and $\overline{T''^2}$ can be related to $\overline{H''^2}$ such that

$$\begin{aligned} \overline{T''^2} = \frac{1}{M^2} [\overline{H''^2} - \overline{u}^2 \overline{u''^2} - \sum_k (m_k D_k \overline{T} + \epsilon_{k_f})^2 \overline{Y_k''^2} \\ - 2\overline{u} \{ \sum_k (m_k D_k \overline{T} + \epsilon_{k_f}) \epsilon_H \frac{\partial \overline{Y}_k}{\partial x} + M \epsilon \frac{\partial \overline{T}}{\partial x} \}] \end{aligned} \quad (149)$$

where gradient closure is employed for turbulent correlations $\overline{u''Y_k''}$ and $\overline{u''T''}$ and correlations $\overline{T''Y_k''}$ and higher order correlations are neglected at present for simplicity. Since the solution of the mean flow equations is coupled to the determination of the mean reaction rate constants, iteration is required for the complete solution. However, for numerical simplicity, the mean rate constants can be determined at any given point (x_i) in terms of the values of \overline{T} and $(\overline{T'^2} + \overline{T''^2})$ from the previous stream-wise location (x_{i-1}) and the iteration procedure can be avoided at the expense of some numerical accuracy.

III. METHOD OF SOLUTION

3.1. Reactive Eigenvalue Problem

The stability equation in terms of pressure perturbation $\hat{p}(\eta)$, equation (55) must be solved subject to appropriate boundary conditions. Since detailed stability analysis of reactive wakes was not available, extensive numerical calculations were carried out to determine the eigenvalues of the problem. In essence, for a given M_∞ and frequency β and with assumed mean flow profiles, equation (49), the eigenvalue problem can be solved using Runge-Kutta integration technique. The boundary conditions used are

(i) On the wake axis ($\eta = 0$)

For Antisymmetrical Oscillations

$$\hat{p}(0) = 0 \quad (150)$$

For Symmetrical Oscillations

$$\hat{v}(0) = \hat{p}'(0) = 0 \quad (151)$$

(ii) Far from wake axis ($\eta \rightarrow \infty$)

$$\hat{p}(\eta) \rightarrow 0 \quad (152)$$

The boundary conditions are homogeneous and therefore are not sufficient to establish any solution of the governing stability equation (55) other than the trivial solution of zero. The stability problem must therefore be formulated as an eigenvalue problem, i.e., non-zero solutions which satisfy the boundary conditions exist only for certain combinations of the complex wave number α and complex phase velocity, c . Since the frequency $\beta = \alpha c$ is constraint to be real, then for fixed β , we need only determine α_R and α_I (and hence c_R and c_I) to obtain the required eigensolutions.

It can be seen that an important analytical feature of

equation (55) is the existence of a singularity at the point $\bar{u} = c$ (critical point). Though \bar{u} is real, the singularity lies on the real axis in the complex-plane only for a neutral disturbance. However, for amplified and damped disturbances ($c_I \gtrless 0$), the singularity lies in the complex η -plane and numerical integration along the real axis is not possible [60].

Essentially, integration begins at large value of η ($\approx \eta_\delta$) and proceeds along an indented contour around the critical point in the complex η -plane. The eigenvalues (α_R, α_I) are obtained by a linear search procedure to satisfy the boundary conditions. The method of solution is basically the approach of Mack [60, 61]. The equations are separated into real and imaginary parts and solved simultaneously. Once the eigenvalues are determined all the eigenfunctions $\hat{u}, \hat{v}, \hat{\rho}, \hat{T}$ and \hat{Y}_k can be calculated using the linear equations (see Appendix A). For neutral eigenvalues, i.e., $c_I = 0$, a linear search is carried out in c_R and α_R because $\alpha_I = 0$ for the spatially developing disturbance studied here.

3.2. Interaction Between Coherent Structure and Mean Motion in Reactive Flow

When all turbulent correlations are neglected in the governing mean flow equations, the integral equations show the balance between the mean motion and coherent structure motion. The integrals appearing in the equations can be calculated in terms of the eigenfunctions (Section 3.1) by Simpson's Rule. To avoid integration to large values of η , η_δ is taken to be ≈ 5.0 , since for $\eta > 5$ the mean flow approaches free stream and the integrals in the range $\eta_\delta < \eta < \infty$ can be shown to be a function of the value of

eigenfunction at $\eta = \eta_\delta$. The governing equations for the mean flow variables V_c , T_c and Y_{k_c} and coherent structure amplitude $|A|^2$ can be written in a general functional form as

$$\frac{d\phi_i}{dx} = f_i(\phi_i; Re, M_\infty, \beta, C_D) \quad , \quad i=1,7 \quad (153)$$

where ϕ_i denotes the unknown variables of the flow, i.e., $V_c, T_c; Y_{k_c}$ ($k=1, \dots, 4$) and $|A|^2$. These equations can then be solved in the streamwise direction from some initial conditions at, say, $x = x_0$ such that $V_c(x_0) = V_{c_0}$, $T_c(x_0) = T_{c_0}$, $Y_{k_c}(x_0) = Y_{k_{c_0}}$ and $|A|^2(x_0) = |A|_0^2$. Since the eigenvalue problem is a function of ϕ_i , at each streamwise location the eigenfunctions and the integrals are evaluated to proceed with the solution of equation (153). The various integrals appearing in the equations are given in Appendix B.

3.3. Fine-Scale Turbulence in Reacting Flow

The integral equations for turbulent-correlations, equations (67), (76), (87), and (106), can also be written in a similar form to equation (153) and solved subject to proper choice of initial conditions for the shape functions (133). In all, there are 11 equations that must be solved along with the mean motion equations described in Section 2.3. However, at present the turbulence model has not been included in the numerical calculation of the interaction problem because of lack of comparison with experimental data, specially for reactive wake. Instead, a numerical parametric study of the turbulent integral equations was carried out to determine the effect of the variation of the constants and correlation coefficients $R_{\phi\psi}$ appearing in the equations. For simplicity, the mean flow was assumed to be self similar in transformed coordinate η and interaction between the coherent structure and turbulence was neglected.

For self similar conditions, all cross correlation coefficients $R_{\phi\psi}$ tends to either -1 or +1 and therefore from past studies [6], $R_{\phi\psi}$ was given a constant value across the shear layer. Effect of the variation of $R_{\phi\psi}$ on the development of the turbulence field is studied parametrically. Effect of adjusting the various constants (i.e., ϵ_p , S_K , C_{D_K} , S_H) was not studied in detail due to lack of experimental data for the physical reaction model employed here. Numerical calculations were carried out using the Runge-Kutta integration technique.

IV. RESULTS AND DISCUSSION

In this chapter the results of the numerical calculations are presented and the various facets of the interaction problem are discussed. Since the basic thrust of this research has been to develop a model to study the interaction stability of a coherent structure in a supersonic reactive flow, detailed analysis of the stability of a disturbance in reactive flow has been carried out. There is a considerable lack of experimental data on the reactive wake phenomena, specially in the $H_2 - O_2$ combustion system studied here. Therefore, no direct comparison was possible for the development of a coherent structure in reactive free shear layer. However, experimental data [27,28,40] is available for nonreactive hypersonic wake of a flat plate and a comparison is possible. The reaction model is at present not of great importance to study the growth and decay of coherent structure except so far as to include finite-rate kinetics in the interaction problem. The presence of finite-rate chemistry results in large species production rates for the reaction model used [54] and therefore imposes stringent stability restrictions on the explicit numerical calculations carried out here. The step size required for stability of the numerical calculations of the reactive interaction problem is so small that detailed computations for reactive cases was computationally prohibitive and therefore only a representative set of solutions are presented. It may be possible to solve this problem by an implicit numerical technique which could result in detailed solutions within reasonable computational time. At present such a numerical solution is beyond the scope of this research and must await future study.

The turbulence model developed in this study is at present untested, and therefore its inclusion into the interaction between coherent structure

and mean motion cannot be justified. Instead, the turbulence model is parametrically studied for a simplified mean flow and with the assumption that there is no interaction between coherent structure motion and fine-scale turbulence. This enables the fine-scale turbulent motion to become uncoupled from the development of the instability wave and with proper choice for the mean flow profiles, the turbulent integral equations can be numerically solved subject to given initial conditions. The various constants and correlation coefficients $R_{\phi\psi}$ appearing in the turbulent equations have been parametrically varied to study their effect on the spatial development of fine-scale turbulence in reactive wakes. Detailed comparison with experimental data for a free shear layers undergoing $H_2 - O_2$ kinetics is again not possible due to the lack of experimental data on the turbulence field of this combustion system. The success of any turbulence model capable of handling finite-rate kinetic effects will depend upon the availability of reasonable comparison between numerical predictions and experimental data and since this is not possible at present, the turbulence model developed here is studied only as an independent problem and was not included in the interaction analysis.

The results presented here therefore falls in three distinct parts. In the first section the results of the detailed study of the stability of reactive wakes is presented. In the second section, the interaction between the coherent structure motion and the mean flow motion is numerically studied. And, finally, the numerical parametric study of the turbulence model is presented for a self similar mean flow field. Effect of varying the cross correlation coefficients is studied for both reactive and non reactive cases.

4.1. Stability of Reactive Laminar Wakes

The eigenvalue problem developed for reactive flow, equation (55), is solved subject to the boundary conditions (150), (151) and (152) and the eigenvalues $\alpha(\alpha_R, \alpha_I)$ are numerically calculated. With proper choice of the the mean flow variables (i.e., V_c , T_c and Y_{k_c}) and for a given free stream Mach number M_∞ , the stability equations can be integrated as described in Section 3.1. Solution proceeds in the complex η -plane (Figure 2) and therefore the equations and the boundary conditions must be separated in their real and imaginary parts and solved simultaneously. With a reasonably good choice of initial guess for α_R and α_I for a given real frequency β , the nonreactive case converged in 4-6 iterations. However, the corresponding reactive cases took 6-9 iterations and the computational time also increased proportionately. A convergence criteria of 10^{-8} was used for both cases.

It was seen from the computations that the eigenvalues for the reactive case depended significantly on the finite-rate kinetics used in this model and therefore it is expected that different rate kinetics mechanism would result in different eigensolutions. However, it was seen that the general trend of solution remains the same and so some generalized conclusions can be drawn from the study of this reactive stability problem. Stability calculations such as this gives some insight into the phenomenon of transition to turbulence in reactive flows which is an area of research of great interest.

Lees and Lin [43] and Lees and Gold [57] have shown for nonreactive flows, that neutral subsonic disturbances exist only when a generalized mean density-vorticity product has an extremum, and then only when the phase velocity corresponding to this location is subsonic relative to an

observer fixed in fluid. This condition is also sufficient (but not necessary) for the existence of amplified subsonic disturbances. It has been shown that the relative velocity $1 - u(x,0)$ governs the stability of the wake and so the proper coordinates for the stability problem is a system fixed "in the fluid" even though the mean flow is calculated in a coordinate system fixed in the body. A disturbance is classified "subsonic," "sonic" or "supersonic" according to whether the relative propagation velocity is less than, equal to, or greater than the ambient sound speed. The local relative Mach number of the wave front is given by [57]

$$M = \frac{M_r (w - c_R)}{\sqrt{T}} \quad (154)$$

where $M_r = M_\infty V_c$ is the relative Mach number. A subsonic disturbance must therefore satisfy the condition

$$-c_R < \frac{1}{M_r} \quad (155)$$

It was also shown for nonreactive case that a neutral subsonic disturbance exists only for certain mean velocity temperature profiles and $-c_R$ is uniquely determined by these profiles. The stability restriction results in the criteria that $-c_R$ must lie in the interval $[0,1]$ for a self-excited disturbance to exist. For subsonic disturbance it results in the requirement that [57,58]

$$0 < -c_R < \frac{1}{M_r} \quad (156)$$

It has been possible to establish some criteria for the existence of neutral subsonic disturbances [57] in compressible nonreactive wakes but it seems impossible to extend such requirements for the reactive case. For two-dimensional compressible nonreactive wakes, the condition that uniquely determines the existence of neutral disturbance is given by

$$\left(\frac{w'}{T}\right)_{c_{R_c}} = 0 \quad \text{and} \quad c_R = c_{R_c} \quad (157)$$

where prime denotes differentiation with respect to η . Using the mean flow profiles and equation (157) results in

$$T_c e^{-\eta_c^2} = \left(\frac{2\eta_c^2 - 1}{2\eta_c^2 + 1}\right) \quad (158)$$

and

$$-(c_R)_c = e^{-\eta_c^2} \quad (159)$$

where η_c is the critical point where $w = c_R$.

This indicates that for nonreactive case, the neutral solution phase velocity c_{R_c} is a function of T_c only and is independent of the relative Mach number. For these values of c_{R_c} , the neutral inviscid eigenvalues for anti-symmetric disturbance (α_c) can be determined as a function of T_c and M_r (Figures 3,4). The solution shown in Figure 4 clearly indicates that whereas for no reactions in the flow, the criteria equation (157) is always satisfied, for finite-rate kinetics however, the neutral phase velocity, $-c_{R_c}$, is no longer a function of T_c only but instead depends on both T_c and M_r . This interesting deviation from the inviscid stability criteria, equation (157), indicates that the requirement given by equation (157) is necessary but not sufficient to theoretically define stability bounds for reactive wakes. At present, an extension of the nonreactive stability criteria to handle reactive stability seem very difficult and has not been attempted.

In Figure 3 results of the neutral eigenvalue solutions for nonreactive flow is presented. For increasing temperature excess T_c , $-c_R$ increases towards zero, i.e., the phase velocity approaches free-stream

velocity. The critical point η_c where $w = c_{Rc}$ increases with T_c . Excellent agreement with the Lees and Gold [57] solution is also obtained (Figure 3). The eigenvalue α_c decreases and almost becomes constant with increase in T_c for the case of $M_r^2 \approx 0$. The dependence of the phase velocity on T_c and M_r is shown in Figure 4 where it can be seen that the reactive case deviates significantly from the nonreactive case. Clearly, the numerical solution shows that a minimum value for $-c_{Rc}$ for each value of T_c is obtained as a function of M_r ($= M_\infty V_c$). In all the neutral eigenvalues calculations a value of $V_c = 0.4$ was maintained at all times. It is also noted from Figure 4 that the $-c_{Rc}$ bottoms out much more sharply for lower T_c . The actual phase velocity, in the coordinates fixed with the body is given by $C_R = 1 + V_c c_{Rc}$ and therefore depends implicitly on the velocity defect in the wake axis. In Figure 5 the solutions for the neutral eigenvalues α_c as a function of M_r and T_c is presented. For fixed value of T_c the wave number α_c decreases with increasing M_r as predicted by Lin [59] and computed by Lees and Gold [57]. Again excellent agreement with the solutions of reference [57] is obtained for the nonreactive case. For reactive case, α_c varies with M_r^2 in a similar manner as the nonreactive case. However, the wave numbers are much larger and the range of relative Mach number over which the neutral (and adjacent amplified) disturbances can exist also increases. This kind of increase is also noted with the increase in temperature excess T_c .

Since we are interested in spatially developing waves, a comparison of the variation of frequency β with relative Mach number M_r is presented in Figure 6. For fixed T_c , β decreases with M_r for both reactive and nonreactive cases. The frequency at which neutral disturbance can exist

increases with increase in T_c and is also greater for the reactive case. The leveling of frequency β for $T_c = 4.0$ during reactions is due to the variation of $-c_R$ observed in Figure 4.

The boundary conditions, equations (150)-(152) allow for both symmetrical and antisymmetrical disturbances in the wake and therefore numerical solutions were obtained for both the disturbances. It has been determined that antisymmetrical disturbances are more unstable in laminar wake transition [29] and similar trend is also observed during the present computation. Figures (7) to (10) give the eigenvalues computed for symmetrical disturbances and Figures (11) to (14) give the corresponding antisymmetrical disturbance solutions. The complex phase velocity $C(C_R, C_I)$ shown in these figures is the velocity with reference to the coordinate system fixed to the body and is defined as $C = 1 + V_c Re c$ where $c (c_R, c_I)$ is the relative phase velocity defined in the local coordinate system (equation (55)).

In general, the reference conditions used for the present computations unless otherwise specified are

$$T_\infty = 1500^\circ K, \quad Y_{k_e} = 0.05, 0.90, 0.025, 0.025$$

$$L_\infty = 0.1m \quad M_\infty = 2.0 \quad \text{and} \quad \beta = 0.2$$

and the centerline values for the mean profile were taken to be

$$V_c = 0.4, \quad T_c = 4.0, \quad Y_{k_c} = (-0.25, -0.25, 3.0, 6.5)$$

In Figures (7) to (9) the reference values for species Y_{k_e} was taken to be (0.3, 0.65, 0.025, 0.025) which is a fuel rich mixture for this present reaction model.

In Figure 7 we see that for nonreactive flow, with $\beta \leq 0.24$ the solutions are amplified ($C_I > 0$) and with $\beta \geq 0.24$ the solutions are

damped ($C_I < 0$). At $\beta \approx 0.24$ we have a neutral eigenvalue solution. However, when the reaction is turned on, all the solutions are amplified and also the degree of amplification is much higher. The maximum amplification occurs around $\beta \approx 0.092$ for nonreactive case but is around $\beta \approx 0.081$ for the corresponding reactive case. This seems to indicate that the disturbance is more likely to become unstable for the reactive case. The phase velocity C_R monotonically increases with β for both cases. However, C_R is lower when chemical reactions are going on. This implies that for reactive flow, though the disturbance gets highly amplified it is travelling slower relative to freestream. This is consistent with experimental observation by Ganji and Sawyer [21] of organized structure motion in a propane-air combustion flow.

In Figure 8 we show the variation of the eigenvalues as a function of freestream Mach number M_∞ . A neutral eigenvalue is observed near $M_\infty = 2.375$ for nonreactive case which disappears when the reaction is turned on. We notice that for $M_\infty < 2.375$ the solutions are amplified ($C_I > 0$) and for $M_\infty > 2.375$ the solutions are damped. This is very interesting because in a very early paper concerning stability of jet flows, Pai [62] had theoretically predicted that there is a critical Mach number above which jet type flow will be stable with respect to all small symmetrical disturbances in the inviscid fluid. He further showed that for the case of no energy transfer the critical Mach number is about 2.5. Our present numerical results for symmetrical disturbances shows that the flow is stable for $M_\infty \geq 2.375$. This close agreement between earlier theory [62] and present analysis indicates the validity of the present numerical results. Another interesting observation in Figure 8 is that when the reaction is turned on there is no neutral eigensolution and the

results are completely amplified. Moreover, the reactive solutions seems to be weakly dependent on M_∞ . A possible explanation of this result is that since the release of chemical energy due to reactions is independent of Mach number, the variation of M_∞ will probably have limited effect on the eigenvalues. The phase velocity C_R is still smaller when reactions is turned on.

Figure 9 shows the variation of the eigenvalues as a function of velocity defect V_C . There is significant differences between the non-reactive and reactive cases. For nonreactive flow the rate of amplification is maximum around $V_C = 0.505$. However for reactive cases calculated here, the disturbances amplification increases continuously with increase in V_C . The phase velocity C_R is again smaller for the reactive case. The results indicate that very close to the rear edge of the flat plate where V_C is large, chemical reactions make the disturbance grow rapidly but on proceeding downstream into the wake where the interaction weakens and V_C decreases, the amplification rate decreases. The phase velocity C_R however, increases as V_C is decreased and approaches free-stream velocity far downstream into the wake.

We further note that for $V_C < 0.45$, the amplification rate is lower for reactive case as compared to reactive case. This indicates that the instability wave is not amplified for all cases considered here and that under some initial conditions reactive wave will be less amplified when compared with the nonreactive case. It was determined during the present calculations that the wave amplification is quite dependent on shape function assumed. The phase velocity, however, is always lower for reactive cases. In Figure 10 we plot the variation of the eigenvalues as a function of temperature increment T_C . Here for small value

of T_c we see that C_I is larger for nonreactive case as compared with the reactive case. The phase velocity C_R is still lower for reactive case. There is a maximum amplification occurring around $T_c = 2.4$ for nonreactive case but is no longer present for the reactive case. This figure shows that with the low value of V_c considered here, and for reactive case with 5% H_2 , the wave is amplified less as compared with nonreactive case but the amplification continuously increases with increase in T_c . With higher value of V_c the amplification again becomes higher for reactive case as compared with nonreactive case. The amplification rates show similar trends as observed experimentally by Ganji and Sawyers [21].

In Figure 11 we present representative calculations of the eigenvalues for the case of antisymmetric boundary conditions, equation (151), as a function of β . In previous wake studies it was determined that antisymmetric boundary conditions resulted in more unstable wave motion and it has also been experimentally confirmed that in wake flows the wave structure correspond more closely to the antisymmetric solution [27,28,29]. As can be seen in the figure, the amplification ($C_I > 0$) is much larger for reactive case as compared to nonreactive case. Furthermore, when compared with the symmetric solutions in Figure 7 we see that amplification is greater for the antisymmetric solution. All the eigenvalues are amplified solutions and no neutral solution exist unlike the case in Figure 7. For nonreactive case there is a maximum amplification occurring around $\beta \approx 0.17$ which is greater than $\beta = 0.092$ for the corresponding symmetrical case. The wave speed C_R is still smaller for reactive case as compared with the nonreactive case.

Figure 12 presents the eigenvalues as a function of M_∞ for

antisymmetrical disturbances. The amplification continuously decreases with increase in M_∞ for no reactions and shows a maximum for very low Mach number. For reactions the amplification shows a maximum around $M_\infty = 3.0$ and is generally much larger than the nonreactive solution. Compared with the corresponding symmetrical disturbance solutions (Figure 8), antisymmetrical disturbance is highly dependent on the freestream Mach number. Figure 8 also shows the stabilizing effect of increasing M_∞ as observed experimentally [27,40].

Figure 13 shows the eigenvalues as a function of velocity defect V_c . In general the amplification rate is higher for reactive case and the overall behavior is quite similar to the corresponding symmetrical case (Figure 9). However, no maximum is directly observed in amplification case within the range calculated except perhaps the tendency to level off near $V_c = 0.8$. Figure 14 gives the variation of the eigenvalues as a function of T_c . The trend shown here is quite different from the symmetric case. The amplification for nonreactive case decreases with increase in temperature excess as observed by Lees and Gold [57] and the wave number also decreases with T_c . For reactive case however, the amplification rate shows a distinct maximum around $T_c = 1.8$ and the wave number variation also shows a maximum. This indicates that the wavelength ($\approx 1/\alpha_R$) first decreases and then increases with increasing temperature excess. The phase velocity C_p is consistently lower for the reactive case as determined by Ganji and Sawyer [21].

Finally, Figures 15 and 16 show the characteristic variation of the pressure eigenvalue amplitude $|\hat{p}|$ and phase ϕ_p across the shear layer for symmetric and antisymmetric disturbance respectively. In

general, the amplitude is much larger for the reactive case in both figures. The phase changes across the shear layer shows significant difference between reactive and nonreactive flows.

Finally in conclusion the study of the stability of reactive wakes has shown remarkable differences with the classical nonreactive stability analysis. Though small disturbance analysis cannot deal with transition, it however has been shown [39] that linear stability theory is a useful guide to the understanding of the main parameters and phenomena governing transition. The growth and decay of amplification rates along the wake axis can be used to give a good indication of nonlinear effects present in the wake. The excellent agreement of laminar stability theory with previous studies for nonreactive cases [57] indicates the applicability of this theory to study the development of disturbances in the flow. The present calculation of the eigenvalues shows good agreement with past theoretical and experimental analysis. For reactive flows, it has been shown that the neutral phase velocity is no longer independent of relative Mach number M_r . The condition for neutral stability equation (157), is no longer sufficient for reactive flows. Furthermore for the amplified solutions calculated here, qualitative agreement has been obtained with the experimental observations of Ganji and Sawyer [21]. In essence, the reacting wakes are more unstable than nonreactive wakes. The amplification of the wave is in general higher for reactive wakes but the wave propagation velocity is consistently lower. The antisymmetric disturbance is more unstable than the symmetrical disturbance in general for both reactive and nonreactive cases which again agrees with experimentally observed data in wake flows. The calculations further show that the choice of

the mean flow velocity, temperature and mass fraction profiles governs to a great extent the spatial stability of laminar reactive and nonreactive wakes.

Since the reactive eigenvalue problem formulated in Appendix A is a very general one it was decided to do some representative calculations of reacting flow fields other than a wake. Essentially, the mean flow assumption has to be modified to account for different physical geometry. For example, a heated symmetric jet has a mean velocity flow profile that can be given in terms of similarity variable η as $\bar{u} = \text{sech}^2 \eta$ [67]. For heated jet, the temperature profile can be still taken as near Gaussian, equation (40). For symmetrical disturbances, the stability problem was solved for a characteristic frequency $\beta = 0.1$ and presented in Figures 17 and 18. Figure 17 shows the variation of the amplitudes of pressure eigenfunction $|\hat{p}|$ and vertical velocity eigenfunction $|\hat{v}|$ across the jet for reactive and non reactive conditions. Comparing with the symmetric solutions for the wake, Figure 15, we see remarkable differences that do not necessarily depend upon the differences in reference conditions alone. The vertical velocity amplitude $|\hat{v}|$ shows a maximum for non reactive case around $\eta \approx 5$. However, for reactive cases no such maximum is observed and the amplitude is lower than the non reactive case. The eigenvalues indicate that amplification is much higher for reactive case and the wavelength ($\sim 1/\alpha_R$) is lower. The corresponding phase changes of the pressure and vertical velocity eigenfunction across the jet is shown in Figure 18. The pressure phase ϕ_p , shows a single phase change at large value of η for both reactive and non reactive cases. On comparison with the corresponding wake solution, Figure 15, it can be seen that reactive wake has two phase changes. The phase changes for the vertical velocity

eigenfunction ϕ_y is also shown in Figure 18. In general, the trends in phase changes are similar for both non reactive and reactive jets. Detailed calculations of reactive jet stability has not been carried out at present. However, it has been shown that the generalized stability problem formulated here is quite versatile and is capable of handling different physical problems. Other reactive models can also be handled by proper modifications to the finite-rate kinetic terms v^* and $\bar{\beta}$ in equation (55). Reactive flow stability of other shear flows like boundary layers and jets would also be of great interest due to the existence of large scale structure in these shear flows [25]. Such stability calculations have, however, not been carried out at present and must await future study.

The study of wave development and the onset of nonlinearity leading to transition has been extensively studied and the general results show both qualitative and quantitative agreement with past experimental and theoretical data. The present study results in some basic insight into the instability wave phenomena in reacting shear layers. By modeling coherent structure as an instability wave the results of such an analysis can be used to study the effect of finite-rate kinetics on the development of organized motion in free shear layers. However, the spatial development of such instability waves is coupled to the variation of the mean flow and therefore their spatial development has to be studied simultaneously. Such an analysis is the topic of study in the next section.

4.2 Coherent Structure Interaction in Reactive Wakes

The development of the interaction between the mean flow and the coherent structure can be studied by integrating the governing equations

for given values of M_∞ , Re , C_D and β_0 . The integration proceeds downstream from an initial location $x = x_0$ with initial values V_{C_0} , T_{C_0} , $Y_{k_{C_0}}$ and $|A|_0^2$. Experimental data [27-29, 40] can be utilized to obtain initial values for the velocity defect and temperature excess for non reactive wakes. However, the initial value for the amplitude of the coherent structure has not been measured experimentally and so the value used must be such that it can simulate experimental conditions. There is also a considerable lack of experimental data on reactive wakes and so the initial values used are the same as that for non reactive wakes and a comparison of the interaction development is studied between the two cases. For non reactive flow, with uniform concentration gradients, i.e., $Y_{k_{C_0}} = 0$, $k=1,4$, the interaction problem is numerically calculated for the experimental data available [27, 40]. Using the initial conditions used by Liu and Gururaj [39] the solutions are obtained for a hypersonic wake [27]. The calculations correspond to the transition behind an adiabatic flat plate. The initial location is chosen such that it is upstream of the nonlinear region. Thus the interaction develops from the linear region into the nonlinear region. In experimental studies the transition from laminar to turbulent arises naturally from body generated noise or other forms of disturbances. In the present numerical calculations the disturbance arises due to the initial value given for the amplitude $|A|_0^2$ and its growth and decay downstream occurs due to the interaction between the mean flow and the coherent structure.

Figures 19 and 20 show, respectively, the variation of the centerline temperature excess and centerline Mach number along the wake axis. The present calculations show excellent agreement with the experimental

data of Batt and Kubota [27] and the theoretical work of Liu and Gururaj [39]. In the initial growth region the disturbance amplitude is small and both the temperature defect T_c and Mach number M_c follow essentially the linear growth and is identical to the 'laminar' case, $|A|_0^2 = 0$. However, as the interaction proceeds downstream the amplitude rapidly increases and the solution deviates from the 'laminar' solution and the temperature and velocity decay is more rapid. The solution follows very closely the experimental data [27]. The decay is more rapid for higher values of $|A|_0^2$ and it was seen that the higher value of $|A|_0^2 (= 2 \times 10^{-5})$ shows a better comparison with the experimental data [27]. Since detailed calculations of the non reactive wake has already been investigated [29, 38, 39, 63], such calculations will not be repeated here in detail. Only some representative solutions for non reactive cases will be presented here.

It was found during the preliminary calculations of the reactive wake that the reaction model used here [54] results in large production rates and therefore imposes stringent stability requirements on the integration of equation (153). In fact the complete reaction model, equation (139), results in integration step size of the order of $10^{-9} \sim 10^{-10}$ that is computationally prohibitive. In their calculations also, Rogers and Chinitz [54] also observed large instantaneous production of the hydroxyl radical thereby requiring very small integration steps. These large production rates were identified with the first reaction in equation (139) and they found typical chemical time for OH production of the order of 10^{-10} seconds [54]. They further estimated that the first reaction, i.e., $H_2 + O_2 \rightleftharpoons 2OH$, may be in chemical equilibrium during much of the time required for a typical integration step that is computationally reasonable.

Due to the limitations imposed by the available computing system, it was decided that in order to alleviate the computational problem caused by large production rates, a simplified procedure would be adopted that would allow finite-rate calculations within reasonable computational time. The present formulation already assumes premixed flow and since we are only interested in presenting a formulation that can account for coherent structure motion in reactive flow, to the first approximation, we assume that the first reaction is in equilibrium and no production of OH radical occurs. The second reaction which is essentially the production of water vapor is a much slower reaction and finite-rate calculations based on this reaction is computationally possible. Therefore, all reactive solutions presented here will assume the above mentioned simplifications. This assumption results in no production of OH radical and also no consumption of O_2 . The premixed model used here did not include N_2 as an inert specie in contrast to the model in reference [54]. By assuming equilibrium for the first reaction, the presence of oxygen essentially assumes an inert form for the second reaction since no consumption of O_2 occurs. The results presented here, therefore, account for the finite-rate production of water vapor at the expense of the hydrogen and hydroxyl radical in the premixed flow. Finite-rate calculations of the second reaction still results in step sizes of the order of $10^{-4} \sim 10^{-5}$ and therefore only representative calculations are presented due to computational system limitations.

It must be noted here that the reactive eigenvalue problem depends significantly on the variation of mean flow profiles and must be solved at each streamwise location which results in increased computational costs. For numerical efficiency it is however possible to store an

eigenvalue map, whereby the eigenvalues (α, c), the eigenfunctions (ϕ_i) and their integrals can be stored as a function of V_c, T_c and Y_{k_c} ($k=1,4$). At each streamwise location this map or table can then be referred to and the interaction integrals (Appendix B) determined by interpolation. At present such numerical optimizations has not been carried out due to storage logistics.

It was also observed during the calculations that the mean flow shape functions assumed may not necessarily be applicable to reactive flow situations. Even though the mean velocity and temperature profiles have been experimentally observed to be nearly Gaussian [65] no detailed measurements are available for the specie concentration profiles in supersonic reactive wakes. Concentration profiles in reactive jets [22] indicate that the profiles do deviate significantly from Gaussian distribution [23]. Since the integral formulation used here requires a priori assumptions of the mean flow shape functions, proper choice of the profiles is necessary for accurate solutions. Here, for numerical simplicity the mean flow shape functions for all variables were assumed to be Gaussian as defined in equation (49). This simplification allowed the reduction of all the integro-differential equations to the form in equation (153). During the course of the numerical calculations, it was determined that this simplification resulted in reactive solutions that were highly dependent on the mean flow specie mass fraction shape function assumptions. Representative mass fraction profiles are shown in Figure 21 (a-d) for a supersonic reactive wake. To see the effect of large concentration gradients near the wake centerline, the mass fraction values at $\eta=0$ were taken to be Y_{k_c} ($= -0.25, -0.25, 3.0, 6.5$). Figures 21a and b show the mean flow mass fraction profiles for hydrogen, \bar{Y}_{H_2} and

oxygen, \bar{Y}_{O_2} at various axial locations. We see that hydrogen levels are reduced as the flow progresses downstream. Similar trend is observed in Figure 21c where the hydroxyl radical mass fraction profiles are presented. The chemical reaction used here results in the depletion of H_2 and OH as the water vapor is formed. This is evident from 21d where \bar{Y}_{H_2O} profiles increase with axial distance. Comparing with the non reactive profiles also plotted in Figure 21, we see that all the non reactive profiles tend to uniform conditions with axial development. However, for reactive conditions, only \bar{Y}_{O_2} profiles still approach uniformity which is directly due to the fact that the first reaction is assumed to be in chemical equilibrium and oxygen molecules act as an inert specie for the second reaction. These figures also indicate that OH radical is consumed more rapidly than the fuel (H_2). This is again consistent with the fact that OH is a very unstable radical and at high temperatures reacts very fast to produce H_2O vapor which is more stable. The numerical computation therefore had to take into account the large rate of depletion of OH as the restricting factor leading to small integration step sizes. When all OH radical mass fraction was used up at the centerline (i.e., $Y_{OH_c} \rightarrow -1$) the numerical computations were terminated. This was necessary to avoid negative mass fractions in the flow field. This limitation of the present calculations can be related to the choice of mean flow specie shape functions and also to the fact that molecular diffusion was neglected in the original formulation. Another reason for this behavior is the basic assumption of premixed conditions which has been shown to be more complicated than non-premixed flames [68]. Furthermore, on comparing the production rates in supersonic H_2-O_2 combustion systems with other hydrocarbon combustion systems [21] it was seen that the

hydrogen-oxygen combustion rates are much higher leading to the point of view that the combustion system used here is 'kinetically' dominated.

However, all the above mentioned restrictions in this formulation can be removed by solving with more appropriate shape functions for the specie and adding diffusion terms, etc. Of course, finite difference calculations would be more accurate instead of integral considerations for reactive flow fields, but step size restrictions would be more stringent in such calculations.

Figures 22 and 23 present respectively the centerline variation of the mean flow temperature excess and velocity defect for a $M_\infty = 3$ turbulent non reacting wake experimentally studied by Demetriades [40, 64]. To account for turbulence simple eddy viscosity models in Spalding [69] (Model I) and Schetz [70] (Model II) (see Appendix C) were utilized. The results indicate that the decay in temperature and velocity is only slightly larger than the case for no turbulence. Coherent structure development as discussed above cannot account for turbulence and the results indicate that the decay observed due to the interaction between the large structure and the mean flow deviates significantly from the turbulent data of reference [40, 64]. Better comparison is observed in the earlier part of the wake where the amplitude $|A|^2$ is increasing. Further downstream, the amplitude decays and the coupling between mean flow and coherent structure motion weakens. This growth and decay behavior of the amplitude can be seen in Figure 24 which also shows the balance between the various terms appearing in the coherent structure kinetic energy conservation. Here the averaged disturbance kinetic energy density $C(x)$ is given by

$$C(x) = v^2 |A|^2 = \frac{1}{2} \int_{-\infty}^{\infty} (|\hat{u}|^2 + |\alpha \hat{v}|^2) dn \quad (160)$$

which is due to the normalizing condition used in equation (59). We further note that the development of the amplitude is essentially governed by the Reynold stress production I_{RS}^c due to the interaction between mean flow and coherent structure. All other terms contributing to the conservation mechanism in equation (58) are relatively smaller than I_{RS}^c . Very similar results were also obtained by Lin and Gururaj [39] and Ko et. al. [38]. Inclusion of turbulence into the governing equations results in lower values for the energy density $C(x)$, stress production I_{RS}^c and coherent structure dissipation I_ϕ^c . However, the mean flow dissipation I_ϕ , also shown here, is larger for the turbulent case as expected. The mean flow dissipation continuously decreases with axial development since the mean flow velocity gradient $(\frac{\partial \bar{u}}{\partial y})$ decreases. The coherent structure dissipation first increases with the increase in the amplitude $|A|^2$ and reaches a maximum value at an axial location that closely corresponds to the amplitude maximum. Further downstream as the amplitude decays the dissipation, I_ϕ^c , also decreases as was observed in other calculations [39].

The calculations for non reactive cases show only limited effects of the inclusion of the eddy viscosity model. The more complete turbulence model formulated in Chapter II was not used due to lack of time to do extensive numerical experiments. Since the present analysis is directed towards an investigation of the interaction between mean flow and coherent structure in turbulent reactive flows, the eddy viscosity model was included to account for some turbulent effects. Due to the lack of experimental data on supersonic turbulent reactive wakes, no detailed analysis was undertaken to investigate the effect of various turbulence models. However, all further results presented here for

reactive cases were calculated with inclusion of the algebraic model for eddy viscosity (Model II).

4.2.1. Effect of Initial Amplitude and Oscillation Frequency

Figures 25-28 present the results for the reactive wake for various initial values of the amplitude, $|A|_0^2$. Figure 25 gives the centerline temperature increase as a function of axial distance. Since the second reaction is exothermic, temperature is increased as water vapor is formed. We see that as the initial amplitude $|A|_0^2$ is increased, the temperature also increases. In contrast, non reactive flow temperature excess decreases with increase in initial amplitude. From the calculation it became evident that the increase in amplitude results in increased contribution from the coherent structure development to the mean flow thermal energy conservation. Essentially, the streamwise gradient of total enthalpy diffusion flux integral, $-\frac{dI_E}{dx}$ and dissipation I_ϕ^c are always positive and increases with increasing initial amplitude which directly contributes to the growth of temperature excess. In contrast, the decay of mean flow velocity defect (Figure 26) increases with increase in initial amplitude. This is due to the fact that the Reynold stress production due to coherent structure, I_{RS}^c increases with increase in initial amplitude and therefore increases the velocity defect decay (equation (36)). The mean flow dissipation, I_ϕ , (equation (46)) is not affected by changes in initial amplitude. Figures 27a and 27b give the evolution of the mean flow centerline specie mass fractions under the same conditions. Increase in initial amplitude increases the decay of hydrogen and hydroxyl centerline values (Figure 27a) and also increases the increase of water vapor (Figure 27b). However, it is clear that in this

kinetically controlled combustion studied here, the effect of changing the initial amplitude is only marginal. Essentially, this is due to the fact that the combustion results in large production rates which are almost independent of the coherent structure development. Furthermore, though the growth of the amplitude increases with increasing initial values (Figure 28), the maximum is significantly lower when compared to the non reactive case. The maximum occurs around $x/L \approx 13.2$ as compared to $x/L \approx 30$ for the non reactive case (Figure 24). One of the interesting results of such calculations is that the growth rate of coherent structure is significantly lower in reactive flow and also the maximum attained is lower. Evidently, this reaction mechanism inhibits the growth of coherent structure, a result consistent with the observation of Ganji and Sawyer [21]. Though the growth and decay behavior of the amplitude is similar in both non reactive and reactive flows, their magnitudes are quite different. This essentially seems to indicate the growth rate of coherent structure amplitude depends quite significantly on the reaction mechanism. In fact, the present calculations show that due to the large production rates associated with the reaction, the coupling between mean flow and coherent structure motion is considerably weakened and the mean flow field variation, especially the thermal and concentration fields are not significantly affected by the coherent motion. The coherent structure motion however is modified due to the presence of finite-rate kinetics. This behavior can again be identified with the dominance of the finite-rate terms appearing in the governing conservation equations.

The present calculations were also carried out to determine the effect of changing the initial peak frequency β_0 . Figure 29 shows the

effect of changing the initial spatial frequency on the growth/decay characteristics of the coherent structure amplitude. It has been observed in non reactive calculations [35] that there exists a frequency for which the local amplification ($-\alpha_1$) is a maximum. The eigenvalue stability problem solved in Section 4.1 indicates the possibility of a peak amplification for the reactive case also. Here we present the solutions calculated for various initial frequencies. As the initial frequency β_0 is increased, the amplitude of the coherent structure also increases. This is again similar to the behavior observed in nonreactive case. The solutions for $\beta_0 = 0.4$ is not shown completely except so far as to show the increase in $|A|^2$. It is evident from these solutions that as far as the interaction is concerned, $\beta_0 = 0.4$ as compared to $\beta_0 = 0.2$ and 0.3 is one for which the initial large-scale structure is most amplified and is thus expected that the large-scale structure at this frequency will be the most efficient extractor of energy from the mean flow. Detailed calculations for various other β_0 are however necessary to determine which initial frequency results in peak amplification. Such calculations have not been carried out at present. Due to the dominance of finite-rate kinetics, it is expected that in general solutions for various β_0 will give very similar results as can be seen from the variation of the mean flow centerline specie mass fraction shown in Figure 31. Therefore, at present, all other reactive solutions computed here were calculated for $\beta_0 = 0.2$ and numerical experiments for various β_0 has not been attempted.

The local eigenvalue problem, hence the local amplification rates, enters the interaction problem only through the integrals of the eigenfunctions. As far as the streamwise development is concerned, because

of the finite amplitude of the disturbance, the local eigenvalue problem essentially lose their identify. Nevertheless, the local amplification rate, $-\alpha_I$, and its streamwise development is of interest due to its effect on the behavior of the local eigenfunctions. Figure 30 shows the streamwise variation of the local wave number, α_R and the local amplification rate, $-\alpha_I$ for various initial frequency. The wave number, α_R increases with streamwise distance and also increases with increase in frequency. This indicates that the wavelength of the disturbance ($\approx 1/\alpha_R$) decreases with increase in β_0 and also decreases as the mean flow develops. A similar trend was observed for the non reactive case, also shown in Figure 30 for the case $\beta_0 = 0.3$. Such decrease in scales were also observed by Demetriades [40] for non reactive wakes. Though no experimental data is available for the reactive case, it is however expected that the trends calculated here will also be observed in future experiments. The local amplification rate, $-\alpha_I$ decreases with streamwise development. An interesting observation here is that on comparing the reactive and non reactive cases for $\beta_0 = 0.3$, the local amplification rate starts higher for reactions as was calculated in Section 4.1. However, as the mean flow develops the reactive amplification rapidly decreases to values below the corresponding non reactive case. There are two reasons for this behavior. As shown before the amplitude of the large-scale structure is significantly lower for the reactive case and also the peak value occurs around $x/L = 13.2$, whereas for the non reactive case the growth of $|A|^2$ continues till $x/L = 30$. This results in lower amplification rates as is observed in Figure 30. With increase in β_0 , the amplification rates also increase as is expected. However, the rate of decrease with streamwise development actually increases with increase

in initial frequency. An interpretation of these results is that in reactive flow, the coherent structure development is actually stabilized more rapidly. A similar trend has been observed experimentally by Ganji and Sawyer [21]. Combustion therefore seems to affect the development of coherent structure in the mean flow in a manner consistent with past experiment and theoretical studies [21 - 24]. Essentially, the large-structure is initially amplified but as the interaction between the coherent structure and the mean flow develops, the growth rate ($d|A|^2/dx$) and the local amplification rate is significantly lower as compared to non reactive case. Detailed calculations for various other combustion models are necessary before any generalized conclusion can be drawn concerning the effect of the finite-rate kinetics on the interaction between the mean flow and large-scale structure. However, it is expected that results very similar to the present calculations will be obtained for other combustion systems.

4.2.2 Effect of Intermittency and Molecular Diffusion

Even in premixed turbulent flows, experimental observations indicate that there are situations in which the instantaneous value of fuel or oxidizer concentration and, therefore, the instantaneous chemical reaction rate vanish [71]. Physically, this is caused by the random variation of local flow properties coupled to high local fluctuations of the specie concentrations, resulting in situations in which the instantaneous value of either fuel or oxidizer is zero. In such situations there is no chemical reaction despite the finite values of average concentrations. The longer such a situation prevails, the stronger is the damping effect. This phenomenon has been called 'unmixedness' or 'intermittency.' There are several definitions of intermittency [71, 72] but since we are

interested in theoretical computation of finite-rate chemistry we modify the model developed by Spiegler et. al. [70]. This model is simple enough to be incorporated into the interaction problem studied here and is described in Appendix C. It has been pointed out that the level of intermittency of a certain reactant may affect the structure and behavior of turbulent flames and is therefore a region of great interest. The model described in Appendix C was incorporated into the general computer code and some preliminary results are presented. Figure 32 shows the variation of the terms contributing to the development of coherent structure for the cases with and without intermittency. For the test conditions presented here, the effect of intermittency is to increase the growth of the amplitude. The stress production mechanism I_{RS}^C is also larger due to the intermittency effects. The coherent structure induced pressure I_p^C and dissipation I_ϕ^C are also larger with intermittency. The mean flow dissipation I_ϕ is not affected by the inclusion of intermittency. The dominant production mechanism is still associated with the Reynold shear stress integral I_{RS}^C as one expects. Both I_ϕ^C and I_p^C convert (the latter reversibly) disturbance kinetic energy into mean flow thermal energy as was observed in non reactive calculations here and elsewhere [39]. In the initial growth stage, the coherent structure development is relatively small and I_ϕ primarily determines the decay rate. However, as the mean flow spreads and the coherent structure amplitude grows I_ϕ plays a much less significant role. The shear stress production I_{RS}^C then plays a more important role in the amplitude growth rate as the shear layer develops. The effect of intermittency, however, is very marginal in the disturbance conservation mechanism essentially due to the fact that intermittency effects the rate constants k_{f_i} and k_{b_i} which

contribute mainly to the finite-rate terms. As discussed before the reaction model used here is kinetically dominated and therefore not very significant changes in the coherent structure development is expected. Figure 33 shows the effect of intermittency on the other integral terms appearing in the conservation equations. In the linear region dissipation I_ϕ primarily determines the development of dV_c/dx . However as the coherent structure grows the diffusion flux for kinetic energy, dI_{KE}/dx , increases and is responsible for the later stages of the mean flow development. Also shown in this figure is the variation of total enthalpy diffusion flux gradient, dI_E/dx . As mentioned before $-dI_E/dx > 0$, and the contribution of coherent structure motion to the thermal field development first increases and then decreases. Essentially, all coherent structure generated terms follow the growth/decay characteristics of the amplitude $|A|^2$. Other terms of interest are the specie diffusion flux integral gradient, dI_{D_k}/dx which vanishes for non reactive case (i.e., for $Y_{k,c_0} = 0$). However, for reactive conditions the variation of these terms essentially follow the rate mechanism. Note that this term appearing in the specie integral equation (13) as $-dI_{D_k}/dx$. We see that as hydrogen and hydroxyl is consumed, $+dI_{D_{H_2}}/dx$ and $+dI_{D_{OH}}/dx$ first increase with increase in $|A|^2$ and then decreases with decay in amplitude. $dI_{D_{H_2O}}/dx$ on the other hand, first decreases and then increases with $|A|^2$. Effect of intermittency is to increase the values of all dI_{D_k}/dx terms. Essentially, these coherent structure induced diffusion flux gradients terms show contributions that increase the reduction of H_2 and OH mass fraction while increasing the H_2O mass fractions. The magnitude of $dI_{D_{H_2}}/dx$ is

much lower than the values of $dI_{D_{OH}}/dx$ and $dI_{D_{H_2O}}/dx$, again consistent with the low values of Y_{H_2C} .

The intermittency terms used to correct the forward and backward rates, k_{f2} and k_{b2} are shown in Figure 34 at various streamwise locations. We see that the intermittency factor for forward rate, U_{2f} is much larger than the backward rate factor, U_{2b} . Furthermore, the magnitude of both the factors increases with increase in streamwise development of the reactive wake. The effect of intermittency on the coherent structure development is marginal as can be seen by comparing the solutions for $|A|^2 = 0$ and 4×10^{-5} . Intermittency is reduced a little when coherent structure development is included. The variation of the intermittency factor across the shear layer shows that there is peak occurring around $\eta \approx 6.5$ at $x = 9.2$ but the peak moves into the outer edges of the shear layer and is around $\eta \approx 8$ at $x = 14.2$. This is an interesting observation because it is in the outer edge of the shear layer where flow is intermittently turbulent and plays a significant role in the phenomenon of flame extinction. As the mean flow develops the intermittency factor becomes quite large with a peak $U_{2f} \approx 0.9$ at $x = 14.2$. This indicates that for the intermittency model used here there is a possibility of extinction at the outer edges of the shear layer as the flow develops. However, this does not effect the finite-rate production rate to a large extent due to the fact that most of the contribution comes from the rate kinetics near the centerline, $\eta < 2$, where as can be seen there is no intermittency. The validity of the model used here (see Appendix C) cannot be confirmed at present due to lack of detailed measurements of intermittency behavior in reactive wakes. The model however, shows good

promise in identifying the physical mechanism involved in intermittence or unmixedness in turbulent flames with finite-rate chemistry.

Since the contribution of the Reynold shear stress production I_{RS}^c was seen to be the dominant reason for the growth/decay characteristics of the coherent structure amplitude, the various terms contributing to I_{RS}^c (see Appendix B) are shown in Figure 35. As expected, the production $I_{RS_1}^c$, associated with the dominant mean flow shear $\partial\bar{u}/\partial y$ contributes the most. Similar results were also obtained for non reactive case. $I_{RS_2}^c$, $I_{RS_3}^c$ and $I_{RS_5}^c$ are much smaller than $I_{RS_1}^c$ and $I_{RS_4}^c$. The term $I_{RS_2}^c$, which is part of the mean flow convection effect, transfers energy from the coherent structure to the mean flow ($I_{RS_2}^c < 0$) in the initial part of the development ($x/L < 11$) but reverses the energy transfer in the later part of the coherent structure development. The terms $I_{RS_3}^c$ and $I_{RS_5}^c$ also transfers energy to the mean flow at the expense of coherent structure development. However, the net effect is still positive and therefore is conducive to the growth of coherent structure. It must be noted that the production terms $I_{RS_1}^c$, $I_{RS_3}^c$ and $I_{RS_5}^c$ have their counterpart in the low speed wakes studied by Sato and Kuriki [29] while $I_{RS_2}^c$ and $I_{RS_4}^c$ are directly due to compressibility effects present in the high speed wake studied here.

It was considered during the course of the calculations that perhaps the absence of molecular diffusion terms in the governing equations may be the main reason for the kinetic controlled combustion restrictions observed and discussed above. Therefore, a simplified form of molecular diffusion term (see Appendix C) was included in equations (8) and (13). Figures 36 and 37 present the mean flow centerline variation of the

temperature excess and velocity defect for the various conditions studied here. The effect of including diffusion is to markedly reduce the temperature increase. However, the velocity decay was not significantly effected by either diffusion or intermittency. The reduction in temperature excess due to diffusion effects is basically because of the lowered rate of change of the specie mass fraction which is shown in Figures 38a and b. The effect of intermittency is still almost insignificant. The inclusion of molecular diffusion was carried out only in the later part of this research and due to lack of time no detailed calculations were carried out. One major conclusion of this theoretical analysis is that the molecular diffusion term must be included for finite-rate calculations.

Finally, since the results indicate that the growth rate of the coherent structure amplitude during reactions is much lower than the non reactive case, Figure 39 presents the ratio of growth rates for the two cases. As expected this ratio is less than one and the growth rate ratio decreases with streamwise development. This is similar to the results in reference [21]. The increase in frequency reduced the ratio even further. This is attributed to the much larger growth rate for the non reactive case as compared to the reactive case.

In conclusion, the interaction between the mean flow and coherent structure has been theoretically investigated for a supersonic non reactive and reactive wake. The non reactive solutions show excellent agreement with the past calculations [38, 39, 63]. For the reactive case, due to lack of experimental data no direct comparison was possible. However, the general trends of the interaction was quite similar to the non reactive case, except so far as to the reduced magnitude for the

coherent structure amplitudes. The effect of different initial amplitude, $|A|_0^2$ and frequency, β_0 on reactive solution has been computed. Turbulence was modeled in a very simple manner and included in all the reactive analysis. Intermittency and molecular diffusion effects were also included in some of the calculations. In general, the reactive solutions show qualitative agreement with experimental observation [21].

4.3 Fine-Scale Turbulence in Self Similar Mean Flow

The turbulence model formulated in Section 4.2 was solved with the assumed shape functions, equation (133) for a self similar mean flow to determine the general trends. No detailed calculations are presented for this model due to lack of data necessary to evaluate the various constants appearing in the equations. The turbulence model utilizes a spectral partition of turbulent kinetic energy, $\frac{1}{2} \overline{q''^2}$ and turbulent total enthalpy, $\overline{H''^2}$ following the approach of Hanjalic et. al. [49] and is shown in Figure 40. In all there are 11 equations that must be solved simultaneously with appropriate initial conditions. The results presented have not been checked and their validity still remains to be seen. However, preliminary calculations indicate general trends similar to the variation observed in far field turbulence decay. This model was essentially formulated to account for the interaction between the mean flow, coherent structure and fine-scale turbulence in reactive flows and as such, an attempt was made to include some physical mechanism that is not present in classical turbulence modeling. Also, gradient approximation was avoided except in third order correlations due to the established fact that in reactive flows gradient approximation has limited validity [3, 4]. Of course, all turbulence modeling such this one have some adjustable constants which have not been determined due to lack of

detailed experimental data for wakes. This model also incorporates a clipped Gaussian probability density distribution, $P(\theta)$ in terms of the normalized temperature θ [55] to evaluate the effect of temperature fluctuations on the mean rates of production of the specie.

Figure 41a and b show, respectively, the temperature profiles and probability distribution used. The shape function for temperature, equation (49) was used to determine θ and the mean square fluctuations, $\overline{\theta^2}$ was determined by using a simple gradient approximation [55]. Figure 42 gives the variation with temperature of the ratio of the mean rate of production of hydrogen, $\overline{r_{H_2}^0(T)}$ to the rate of production of hydrogen based on mean temperature, $r_{H_2}^0(\bar{T})$. The results show that with increase in temperature this ratio becomes very large indicating that the inclusion of temperature fluctuation increases the production rates. This result is very similar to the one obtained in reference [6] and is consistent with past studies. Similar variation was observed for other specie too. The effect of changing the shape of $P(\theta)$ (i.e., ν, σ^2) is also quite significant.

Finally, Figures 43 and 44 give the streamwise variation of the centerline values of turbulent kinetic energy, $E(x)$, turbulent total enthalpy, $N(x)$ and mass density fluctuation, $\sigma(x)$. Only non reactive cases are presented here. The reference conditions used were:

$$M_\infty = 2.0, T_\infty = 1500^\circ\text{K}, L = 2.54\text{cm}, C_D = 0.01, Re_L = 2 \times 10^6,$$

$$Y_{k_\infty} = 0.05, 0.90, 0.025, 0.025, x_0 = x_0^*/L = 1000.$$

The initial conditions at $x_0 = 1000$ were taken at present as follows:

$$\sigma(x_0) = E(x_0) = N(x_0) = C_k(x_0) = 10^{-4}$$

$$D_p(x_0) = D_{H_p}(x_0) = D_s(x_0) = D_{H_s}(x_0) = 10^{-2}$$

All constants were taken to be equal to unity except for ϵ_ρ and

$$S_H = S_{H_1} = 0.1, \quad k_3^* = 0.01, \quad \text{and} \quad k_4^* = S_{\rho_1} = 0$$

Figure 43 shows the variation of $E(x)/E(x_0)$ and $N(x)/N(x_0)$ for different values of correlation coefficient $r_{\phi\psi}$ and Figure 44 shows the effect of changing ϵ_ρ (equation (71)). All solutions show decay characteristics as expected. The correlation coefficients $r_{\phi\psi}$ are not constant across a developing turbulent shear layer except perhaps far downstream [6] and detailed numerical experiments are necessary to determine the effect of their variation.

V. CONCLUDING REMARKS

A theoretical analysis of the interaction between the mean flow and large-scale structure has been presented for a supersonic reactive wake. For numerical simplicity, von Karman integral considerations were used for the present solutions. The integral shape assumptions were shown to be quite accurate in determining the non reactive mean flow development. For reactive cases, the species shape function assumptions were found to be quite restrictive. However, better choice of shape functions would depend on the availability of experimental data for the H_2-O_2 supersonic combustion system studied here. Furthermore, due to the single frequency model and other assumptions, point-by-point analysis of the interaction may not be very significant. The salient physical mechanism responsible for the development of the nonlinear transition region in compressible reactive wake has been studied for various initial conditions and the results are consistent with some experimental observations in other combustion studies. Improvements in the modeling of large-scale structure must await more refined experimental studies under well controlled conditions, especially for reactive conditions.

Integral considerations were found to be quite restrictive on the shape assumptions for species but were used here for numerical simplicity. Finite difference calculations are, of course, possible except for the increase in computational costs. Since all flow fields are three dimensional, the interaction of a three dimensional coherent structure must be included for better understanding of the developing interaction. Furthermore, the effect of the subharmonics must also be included in future studies due to the observed phenomenon of pairing and breakup of large structure. Linear stability analysis of the reactive eigenvalue problem

can be extended to include both three dimensional effects and subharmonics but must await further guidance of more detailed experimental studies.

The turbulence model developed here can be included into the general interaction problem without too many complications. However, it must first undergo detailed numerical testing for various combustion flow, which is again restricted due to lack of available data.

The results presented here is the first theoretical attempt to include finite-rate kinetic effects in the study of the stability and interaction of coherent structure in free shear layers. The inclusion of coherent structure motion in reactive flows is very important due to the established existence of large-scale structures in all kinds of shear layer and theoretical studies must therefore account for such interaction phenomenon.

APPENDIX A
THE EIGENVALUE PROBLEM FOR REACTIVE FLOWS

In this Appendix, the generalized eigenvalue problem for a two-dimensional reactive flow is formulated. The linearized form of the dimensionless equations for coherent structure motion is transformed using local coordinate transformation (equation (52)) and reduced to the stability equations by the application of the assumed shape function, equation (53). For constant transport properties the general viscous stability equations are

$$\begin{aligned} i[(w-c)\bar{\rho} + \bar{\rho}\hat{u}] + (\bar{\rho}\hat{v})' &= 0 \\ i\alpha(w-c)\hat{Y}_k + \bar{\rho}\bar{Y}_k' \alpha \hat{v} &= \gamma_k^* + d_k \quad k=1, \dots, v \\ \bar{\rho}(w-c)\hat{u} + C_1^* \hat{p} - i\bar{\rho}^2 w' \hat{v} &= V_u \\ i\alpha^2(w-c)\hat{v} + C_1^* \hat{p}' &= V_v \end{aligned} \quad (A1)$$

$$\begin{aligned} i\bar{\rho}(w-c)[(1+V_c w)V_c \hat{u} + \sum_{k=1}^v (m_k D_k \bar{T} + \epsilon_{k_f}) \hat{Y}_k \\ + M \hat{T}] + i(1+V_c c)C_1^* V_c \hat{p} + \bar{\rho}^2 \bar{H}' \hat{v} &= E_d \end{aligned}$$

$$\hat{p} = \sum_{k=1}^v C_k^* [\bar{\rho} \bar{T} \hat{Y}_k + \bar{\rho} \bar{Y}_k \hat{T} + \bar{T} \bar{Y}_k \hat{p}]$$

where

$$-w = \frac{(1-\bar{u})}{V_c} \quad \text{and} \quad -c = \frac{(1-c^*)}{V_c} \quad (A2)$$

c^* is the complex phase velocity with respect to the observer. The viscous contributions appearing on the right hand side of equations (A1) are given by the species diffusion,

$$\begin{aligned} d_k = \frac{\bar{D}_k}{V_c} [\bar{\rho}^2 \hat{Y}_k'' + 2\bar{\rho}\bar{\rho}' \hat{Y}_k' - \alpha^2 \hat{Y}_k + \bar{\rho}\bar{Y}_k' \hat{p}' \\ + (\bar{\rho}\bar{Y}_k'' + \bar{\rho}'\bar{Y}_k') \hat{v}] \quad k=1, \dots, v \end{aligned} \quad (A3)$$

the viscous dissipations,

$$V_u = -i \frac{\bar{\mu}}{\alpha \text{Re} V_c} \left[i \frac{\alpha^2}{3} \bar{\rho} \hat{v}' + \bar{\rho}^2 \hat{u}'' - \frac{4}{3} \alpha^2 \hat{u} \right] \quad (\text{A4})$$

$$V_v = \frac{\bar{\mu}}{\alpha \text{Re} V_c} \left[i \frac{\alpha}{3} \hat{v}' + \frac{4}{3} \bar{\rho}^2 \alpha \hat{v}'' - \alpha^3 \hat{v} \right]$$

and the energy dissipation

$$E_d = \frac{\bar{\mu}}{\alpha \text{Re}} \left[i \alpha^2 \bar{\rho} \left(\frac{\bar{u}}{3} \hat{v}' + 2\bar{u}' \hat{v} \right) + \bar{\rho}^2 \bar{u} \hat{u}'' \right. \\ \left. + \bar{\rho} (2\bar{\rho} \bar{u}' + \bar{\rho}' \bar{u}) \hat{u}' + (\bar{\rho}^2 \bar{u}'' + \bar{\rho} \bar{\rho}' \bar{u}' - \frac{4}{3} \bar{u} \alpha^2) \hat{u} \right. \\ \left. + \bar{\kappa} C_T^* [\bar{\rho}^2 \hat{T}'' - \alpha^2 \hat{T}] \right] \quad (\text{A5})$$

$$+ \frac{\bar{\rho}^3}{\alpha V_c} \frac{\bar{D}_k}{\alpha V_c} \sum_k m_k D_k (\bar{T} \hat{Y}_k'' + \bar{T}' \hat{Y}_k')$$

$$+ \frac{\bar{\rho}^2}{\alpha V_c} \frac{\bar{D}_k}{\alpha V_c} \sum_k \{ m_k D_k \bar{Y}_k' (\bar{\rho} \hat{T} + \bar{T} \hat{\rho}) \}'$$

where \bar{D}_k , $\bar{\mu}$, $\bar{\kappa}$ are the mean molecular diffusivity, molecular viscosity and thermal conductivity and are assumed known at present. Here prime denotes differentiation with respect to η . Furthermore,

$$C_1^* = \frac{C_1}{V_c^2} \quad \text{and} \quad C_T^* = 1/(\gamma - 1) M_e^2 \text{Re}_L \text{Pr} \quad (\text{A6})$$

and all other terms are defined in the text.

i) Inviscid Solution

The inviscid equations are obtained from equations (A1) by neglecting all terms containing diffusivity, viscosity and thermal conductivity. The resulting equations can be manipulated to obtain a second order differential equation in terms of the pressure perturbation $\hat{p}(\eta)$.

$$\hat{p}'' - \frac{w'}{w-c} \hat{p}' + \alpha^2 S^2 \bar{T}^2 \left[\frac{V_c^2 (w-c)^2}{\bar{T}} \left(\frac{1}{C_1 S} - \frac{1}{M} \right) - 1 \right] \hat{p} + i R(\eta) = 0 \quad (\text{A7})$$

where

$$R(\eta) = \alpha V_c S^2 \bar{T}^2 (w-c) \sum_{k=1}^v \left[\frac{C_k^*}{S} - \frac{1}{M \bar{T}} (m_k D_k \bar{T} + \epsilon_{k_f}) \right] G_k \quad (\text{A8})$$

Here G_k corresponds to the k th specie production rate due to instability

wave. It can be shown that for nonreactive flow equation (A7) reduces to the classical pressure perturbation equation of Lees and Lin [43]. However, for reactive flows the term G_k is determined such that

$$\begin{aligned} G_1 &= \bar{\rho}^{-2} [\hat{Y}_1 T_{11} + \hat{Y}_2 T_{21} + \hat{Y}_3 T_{31} + \hat{Y}_4 T_{41} + \hat{p} T_{51}] \\ G_2 &= \bar{\rho}^{-2} [\hat{Y}_1 T_{12} + \hat{Y}_2 T_{22} + \hat{Y}_3 T_{32} + \hat{p} T_{52}] \\ G_3 &= \bar{\rho}^{-2} [\hat{Y}_1 T_{13} + \hat{Y}_2 T_{23} + \hat{Y}_3 T_{33} + \hat{Y}_4 T_{43} + \hat{p} T_{53}] \\ G_4 &= \bar{\rho}^{-2} [\hat{Y}_1 T_{14} + \hat{Y}_3 T_{34} + \hat{Y}_4 T_{44} + \hat{p} T_{54}] \end{aligned} \quad (A9)$$

where G_i ($i=1,4$) and \hat{Y}_i ($i=1,4$) indicate species H_2 , O_2 , OH and H_2 respectively. The matrix T_{ij} ($i=1,5$ $j=1,4$) are coefficients which are described below. On using equation (A9) in (A8) and on some algebraic manipulations we get

$$\begin{aligned} \hat{p}'' + \hat{p}' \left[-\frac{2w'}{w-c} + \frac{\bar{T}'}{\bar{T}} (v^* - 1) - \frac{S'}{S} - \bar{B} \right] \\ + \hat{p} \left[\frac{v_c^2 (w-c)^2 v^*}{\bar{T}} \left(\frac{1}{c_1 S} - \frac{1}{M} \right) - 1 \right] \alpha^2 S^2 \bar{T}^2 = 0 \end{aligned} \quad (A10)$$

where v^* and \bar{B} are complex constants appearing due to finite rate kinetics and are defined as

$$v^* = \left[G_0 + i \frac{\bar{\rho}^{-2} \beta_0}{E(\bar{u}-c)\alpha\bar{T}} \right]^{-1} = v_R^* + i v_I^* \quad (A11)$$

and

$$\bar{B} = \frac{\alpha^2 (\bar{u}-c)^2}{c_1 \bar{\rho}^{-2} \hat{p}'} \left[G_1 + i \frac{\bar{\rho}^{-2} \beta_0}{E(\bar{u}-c)\alpha\bar{T}} \right] = \bar{B}_R + i \bar{B}_I \quad (A12)$$

where prime denotes differentiation with respect to η and

$$G_0 = 1 + \frac{\rho}{S} \sum_{k=1}^4 C_k^* N_k \quad (A13)$$

$$G_1 = \frac{\rho}{S} \sum_{k=1}^4 C_k^* M_k$$

$$B_0 = \sum_{j=1}^5 a_j N_j, \quad N_5 = 1 \quad (A14)$$

$$B_1 = \sum_{k=1}^4 a_k M_k$$

and

$$E = \sum_{k=1}^4 m_k D_k \bar{Y}_k \quad (A15)$$

The constants C_1 , C_k^* and D_k are defined in the text. The terms in (A13) and (A14) are due to the algebraic manipulation involved and are given by

$$a_j = T_{jk} (m_k D_k \bar{T} + \epsilon_{k_f}) \quad \begin{matrix} j = 1,5 \\ k = 1,4 \end{matrix} \quad (A16)$$

The matrix T_{jk} which also appears in equation (A9) is the finite rate production of each specie due to the disturbance field and is given as

$$T_{12} = X_2 A \bar{k}_{f_1} \bar{Y}_2$$

$$T_{22} = X_2 A \bar{k}_{f_1} \bar{Y}_1$$

$$T_{32} = -2 X_2 B \bar{k}_{b_1} \bar{Y}_3$$

$$T_{42} = 0$$

$$T_{52} = 2 X_2 \frac{1}{P} (A \bar{k}_{f_1} \bar{Y}_1 \bar{Y}_2 - B \bar{k}_{b_1} \bar{Y}_3^2)$$

$$T_{14} = X_4 C \bar{\rho} \bar{k}_{f_2} Y_3^2$$

$$T_{24} = 0$$

$$T_{34} = 2 X_4 C \bar{\rho} \bar{k}_{f_2} Y_1 Y_3$$

$$T_{44} = -2 X_4 D \bar{k}_{b_2} Y_3$$

$$T_{54} = X_4 [3 C \bar{k}_{f_2} Y_1 Y_3^2 - \frac{2}{\rho} D \bar{k}_{b_2} Y_4^2]$$

$$T_{11} = X_1 \left[\frac{T_{12}}{X_2} + \frac{T_{14}}{X_4} \right]$$

$$T_{21} = X_1 T_{22}/X_2$$

$$T_{31} = X_1 [T_{34}/X_4 - T_{32}/X_2]$$

$$T_{41} = X_1 [T_{44}/X_4]$$

$$T_{51} = X_1 [T_{52}/X_2 - T_{54}/X_4]$$

$$T_{13} = X_3 [T_{12}/X_2 - T_{14}/X_4]$$

$$T_{23} = X_3 [T_{22}/X_2]$$

$$T_{33} = X_3 [T_{32}/X_2 - T_{34}/X_4]$$

$$T_{43} = -X_3 T_{44}/X_4$$

$$T_{53} = X_3 [T_{52}/X_2 - T_{54}/X_4]$$

(A17)

where

$$\begin{aligned}
 A &= \frac{Y_{1e} Y_{2e}}{M_1 M_2} \quad , \quad B = \frac{Y_{3e}^2}{M_3^2} \\
 C &= \rho_e \frac{Y_{1e} Y_{3e}^2}{M_1 M_2^3} \quad , \quad D = \frac{Y_{4e}^2}{M_4^2}
 \end{aligned}
 \tag{A18}$$

and

$$\begin{aligned}
 X_1 &= - \frac{\rho_e L}{u_e} \frac{M_1}{Y_{1e}} \\
 X_2 &= - \frac{\rho_e L}{u_e} \frac{M_2}{Y_{2e}} \\
 X_3 &= 2 \frac{\rho_e L}{u_e} \frac{M_3}{Y_{3e}} \\
 X_4 &= 2 \frac{\rho_e L}{u_e} \frac{M_4}{Y_{4e}}
 \end{aligned}
 \tag{A19}$$

where M_i are the i -th species molecular weight and subscript e indicates reference edge values.

The terms N_k and M_k appearing in (A13) are further defined as follows.

$$N_1 = N_1^2 N_1^1 + N_2^2$$

$$N_2 = N_1^1$$

$$N_3 = N_1^3 N_1 + N_2^3 N_2^1 + N_3^3$$

$$N_4 = N_1^4 N_1 + N_2^4 N_2 + N_3^4$$

$$M_1 = M^1 N_1^2 + M^2$$

$$M_2 = M^1$$

$$M_3 = N_1^3 M_1 + N_2^3 M_2 + M^3$$

$$M_4 = N_1^4 M_1 + N_2^4 M_2 + M^4$$

(A20)

$$N_1^1 = \psi_1 [T_{12} N_2^2 + T_{32} (N_1^3 N_2^2 + N_3^3) + T_{52}] / D$$

$$D = [(1 - \psi_1 T_{22}) - \psi_1 T_{12} N_1^2 - \psi_1 T_{32} (N_1^3 N_1^2 + N_2^3)]$$

$$M = [\psi_1 T_{12} M^2 + T_{32} (N_1^3 M^2 + M^3) - \psi_2 \nabla_2' \hat{p}'] / D$$

(A21)

$$N_1^2 = \psi_1 [T_{21} + T_{31} N_2^3 + T_{41} N_2^4] / D_2$$

$$N_2^2 = \psi_1 [T_{51} + T_{31} N_3^3 + T_{41} N_3^4] / D_2$$

$$M^2 = [\psi_1 \{T_{31} M^3 + T_{41} M^4\} - \psi_2 \nabla_1' \hat{p}'] / D_2$$

$$D_2 = (1 - \psi_1 T_{11}) - \psi_1 \{T_{31} N_1^3 + T_{41} N_1^4\}$$

(A22)

$$N_1^3 = \psi_1 [T_{13} + T_{43} N_1^4] / (1 - \psi_1 T_{33})$$

$$N_2^3 = \psi_1 [T_{23} + T_{43} N_2^4] / (1 - \psi_1 T_{33})$$

$$N_3^3 = \psi_1 [T_{53} + T_{43} N_3^4] / (1 - \psi_1 T_{33})$$

$$M^3 = [-\psi_2 \nabla_3' \hat{p}' + \psi_1 T_{43} M^4] / (1 - \psi_1 T_{33})$$

(A23)

$$N_1^4 = \frac{\psi_1}{D_4} [(1 - \psi_1 T_{33}) T_{14} + \psi_1 T_{34} T_{13}]$$

$$N_2^4 = \frac{\psi_1^2}{D_4} T_{34} T_{32}$$

$$N_3^4 = \frac{\psi_1}{D_4} [(1 - \psi_1 T_{33}) T_{54} + \psi_1 T_{34} T_{53}]$$

$$M^4 = -\frac{\psi_2 \hat{p}'}{D_4} [(1 - \psi_1 T_{33}) \bar{Y}_4' + \psi_1 T_{34} \bar{Y}_3']$$

$$D_4 = [(1 - \psi_1 T_{33})(1 - \psi_1 T_{44}) - \psi^2 T_{34} T_{43}] \quad (A24)$$

where

$$\psi_1 = \frac{\bar{\rho}}{i \alpha (w - c) V_c} \quad (A25)$$

$$\psi_2 = \frac{C_1 \bar{\rho}}{\alpha^2 (w - c)^2 V_c^2}$$

ii) Viscous Solution

The full viscous equations for this stability problem equation (A1) is very complicated and no solution has been obtained so far. Lees and Lin [43], Dunn-Lin [66] and Lees and Reshotko [58] have in the past presented solutions for the viscous equations by solving a set of reduced equations that retain terms up to a certain order, either near the critical point or near the surface. Dunn-Lin [66] ordering of the various terms accounts for supersonic flows and for the propagation wave velocity c to be a substantial portion of the free-stream velocity. Therefore, at present a similar ordering is applied here whereby

$$\begin{aligned}
\bar{\phi}, \bar{\phi}' &\sim \mathcal{O}(1) \\
\frac{d}{dy} &\sim \mathcal{O}\left(\frac{1}{e}\right), \quad (w-c) \sim \mathcal{O}(1) \\
\hat{u} &\sim \mathcal{O}(1), \quad \hat{v} \sim \mathcal{O}(e\hat{u}), \quad T \sim \hat{u}, \quad \hat{Y}_k \sim \hat{u}, \quad \hat{\rho} \sim u \\
\hat{p} &\sim e^2 \hat{u} \\
e^2 &\sim \frac{1}{\alpha Re} \sim \bar{D}_k / \alpha \sim C_T^* / \alpha
\end{aligned} \tag{A26}$$

Using these ordering, equation (A1) can be reduced to a form similar to Dunn-Lin viscous equations

$$\hat{u}''' - i \alpha Re v^{-1} \frac{V_c}{\rho^2} (\bar{w}-c) \hat{u}' = 0 \tag{A27}$$

$$\hat{v}' + i \frac{\hat{u}}{\rho} = i \frac{(w-c)}{\rho} \left[\frac{\hat{T}}{T} + \frac{1}{S} \sum_{k=1}^v C_k^* \hat{Y}_k \right] \tag{A28}$$

$$\hat{Y}_k'' - i \left(\frac{\alpha V_c}{D_k} \right) \frac{1}{\rho^2} (w-c) = - \frac{1}{D_k} \frac{\gamma_k^*}{\rho^3}, \quad k=1, \dots, v \tag{A29}$$

$$\begin{aligned}
\hat{T}'' - i \left(\frac{\alpha}{\kappa C_T^*} \right) \frac{V_c}{\rho} (w-c) M \hat{T} \\
= \left(\frac{\alpha}{\kappa C_T^*} \right) \sum_{k=1}^v \frac{1}{\alpha \rho^2} \bar{h}_k \gamma_k^* \\
+ \left(i \left(\frac{\alpha}{\kappa C_T^*} \right) \frac{V_c}{\rho} (w-c) \sum_{k=1}^v (m_k D_k T + \epsilon_{k_f} - \bar{h}_k) \hat{Y}_k \right)
\end{aligned} \tag{A30}$$

We see that this is a eighth-order system of ordinary differential equations dependent basically on one parameter (αRe). For nonreactive case, the equation (A29) and all terms containing \hat{Y}_k drop out and the resulting equations are then identically Dunn-Lin [66] viscous equations. Lees-Reshotko [58] ordered terms in two parameters (αRe) and M_e^2 and retained additional terms containing temperature and viscosity fluctuations. Such an ordering would eventually be necessary to deal with viscous reactive stability but have been presently neglected by

assuming all transport properties are function of mean variables only. Of course, equations (A27) to (A30) can be directly solved simultaneously with appropriate boundary conditions. However, due to the analytical nature of these equations, some modification is possible. Consider the behavior of these equations in the outer flow where all mean flow variables have attained their external values. A solution for equation (A27) in the outer flow can be immediately written as

$$\hat{u}'(\eta) = \exp[\pm i\{\alpha \text{Re } v^{-1} V_c c\}^{1/2} \eta] \quad , \quad \eta \rightarrow \pm \infty \quad (\text{A31})$$

However all other equations are coupled and no direct solution can be written for the general reactive case. This is in contrast to nonreactive case for $\gamma_k^* = 0$) when we get a solution for equation (A28) as

$$\hat{Y}_k \sim \exp[\pm i\{\alpha \bar{D}_k^{-1} V_c c\}^{1/2} \eta] \quad , \quad \eta \rightarrow \pm \infty \quad (\text{A32})$$

and when \hat{Y}_k terms are neglected, equation (A30) gives

$$\hat{T} \sim \exp[\pm i\{\alpha (\bar{\kappa} C_T^*)^{-1} V_c M\}^{1/2} \eta] \quad , \quad \eta \rightarrow \pm \infty \quad (\text{A33})$$

Solutions (A31) and (A33) are identical to the ones obtained by Lees-Reshotko [58]. These are all linearly independent solutions and governing equations must satisfy these solutions in the outer edge. However, for reactive wakes only equation (A31) is a direct solution since all other equations are coupled. For $\eta \rightarrow \infty$, the positive exponent cannot satisfy the outer inviscid boundary conditions and must be neglected.

Then on applying transformations [58]

$$h = \hat{v}/\hat{u} \quad , \quad f = \hat{u}'/\hat{u} \quad , \quad \theta = \hat{T}/\hat{u} \quad \text{and} \quad \ell_k = \hat{Y}_k/\hat{u} \quad , \quad k=1, \dots, v \quad (\text{A34})$$

we get

$$h' = -h f - \frac{1}{\rho} - \frac{i(w-c)}{\rho \bar{T}} \theta + \sum_k \frac{C_k^* \ell_k}{S} \quad (\text{A35})$$

$$f'' = -f(f^2 + 3f') + \frac{i \alpha \text{Re } v^{-1}}{\rho^2} V_c (w-c) f \quad (\text{A36})$$

$$\begin{aligned}
\ell_k'' &= -2f \ell_k' - (f^2 + f') \ell_k + \frac{i\alpha V_c}{\bar{D}_k \bar{\rho}^2} (w-c) \ell_k - G_k, \quad k=1, \dots, v \\
\theta'' &= -2f \theta' - (f' + f^2) \theta + \frac{1}{(\bar{\rho} \kappa C_T^*)} [i\alpha V_c (w-c) \{ \sum_{k=1}^v (m_k D_k \bar{T} \\
&\quad + \epsilon_{k_f} - \bar{h}_k) \ell_k + f \theta \} + \sum_{k=1} \bar{h}_k G_k]
\end{aligned} \tag{A37}$$

An approximate set of boundary conditions at

$$\begin{aligned}
\eta \rightarrow \infty \quad f(\eta \rightarrow \infty) &= -i [i\alpha Re \bar{v}^{-1} V_c C]^{1/2} \\
h(\eta \rightarrow \infty) &= \frac{1}{[\bar{\rho} \{i\alpha Re \bar{v}^{-1} V_c C\}^{1/2}]} \\
\ell_k(\eta \rightarrow \infty) &= 0 \\
\theta(\eta \rightarrow \infty) &= 0
\end{aligned} \tag{A38}$$

$\eta = 0$

For antisymmetrical disturbance

$$\begin{aligned}
f(0) = h(0) &= 0 \\
\theta'(0) = \ell_k'(0) &= 0
\end{aligned} \tag{A39}$$

For the general solution of viscous reactive flow stability, the equations (A35) to (A37) must be solved for the given boundary conditions such that the outer solution satisfies the inviscid conditions. Essentially two characteristic values α and Re must be determined for the general viscous case in contrast to only α for the inviscid part. Neutral stability characteristics can then be obtained as a function of (α, Re) for a given Mach number. This generalized stability analysis of viscous reactive wakes will be an interesting research area for future study.

APPENDIX B

INTERACTION INTEGRALS FOR COHERENT STRUCTURE MOTION

The integrals appearing in the governing conservation equations in Chapter II can be rewritten using the assumed mean flow profiles and using the coherent structure and fine-scale turbulent representations. Since at present only the interaction between mean motion and coherent structure has been studied therefore only the integrals relevant for this analysis is presented here.

Species diffusion flux:

$$I_{D_k}^c = 2\delta |A|^2 \left[\int_{-\infty}^{\infty} \left\{ \frac{1}{\bar{\rho}} (\bar{Y}_k - 1) \text{Re}(\hat{\rho} \hat{u}^*) + \text{Re}(\hat{u} \hat{Y}_k^*) \right\} d\eta \right. \\ \left. + \int_{-\infty}^{\infty} \frac{u}{\bar{\rho}} \text{Re}(\hat{Y}_k \hat{\rho}^*) d\eta \right] \quad , \quad k = 1, \dots, v \quad (B1)$$

Species production:

$$R_k = \delta \int_{-\infty}^{\infty} \frac{r_k^0}{\bar{\rho}} d\eta \quad , \quad k = 1, \dots, v \quad (B2)$$

where r_k^0 is the total mean production rate for the k-th species and can be rewritten using equation (140) as follows

$$\overline{r_{O_2}^0} = X_{O_2} [B \bar{k}_{b1} \{ \bar{\rho}^{-2} \bar{Y}_{OH}^2 + 2|A|^2 (\bar{\rho}^{-2} |\hat{Y}_{OH}|^2 + 4 \bar{\rho} \bar{Y}_{OH} \text{Re}(\hat{\rho} \hat{Y}_{OH}^*) \\ + \bar{Y}_{OH} 2|\hat{\rho}|^2) \} - A \bar{k}_{f1} \{ \bar{\rho}^{-2} \bar{Y}_{H_2} \bar{Y}_{O_2} + 2|A|^2 (\bar{\rho}^{-2} \text{Re}(\hat{Y}_{H_2} \hat{Y}_{O_2}^*) \\ + 2 \bar{\rho} \bar{Y}_{H_2} \text{Re}(\hat{\rho} \hat{Y}_{O_2}^*) + 2 \bar{\rho} \bar{Y}_{O_2} \text{Re}(\hat{\rho} \hat{Y}_{H_2}^*) + \bar{Y}_{H_2} \bar{Y}_{O_2} |\hat{\rho}|^2) \}]] \quad (B3)$$

$$\overline{r_{H_2O}^0} = X_{H_2O} [C \bar{k}_{f2} \{ \bar{\rho}^{-3} \bar{Y}_{OH}^2 \bar{Y}_{H_2} + 2|A|^2 \bar{\rho}^{-3} (\bar{Y}_{OH} \text{Re}(\hat{Y}_{OH} \hat{Y}_{H_2}^*) \\ + \bar{Y}_{H_2} |\hat{Y}_{OH}|^2) + 6|A|^2 \bar{\rho}^{-2} (2 \bar{Y}_{OH} \bar{Y}_{H_2} \text{Re}(\hat{\rho} \hat{Y}_{OH}^*) + \bar{Y}_{OH}^2 \text{Re}(\hat{\rho} \hat{Y}_{H_2}^*)) \\ + 6|A|^2 \bar{\rho} \bar{Y}_{H_2} \bar{Y}_{OH}^2 |\hat{\rho}|^2 \} - D \bar{k}_{b2} \{ \bar{\rho}^{-2} \bar{Y}_{H_2O} + 2|A|^2 (\bar{\rho}^{-2} |\hat{Y}_{H_2O}|^2 \\ + \bar{Y}_{H_2O} |\hat{\rho}|^2 + 4 \bar{\rho} \bar{Y}_{H_2O} \text{Re}(\hat{\rho} \hat{Y}_{H_2O}^*)) \}]] \quad (B4)$$

$$\overline{r_{H_2O}} = E \overline{r_{O_2}} - \frac{1}{2} F \overline{r_{H_2O}} \quad (B5)$$

$$\overline{r_{OH}} = -2 G \overline{r_{O_2}} - H \overline{r_{H_2O}} \quad (B6)$$

where all the constants are defined in the text (Section 2.7) and * denotes the complex conjugate. $\overline{k_{f_i}}$ and $\overline{k_{b_i}}$ are the mean rate constants which for this interaction problem is the function of the mean temperature. Here Re stands for the real part of the complex product.

Mean flow total enthalpy flux:

$$I_E^c = I_{E_1}^c + I_{E_2}^c + I_{E_3}^c \quad (B7)$$

where

$$I_{E_1}^c = 2\delta |A|^2 V_c \int_{-\infty}^{\infty} \frac{1}{\rho} (\overline{H} - 1) Re(\hat{\rho} \hat{u}^*) d\eta \quad (B8)$$

$$I_{E_2}^c = 2\delta |A|^2 V_c \int_{-\infty}^{\infty} [V_c \overline{u} |\hat{u}|^2 + M Re(\hat{u} \hat{T}^*) + \sum_k (m_k D_k \overline{T} + \epsilon_{k_f}) Re(\hat{u} \hat{Y}_k^*)] d\eta \quad (B9)$$

$$I_{E_3}^c = 2\delta |A|^2 \int_{-\infty}^{\infty} [V_c \overline{u} Re(\hat{u} \hat{\rho}^*) + M Re(\hat{\rho} \hat{T}^*) + \sum_k (m_k D_k \overline{T} + \epsilon_{k_f}) Re(\hat{\rho} \hat{Y}_k^*)] \frac{\overline{u}}{\rho} d\eta \quad (B10)$$

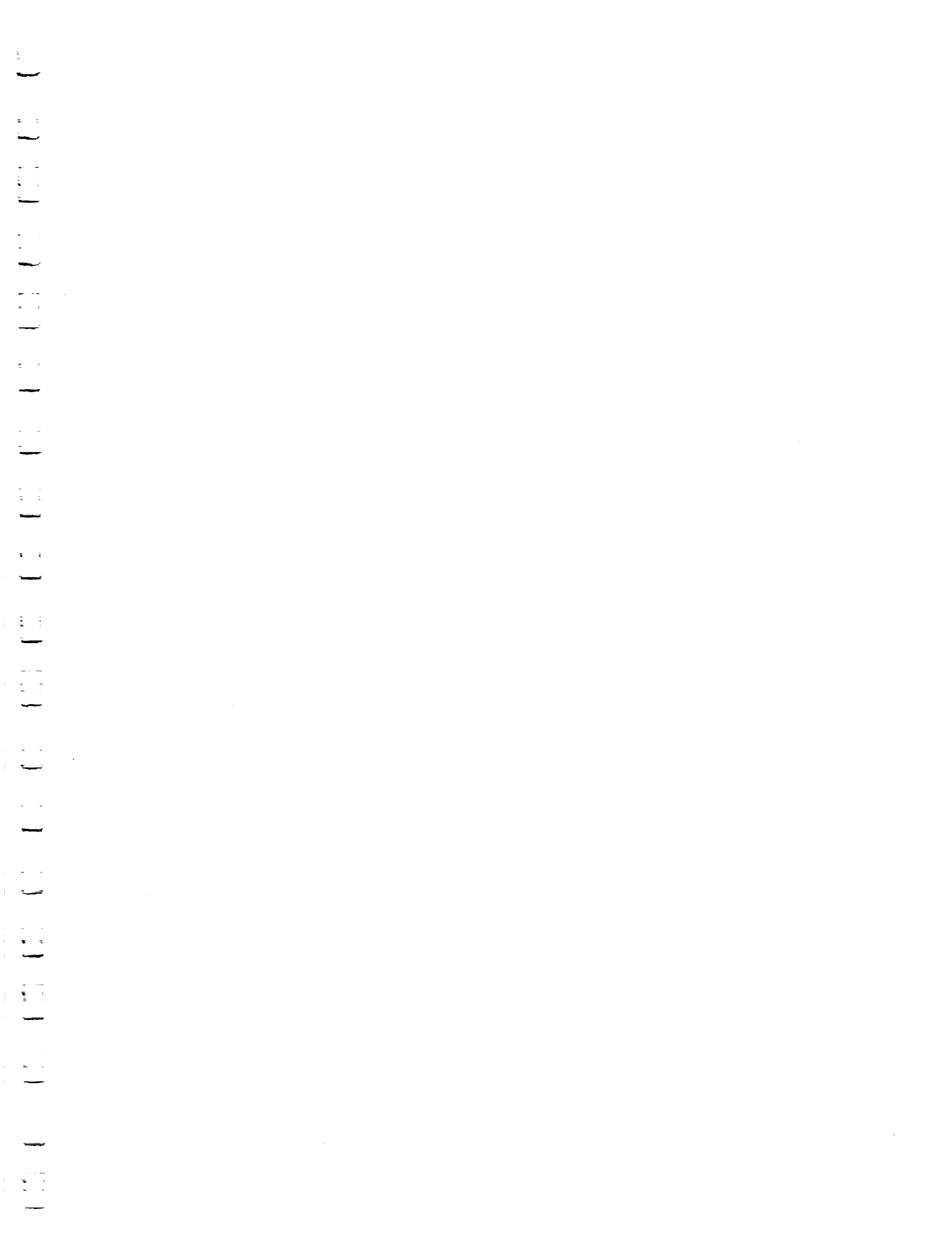
The integral for disturbance generated diffusion flux in the mean flow kinetic energy conservation is

$$I_{KE}^c = \delta V_c |A|^2 \int_{-\infty}^{\infty} \left[\frac{(3\overline{u}^2 - 1)}{\rho} Re(\hat{\rho} \hat{u}^*) + 2 V_c \overline{u} |\hat{u}|^2 \right] d\eta \quad (B11)$$

The Reynolds stress production I_{RS}^c is given by

$$I_{RS}^c = I_{RS_1}^c + I_{RS_2}^c + I_{RS_3}^c + I_{RS_4}^c + I_{RS_5}^c \quad (B12)$$

where



$$\begin{aligned}
I_{RS_1}^c &= -2|A|^2 V_c^2 \int_{-\infty}^{\infty} \bar{\rho} \operatorname{Re}(\hat{u} \alpha^* \hat{v}^*) \frac{\partial \bar{u}}{\partial \eta} d\eta \\
I_{RS_2}^c &= -2\delta |A|^2 V_c \int_{-\infty}^{\infty} \frac{\bar{u}}{\rho} \operatorname{Re}(\hat{\rho} \hat{u}^*) \left(\frac{\partial \bar{u}}{\partial x}\right)_y d\eta \\
I_{RS_3}^c &= -2\delta |A|^2 V_c^2 \int_{-\infty}^{\infty} |\hat{u}|^2 \left(\frac{\partial \bar{u}}{\partial x}\right)_y d\eta \\
I_{RS_4}^c &= -2|A|^2 V_c \int_{-\infty}^{\infty} \bar{v} \operatorname{Re}(\hat{\rho} \hat{u}^*) \frac{\partial \bar{u}}{\partial \eta} d\eta \\
I_{RS_5}^c &= -2|A|^2 V_c^2 \int_{-\infty}^{\infty} \bar{\rho} |\alpha \hat{v}|^2 \frac{\partial \bar{v}}{\partial \eta} d\eta
\end{aligned} \tag{B13}$$

where

$$\left(\frac{\partial}{\partial x}\right)_y = \left(\frac{\partial}{\partial x}\right)_\eta - \frac{\eta}{\delta} \frac{d\delta}{dx} \frac{\partial}{\partial \eta} \tag{B14}$$

The pressure work integrals are

$$\begin{aligned}
I_{p_1} &= -C_1 \frac{d}{dx} \delta \int_{-\infty}^{\infty} (\bar{p} - 1) \frac{\bar{u}}{\rho} d\eta \\
I_{p_2} &= C_1 \delta \int_{-\infty}^{\infty} (\bar{p} - 1) \left[\left(\frac{\partial \bar{u}}{\partial x}\right)_y + \frac{\bar{\rho}}{\delta} \frac{\partial \bar{v}}{\partial \eta} \right] d\eta
\end{aligned} \tag{B15}$$

The mean flow pressure is determined in general, from

$$\bar{p} = 1 - \frac{V_c^2}{C_1} [2\bar{\rho} |A|^2 |\alpha \hat{v}|^2] \tag{B16}$$

The organized motion pressure work integral is

$$I_p^c = -2 C_1 \delta |A|^2 V_c \int_{-\infty}^{\infty} \operatorname{Re}\{i \alpha \hat{p} \hat{u}^* + \alpha \hat{v} \hat{p}'^*\} d\eta \tag{B17}$$

The mean flow viscous dissipation integral is

$$I_\phi = \frac{1}{\delta \operatorname{Re}} \int_{-\infty}^{\infty} \bar{\rho} \bar{\mu} \left(\frac{\partial \bar{u}}{\partial \eta}\right)^2 d\eta \tag{B18}$$

where, for a linear viscosity-temperature relation, $\bar{\mu} = C\bar{T}$, $C \approx 1$,

$$\bar{\rho} \bar{\mu} = 1 - 2|A|^2 [\operatorname{Re}(\hat{\rho} \hat{T}^*) + \frac{\bar{\rho}}{C_1} V_c^2 |\alpha \hat{v}|^2] \tag{B19}$$

The organized motion viscous dissipation integral is

$$I_{\phi}^c = \frac{2V_c^2 |A|^2 C}{\delta Re} \int_{-\infty}^{\infty} \left[\frac{|\alpha|^2}{\rho^2} \left(\frac{4}{3} |\hat{u}|^2 + |\alpha \hat{v}|^2 \right) + \frac{4}{3} |\alpha \hat{v}'|^2 + |\hat{u}'|^2 \right] + \frac{1}{\rho} \{ \text{Re}(2i\alpha^2 \hat{v} \hat{u}'^* - \frac{4}{3} i |\alpha|^2 \hat{u} \hat{v}'^*) \}] d\eta \quad (B20)$$

The relationship between shear layer thickness and velocity defect is given by equation (48) which results in

$$\delta = \frac{C_D/2}{V_c(C_1 - V_c C_2)} \quad (B21)$$

where $C_1 = \sqrt{\pi}$ and $C_2 = \sqrt{\pi/2}$ and C_D is the drag coefficient of the body.

The disturbance kinetic energy integral is

$$\frac{\delta}{2} \int_{-\infty}^{\infty} \overline{u'^2 + v'^2} d\eta = \delta |A|^2 (I_{K_1} - V_c I_{K_2}) \quad (B22)$$

where

$$I_{K_1} = \int_{-\infty}^{\infty} (|\hat{u}|^2 + |\alpha \hat{v}|^2) d\eta = 1 \quad (B23)$$

$$I_{K_2} = \int_{-\infty}^{\infty} (|\hat{u}|^2 + |\alpha \hat{v}|^2) e^{-\eta^2} d\eta$$

The filtering procedure:

On using equation (10) the mean value is given by

$$\overline{\phi\psi} = (\overline{\phi} + \overline{\phi'} + \overline{\phi''})(\overline{\psi} + \overline{\psi'} + \overline{\psi''}) = \overline{\phi}\overline{\psi} + \overline{\phi'}\overline{\psi'} + \overline{\phi''}\overline{\psi''} \quad (B24)$$

On subtracting the mean value from the total value and taking conditional average we get

$$\langle \phi\psi - \overline{\phi\psi} \rangle = \overline{\phi}\overline{\psi'} + \overline{\phi'}\overline{\psi} + R_{\phi\psi} \quad (B25)$$

Fine-scale turbulence contribution is obtained by

$$\phi\psi - \langle \phi\psi - \overline{\phi\psi} \rangle - \overline{\phi\psi} = \overline{\phi}\overline{\psi''} + \overline{\phi''}\overline{\psi} + L_{\phi\psi} \quad (B26)$$

Similar filtering is also applicable to the 0(3) or higher fluctuation correlation.

APPENDIX C
MODELS FOR TURBULENCE, INTERMITTENCY AND DIFFUSION

Turbulence Models

The algebraic eddy viscosity models used in these calculations were modified from the formulation of Spalding [69] and Schlichting and Hinze [70]. They are given in dimensional form as follows.

Model I [69]

$$\mu_t^* = 0.037 \delta^* |U_{\max} - U_{\min}| \bar{\rho}^* \quad (C1)$$

where U_{\max} and U_{\min} are the local maximum and minimum values of the stream-wise velocity and μ_t^* is the dimensional turbulent viscosity.

Model II [70]

$$\mu_t^* = 0.044 \Delta^* \quad (C2)$$

where the characteristic density thickness Δ^* is given in the dimensional form as

$$\Delta^* = \left| \int_{-\infty}^{\infty} \bar{\rho}^* (u_{\infty} - \bar{u}^*) dy^* \right| \quad (C3)$$

On nondimensionalizing equation (C1) we get

$$\epsilon_I = 0.037 \delta V_c \bar{\rho} \quad (C4)$$

where $\epsilon_I = \mu_t^* / \rho_{\infty} U_{\infty} L$ is then identified as the dimensionless turbulent eddy viscosity. Equation (C2) then becomes

$$\epsilon_{II} = 0.044 \Delta \quad (C5)$$

where the nondimensional density thickness

$$\Delta = \left| \int_{-\infty}^{\infty} \bar{\rho} (1 - \bar{u}) dy \right| = \sqrt{\pi} \delta V_c \quad (C6)$$

and $\epsilon_{II} = \mu_t^* / \rho_{\infty} U_{\infty} L$.

During the calculations it was found that the turbulent eddy

viscosity Model II gave slightly better results and was used for all the reactive calculations.

Intermittency Models

The intermittency model used here is basically the model proposed by Spiegler et. al. [71] and is repeated here for completeness. This model is applied to the reaction



and the determination of the intermittency factors for the forward and backward rates are given by the following steps.

For each specie (k), the mean square fluctuation of mass fraction $\overline{Y_k^2}$ is determined from the dimensional relations

$$\overline{Y_k^2} = c_I \delta^{*2} \left| \frac{\partial \overline{Y}_k}{\partial y^*} \right| \left| \frac{\partial \overline{Y}_k}{\partial y^*} \right|, \quad c_I \approx 20.25 \quad (\text{C8})$$

We then compute

$$\lambda_k = \frac{|\overline{Y_k^2}|}{\overline{Y}_k^2} \quad (\text{C9})$$

and

$$U_k = \frac{\lambda_k - 0.233}{\lambda_k + 1} \quad (\text{C10})$$

Then we determine the intermittency factor for reaction (i) as follows:

$U_i = \max(U_k)$, if the respective $\overline{Y_k^2}$'s have the same sign.

$U_i = \sum_{ki} (U_{ki})$, if the respective $\overline{Y_k^2}$'s have different signs.

The finite-rate constants for each reaction (i) and direction (m = f, b) then becomes

$$k_{m_i} = k_{m_i} (1 - U_i) \quad (\text{C11})$$

These rate constants are then used in the finite-rate production terms appearing in the governing equations.

Diffusion Model

The diffusion term due to molecular diffusivity in the integral form is given in the nondimensional form as

$$I_{d_k}^* = \int_{-\infty}^{\infty} \frac{1}{\rho} \bar{D}_k \left[\left(\frac{\partial \bar{Y}_k}{\partial y} \right)^2 + \left(\frac{\partial \bar{Y}_k'}{\partial y} \right)^2 \right] dy \quad (C12)$$

Applying the transformations we get

$$I_{d_k} = \frac{1}{\delta} \int_{-\infty}^{\infty} \frac{1}{\rho} \bar{D}_k \left[\bar{Y}_k'^2 + 2|A|^2 |\hat{Y}_k'|^2 \right] d\eta \quad (C13)$$

where prime denotes differentiation with respect to η . For simplicity, we relate the mean molecular diffusivity to the kinematic viscosity by the Schmidt Number $Sc (= \nu/\bar{D}_k)$ which at present we take to be unity. This term I_{d_k} is then added to the right hand side of equation (13) which results in an additional term in the thermal energy balance by virtue of the heat flux term equation (8).

REFERENCES

- [1] Drummond, J.P., Rogers, R.C. and Evans, J.S., "Combustor Modelling for ScramJet Engines," AGARD 5th(b) Specialist's Meeting on Combustor Modelling, Cologne, Germany, 1979.
- [2] Jones, W.P. and McQuirk, J.J., "Mathematical Modelling of Gas-Turbine Combustion Chamber," AGARD CP-275.
- [3] Libby, P.A. and Williams, F.A., "Some Implications of Recent Theoretical Studies in Turbulent Combustion," AIAA Journal, Vol. 19, No. 3, pp. 261-274, March 1981.
- [4] Broadwell, J.E. and Briendenthal, R.E., "A Simple Model of Mixing and Chemical Reaction in a Turbulent Shear Layer," Journal of Fluid Mechanics, 125, pp. 397-410, 1982.
- [5] Dopazo, C. and O'Brien, E.E., "Statistical Treatment of Non-Isothermal Chemical Reactions in Turbulence," Combustion Science and Technology, Vol. 13, pp. 99-122, 1976.
- [6] Borghi, R., "Computational Studies of Turbulent Flows with Chemical Reactions," in Turbulent Mixing in Non-Reactive and Reactive Flows, ed. S.N.B. Murthy, Plenum Press, NY, 1974.
- [7] Borghi, R. and Moreau, P., "Turbulent Combustion in a Pre-Mixed Flow," Acta Aeronautica, Vol. 4, pp. 321-341, 1977.
- [8] Dopazo, C. and O'Brien, E.E., "Functional Formulation of Non-Isothermal Turbulent Reactive Flows," Physics of Flows, Vol. 17, No. 11, pp. 1968-1975, Nov. 1974.
- [9] Crow, S.C. and Champagne, F.H., "Orderly Structure in Jet Turbulence," Journal of Fluid Mechanics, 48, pp. 547-591, 1971.
- [10] Brown, G. and Roshko, A., "On Density Effects and Large Structure in Turbulent Mixing Layers," Journal of Fluid Mechanics, 64, pp. 775-816, 1974.
- [11] Kline, S.J., Reynolds, W.C., Schraub, F.A. and Rumstalter, P.W., "The Structure of Turbulent Boundary Layers," Journal of Fluid Mechanics, 30, pp. 741-773, 1967.
- [12] Blackwelder, R.F. and Eckelmann, H., "Streamwise Vortices Associated with the Bursting Phenomenon," Journal of Fluid Mechanics, 94, pp. 577-594, 1979.
- [13] Spalding, D.B., "The ESCIMO Theory of Turbulent Combustion," Imperial College, London, Mechanical Engineering Dept., Report No. HTS/73/13, 1976.

- [14] Spalding, D.B., "Chemical Reactions in Turbulent Fluids," Imperial College, London, Mechanical Engineering Dept., Report No. HTS/77/11, 1977.
- [15] Marble, F.E. and Broadwell, J.E., "The Coherent Flame Model for Turbulent Chemical Reactions," Project SQUID Technical Report, TRW-9-PU, 1977.
- [16] Chorin, A.J., "Numerical Studies in Slightly Viscous Flow," Journal of Fluid Mechanics, 57, pp. 785-796, 1973.
- [17] Ghoniem, A.F., Chorin, A.J. and Oppenheim, A.K., "Numerical Modeling of Turbulent Combustion in Premixed Gases," Eighteenth Symposium (International) on Combustion, The Combustion Institute, 1981.
- [18] Cantwell, Brian J., "Organized Motion in Turbulent Flow," Annual Review of Fluid Mechanics, 13, pp. 457-515, 1981.
- [19] Moore, C.J., "The Role of Shear-Layer Instability Waves in Jet Exhaust Noise," Journal of Fluid Mechanics, 80, pp. 321-361, 1977.
- [20] Pai, S.I., "Turbulent Flow Between Rotating Cylinders," NACA TN No. 892, 1943.
- [21] Ganji, A.R. and Sawyers, R.E., "An Experimental Study of the Flow Field and Pollutant Formation in a Two-Dimensional Premixed Turbulent Flame," NACA CR 3230, 1980.
- [22] Yule, A.J., Chigier, N.A., Ralph, S., Boulderstone, R. and Ventura, J., "Combustion Transition Interaction in a Jet Flame," AIAA Paper 80-0077, 18th Aerospace Science Meeting, Pasadena, CA., 1980.
- [23] Yule, A.J., Chigier, N.A. and Thompson, N., "Coherent Structure in Combustion," Symposium on Turbulent Shear Flows, Pennsylvania State University, 1977.
- [24] Peters, N. and Williams, F.A., "Coherent Structures in Turbulent Combustion," in The Role of Coherent Structures in Modelling Turbulence Proc., Madrid, ed. J. Jimenez, pp. 364-385, Springer-Verlag, 1980.
- [25] Roshko, A., "Structure of Turbulent Shear Flows: A New Look," AIAA Journal, Vol. 14, pp. 1349-1357, 1976.
- [26] Chigier, N.A. and Yule, A.J., "The Physical Structure of Turbulent Flames," AIAA Paper No. 79-0217, 17th Aerospace Sciences Meeting, New Orleans, LA., Jan. 15-17, 1979.
- [27] Batt, R.G. and Kubota, T., "Experimental Investigation of the Far Wakes Behind Two-Dimensional Slender Bodies at $M_\infty = 6$," AIAA Journal, Vol. 7, No. 11, pp. 2064-2071, 1969.

- [28] Behrens, W., Lewis, J.E. and Webb, W.H., "Transition and Turbulence Phenomena in Supersonic Wakes of Wedges," AIAA Journal, Vol. 9, No. 10, pp. 2083-2084, 1971.
- [29] Sato, H. and Kuriki, K., "The Mechanism of Transition in the Wake of a Thin Flat Plate Placed Parallel to a Uniform Flow," Journal of Fluid Mechanics, 11, Part 3, pp. 321-353, 1961.
- [30] Reynolds, W.C. and Hussain, A.K.M.F., "The Mechanics of an Organized Wave in Turbulent Shear Flow, 3. Theoretical Models and Comparison with Experiments," Journal of Fluid Mechanics, 54, pp. 263, 1972.
- [31] Liu, J.T.C., "Developing Large-Scale Wave-Like Eddies and the Mean Jet Noise Field," Journal of Fluid Mechanics, 62, pp. 437-464, 1974.
- [32] Liu, J.T.C., "Nonlinear Development of an Instability Wave in a Turbulent Wake," Physics of Fluids, Vol. 14, pp. 2251-2257, 1971.
- [33] Liu, J.T.C. and Merckine, L., "On the Interaction Between Large-Scale Structure and Fine-Grained Turbulence in a Free Shear Flow, I. The Development of Temporal Interactions in the Mean," Proc. of Royal Society, London, A352, pp. 213-247, 1976.
- [34] Liu, J.T.C. and Alper, A., "On the Large-Scale Structure in Turbulent Shear Flows," Proc. Symp. on Turbulent Shear Flows, pp. 11.1-11.11, Pennsylvania State University, 1977.
- [35] Alper, A. and Liu, J.T.C., "On the Interaction Between Large-Scale Structure and Fine-Grained Turbulence in a Free Shear Flow, II. The Development of Spatial Interaction in the Mean," Proc. of Royal Society, London, A359, pp. 497-527, 1978.
- [36] Gatski, T.B. and Liu, J.T.C., "On the Interaction Between Large-Scale Structure and Fine-Grained Turbulence in a Free Shear Flow, III. A Numerical Solution," Phil. Transactions of the Royal Society, London, Series A, V293, pp. 473-509, No. 1403, 1980.
- [37] Stuart, J.T., "On the Nonlinear Mechanics of Hydrodynamic Stability," Journal of Fluid Mechanics, 4, pp. 1-21, 1958.
- [38] Ko, D.R.S., Kubota, T. and Lees, L., "Finite Disturbance Effect on the Stability of a Laminar Incompressible Wake Behind a Flat Plate," Journal of Fluid Mechanics, 40, pp. 315-341, 1970.
- [39] Liu, J.T.C. and Gururaj, P.M., "Finite-Amplitude Instability of the Compressible Laminar Wake: Comparison with Experiments," Physics of Fluids, Vol. 17, No. 3, pp. 532-543, March 1974.
- [40] Demetriades, A., "Observations on the Transition Process of Two-Dimensional Supersonic Wakes," AIAA Journal, Vol. 9, No. 11, pp. 2128-2134, 1971.

- [41] Liu, J.T.C. and Lees, L., "Finite Amplitude Instability of the Compressible Laminar Wake: Strongly Amplified Disturbances," *Physics of Fluids*, Vol. 13, No. 12, pp. 2932-2938, 1970.
- [42] Bouchard, G.E. and Reynolds, W.C., "Control of Vortex Pairing in a Round Jet," *Bulletin American Physical Society*, 23, pp. 1013, 1978.
- [43] Lees, L. and Lin, C.C., "Investigation of the Stability of the Laminar Boundary Layer in a Compressible Fluid," NACA TN-1115, 1946.
- [44] Varma, A.K., Fishburne, E.S. and Beddini, R.A., "A Second Order Closure Analysis of Turbulent Diffusion Flames," NACA CR 145226, June 1977.
- [45] Launder, B.E., Reece, G.J. and Rodi, W., "Progress in the Development of a Reynolds Stress Turbulence Closure," *Journal of Fluid Mechanics*, 68, Part 3, p. 537-566, 1975.
- [46] Rogallo, R.S., "An ILLIAC Program for the Numerical Simulation of the Homogeneous Incompressible Turbulence," NASA TM-73,203, 1977.
- [47] Launder, B.E., "Turbulence Reynolds Stress Closure - Status and Prospects," AGARD CP-271, 1979.
- [48] Mankbadi, R. and Liu, J.T.C., "A Study of the Interactions Between Large-Scale Coherent Structures and Fine-Grained Turbulence in a Round Jet," *Phil. Transactions of the Royal Society, London*, A298, pp. 541-602, No. 1443, 1981.
- [49] Hanjalic, K., Launder, B.E. and Schiestal, R., "Multiple-Time Scale Concepts in Turbulent Transport Modelling," *Proc. 2nd Turbulence Shear Flows Symp.*, London, 1979.
- [50] Mathieu, J. and Charnay, J., "Experimental Methods in Turbulent Structure Research," in *The Role of Coherent Structure in Modelling Turbulence and Mixing*, Proc., Madrid, ed. J. Jimenez, pp. 146-187, 1980.
- [51] Goldschmidt, V.W., Moellami, M.K. and Oler, J.W., "Structures and Flow Reversal in Turbulent Plane Jets," *Physics of Fluids*, Vol. 26, No. 2, p. 428, 1983.
- [52] Lee, S.C. and Harsha, P.T., "Use of Turbulent Kinetic Energy in Free Mixing Studies," *AIAA Journal*, Vol. 8, p. 1026, 1970.
- [53] Fabris, G., "Third Order Conditional Transport Correlations in the Two-Dimensional Turbulent Wake," *Physics of Fluids*, Vol. 26, No. 2, p. 422, 1983.
- [54] Rogers, R.C. and Chinitz, W., "On the Use of a Global Hydrogen-Air Combustion Model in the Calculation of Turbulent Reacting Flows," *AIAA Journal*, Vol. 21, No. 4, pp. 586-592, April 1983.

- [55] Chinitz, W., "A Model to Determine the Effect of Temperature Fluctuations on the Reaction Rate Constant in Turbulent Reactive Flows," Communications to NASA/LRC.
- [56] Lockwood, R.C. and Naquib, A.S., "The Prediction of the Fluctuations in the Properties of Free, Round-Jet, Turbulent, Diffusion Flames," Combustion and Flame, Vol. 24, pp. 109-126, 1975.
- [57] Lees, L. and Gold. H., "Stability of Laminar Boundary Layers and Wakes at Hypersonic Speeds, Part I. Stability of Laminar Wakes," in Proceedings of the International Symposium on Fundamental Phenomena in Hypersonic Flow, Cornell University Press, pp. 310-342, 1966.
- [58] Lees, L. and Reshotko, E., "Stability of the Compressible Laminar Boundary Layer," Journal of Fluid Mechanics, 12, pp. 555-590, 1962.
- [59] Lin, C.C., "On the Stability of the Laminar Mixing Region Between Two Parallel Streams in a Gas," NACA TN 2887, 1953.
- [60] Mack, L.M., "Computation of the Stability of the Laminar Compressible Boundary Layer," Methods in Computational Physics, Vol. 4, pp. 247-299, 1965.
- [61] Mack, L.M., "The Stability of the Compressible Laminar Boundary Layer According to a Direct Numerical Solution," AGARDograph 97, May 1965.
- [62] Pai, S.I., "On the Stability of Two-Dimensional Laminar Jet Flow of Gas," Journal of Aeronautical Sciences, Vol. 13, pp. 731-742, Nov. 1951.
- [63] Ko, D.R.S., "Integral Theory for the Instability of Laminar Compressible Wakes Behind Slender Bodies," AIAA J., Vol. 9, No. 9, pp. 1777-1784, September 1971.
- [64] Demetriades, A., "Turbulent Mean-Flow Measurements in a Two-Dimensional Supersonic Wake," Physics of Fluids, Vol. 12, No. 1, pp. 24-32, 1969.
- [65] Demetriades, A., "Heat Transfer Effect on Supersonic Wake Transition," Physics of Fluids, Vol. 13, No. 1, pp. 204-206, 1979.
- [66] Dunn, D.W. and Lin, C.C., "On the Stability of the Laminar Boundary Layer in a Compressible Fluid," J. of Aeronautical Sciences, Vol. 22, pp. 455-477, 1955.
- [67] Betchov, R. and Criminale, W.O., Jr., "Spatial Instability of the Inviscid Jet and Wake," Physics of Fluids, Vol. 9, No. 2, pp. 359-362, February 1966.
- [68] Libby, P.A. and Williams, F.A., "Turbulent Reacting Flows," Topics in Applied Physics, Vol. 44, Springer-Verlag, New York, 1980.

- [69] Spalding, D.B., "Combustion and Mass Transfer," Pergamon Press, New York, 1979.
- [70] Schetz, J.A., "Injection and Mixing in Turbulent Flow," Progress in Astronautics and Aeronautics, Vol. 68, New York University, New York, 1980.
- [71] Spiegler, E., Wolfshtein, M. and Manheimer-Timnat, Y., "A Model of Unmixedness for Turbulent Reacting Flows with Finite-Rate Chemistry," Progress Report to NASA/LRC.
- [72] Gunther, R. and Lenze, B., "Exchange Coefficients and Mathematical Models of Jet Diffusion Flames," 14th Symposium on Combustion, The Combustion Institute, Pittsburgh, pp. 675-687, 1972.

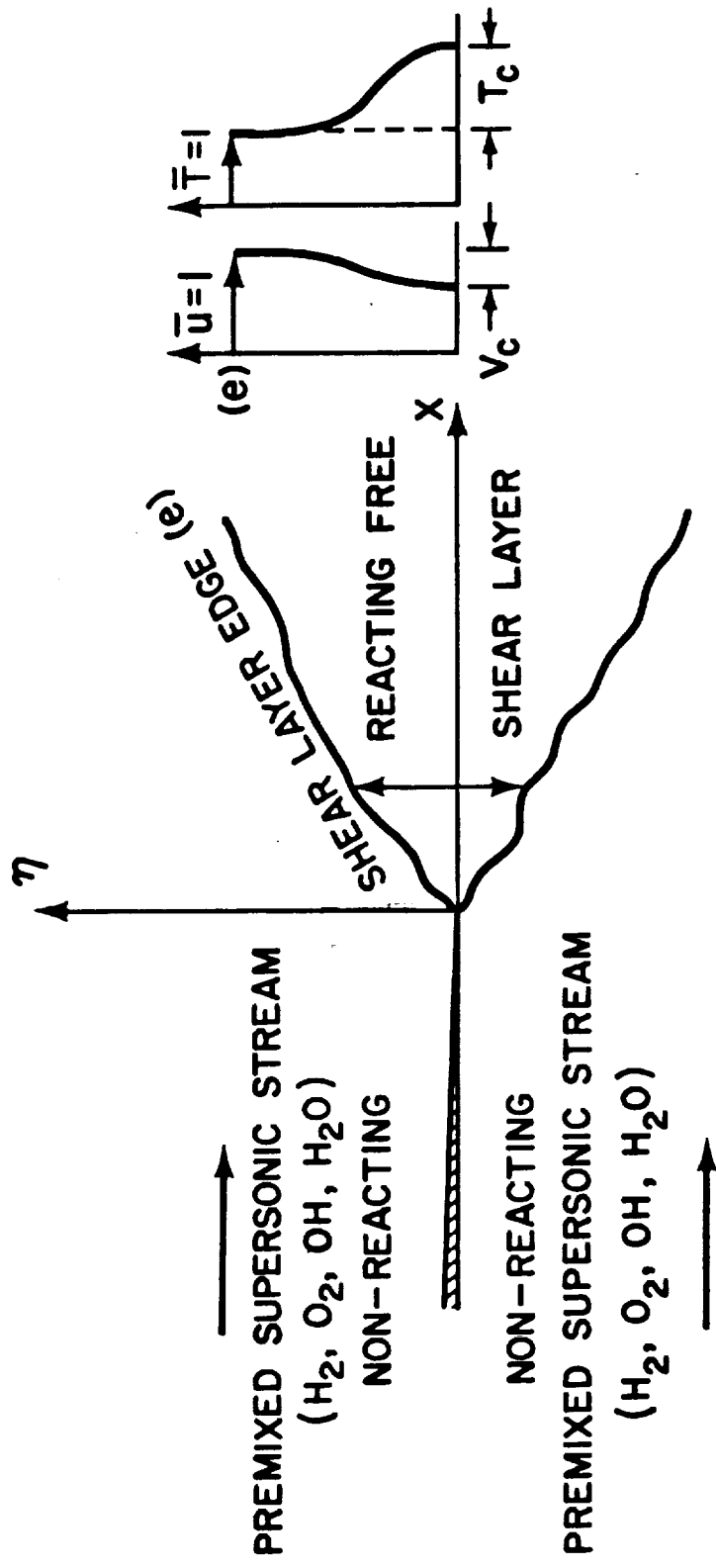


Figure 1 The geometry of the physical problem: Reacting free shear layer in the wake of a flat plate.

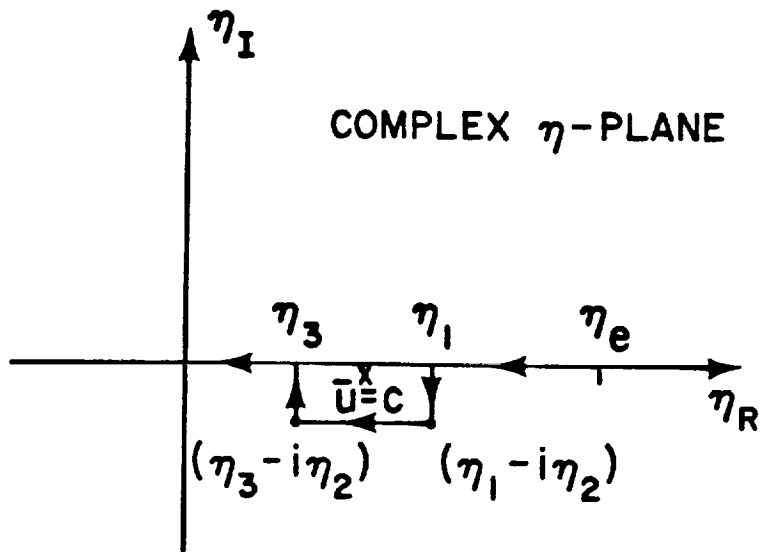


Figure 2 The path of numerical integration in the complex η -plane for the reactive eigenvalue problem.

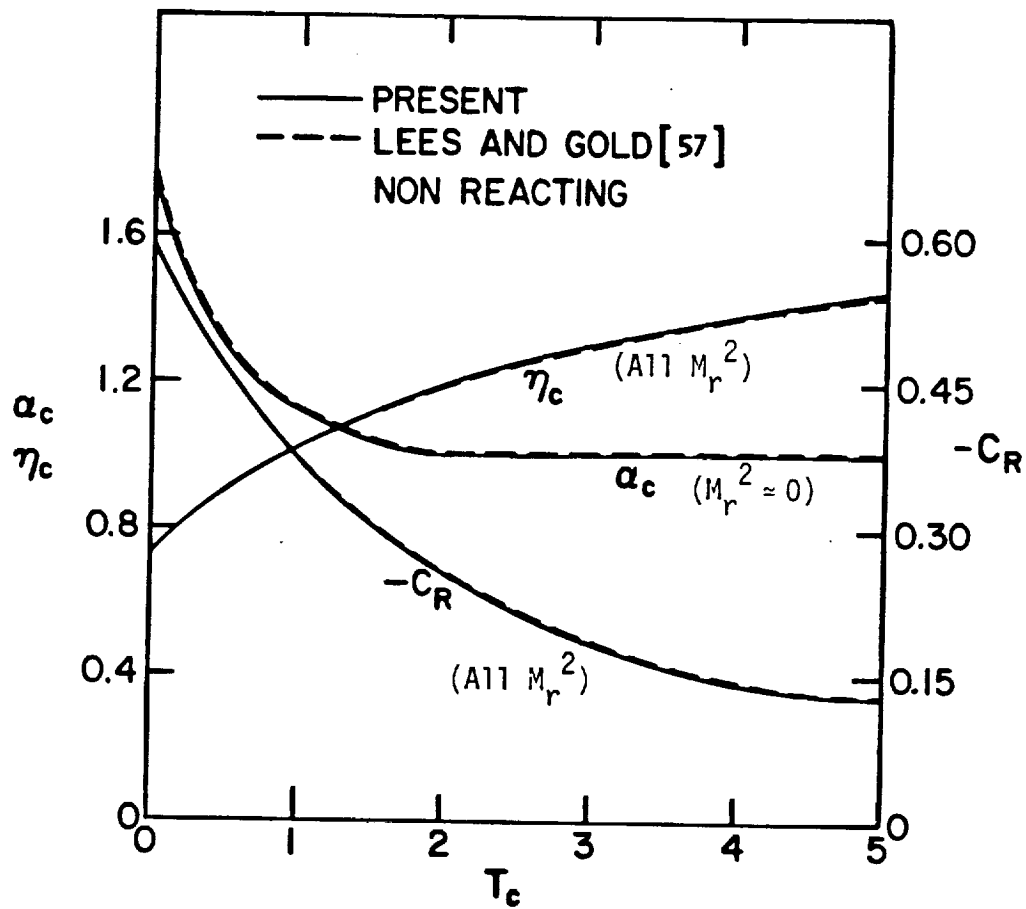


Figure 3 Neutral stability characteristics for non-reacting flow: critical point, wave number and relative phase velocity as a function of temperature excess.

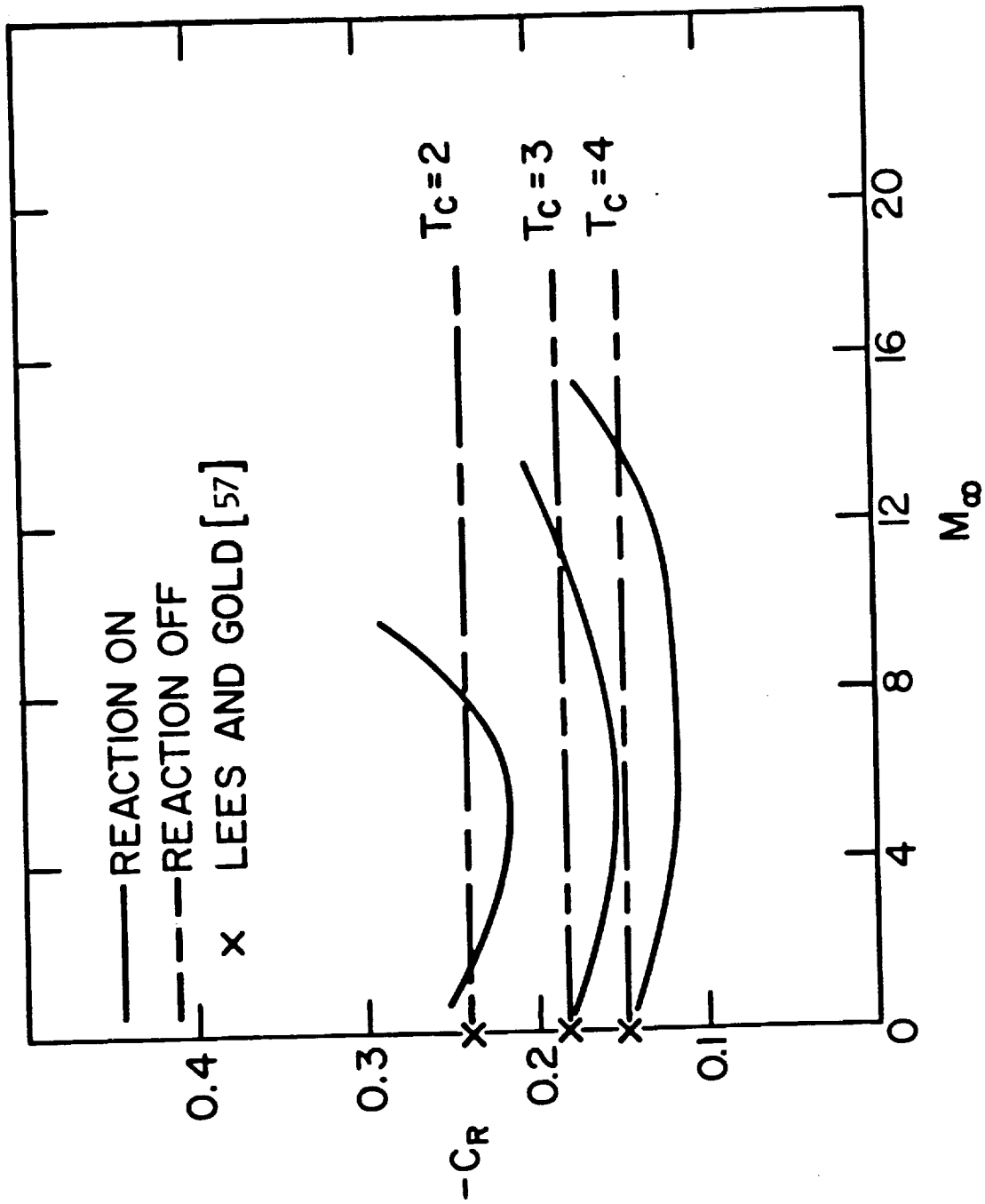


Figure 4 Variation of the neutral wave speed as a function of free stream Mach number and wake temperature excess.

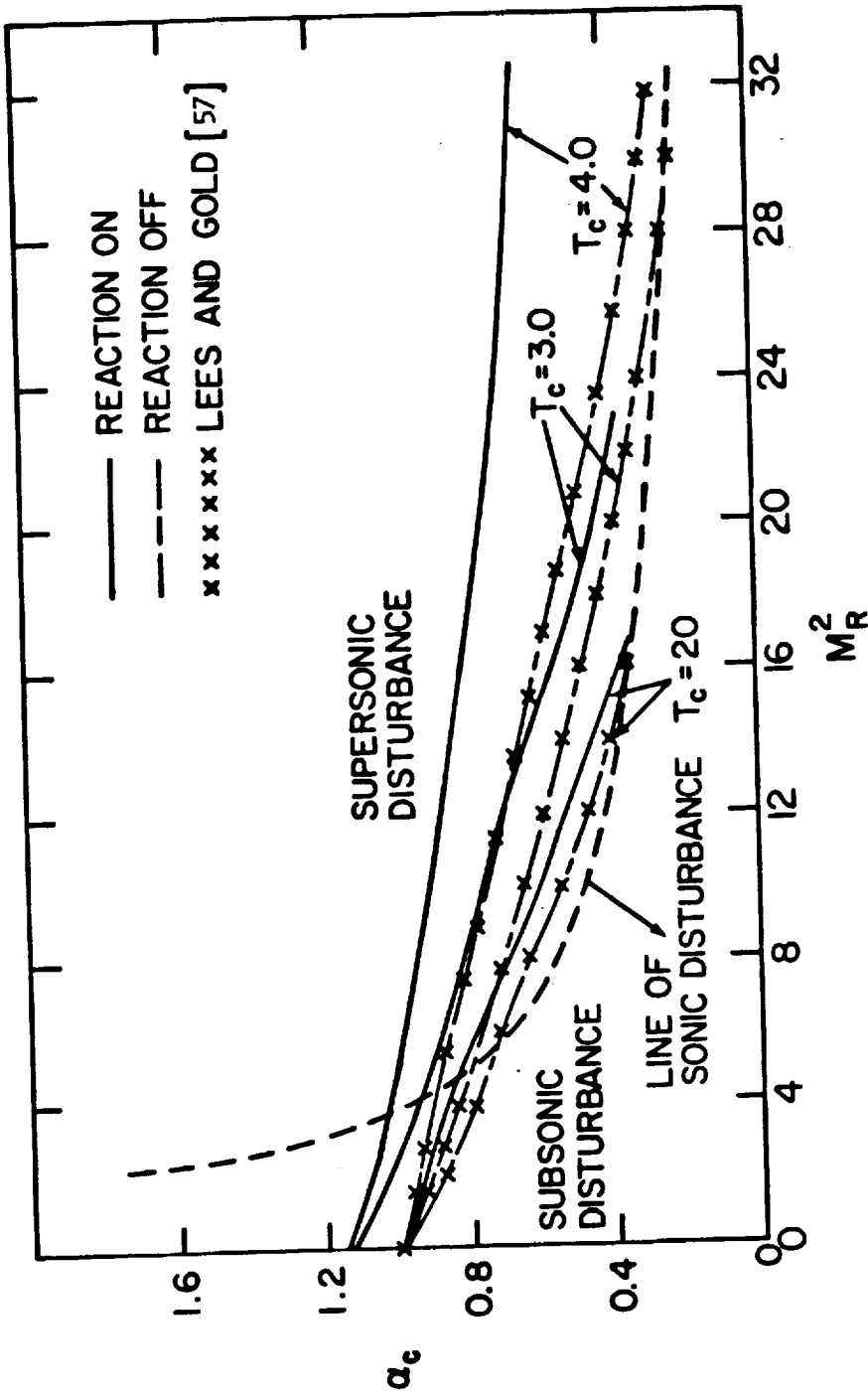


Figure 5 Neutral wave numbers as a function of relative Mach number and wake temperature excess.

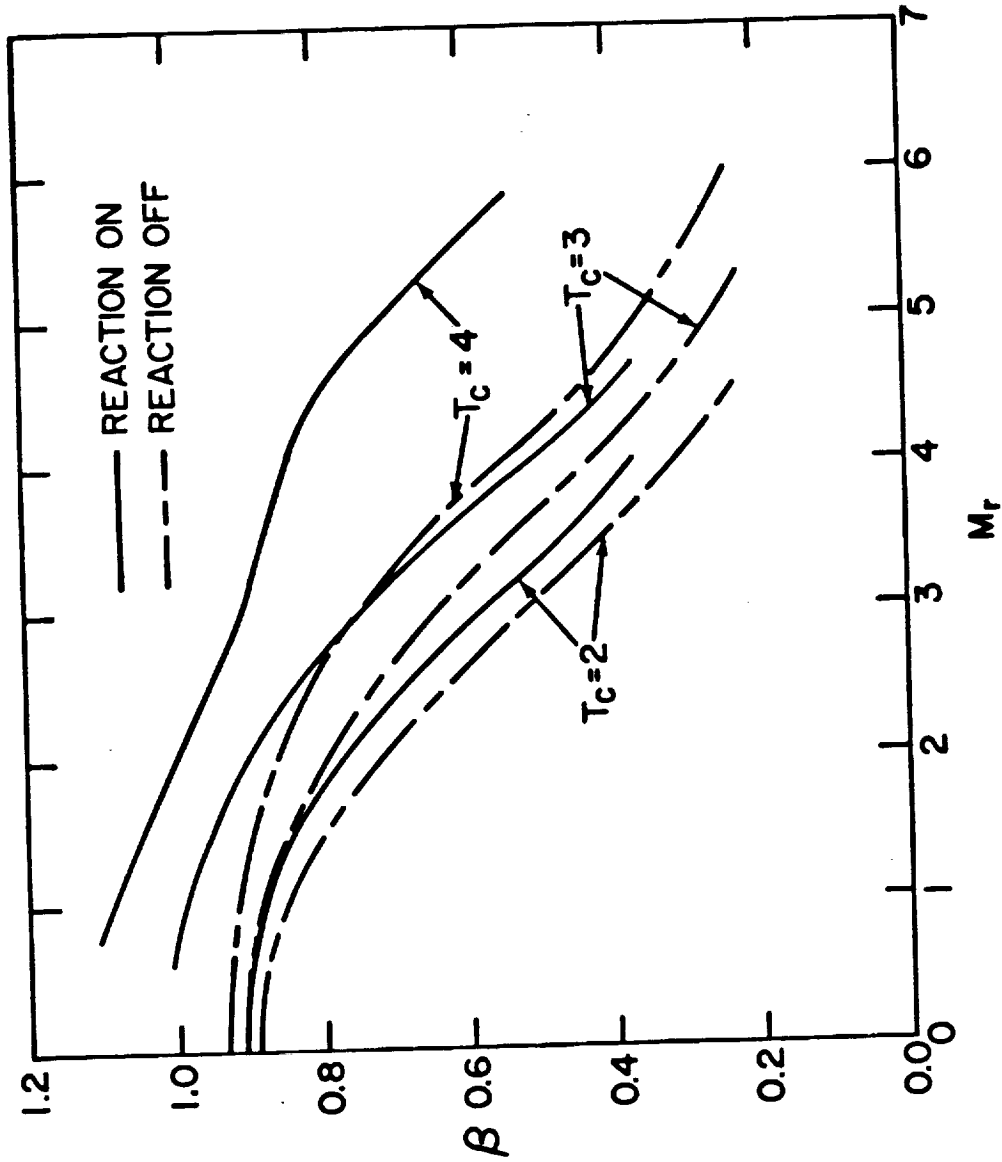


Figure 6 Spatial neutral wave frequency as a function of relative Mach number and wake temperature excess.

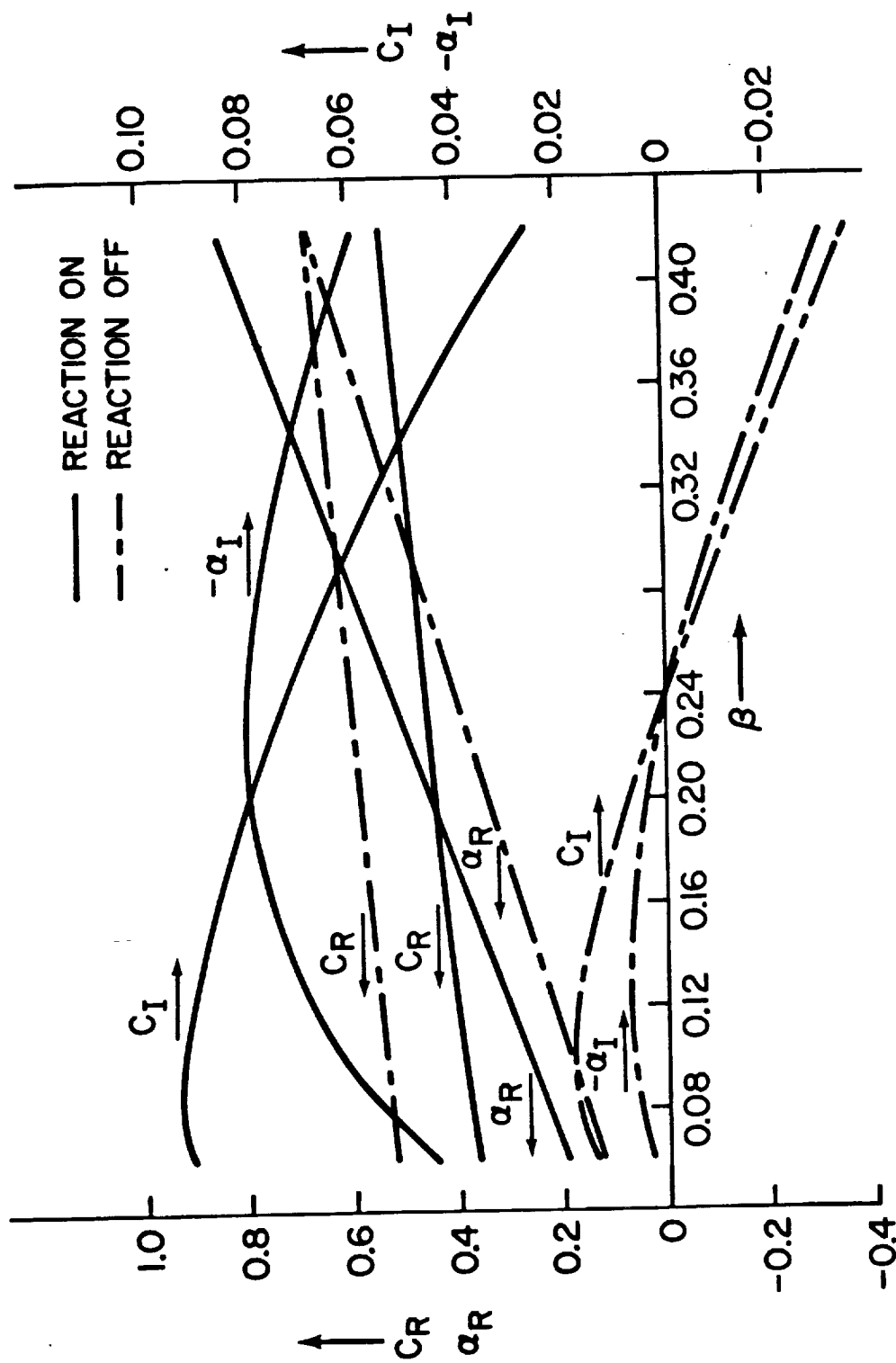


Figure 7 The eigenvalues for symmetrical oscillations as a function of wave frequency.

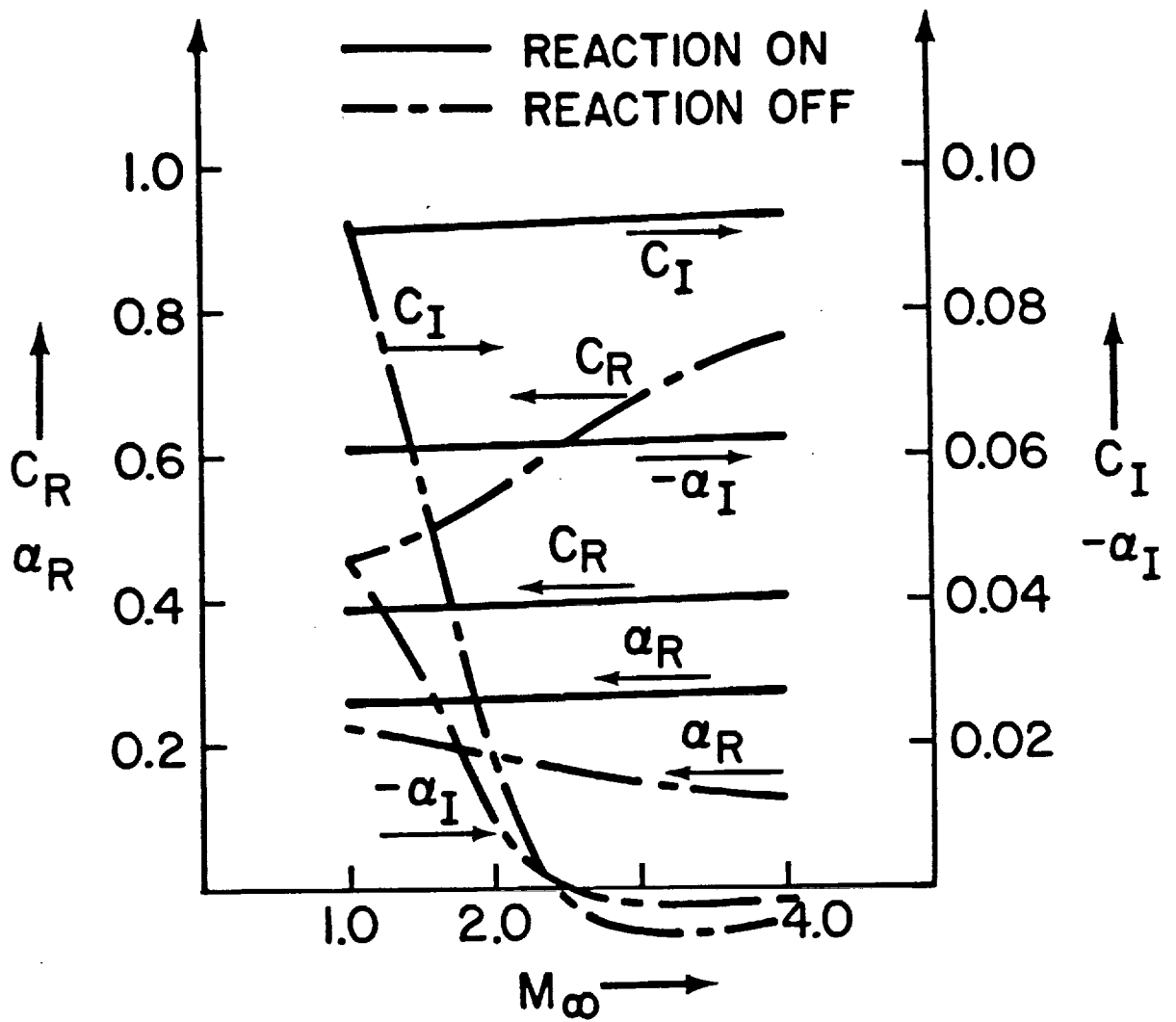


Figure 8 The eigenvalues for symmetrical oscillations as a function of free stream Mach number.

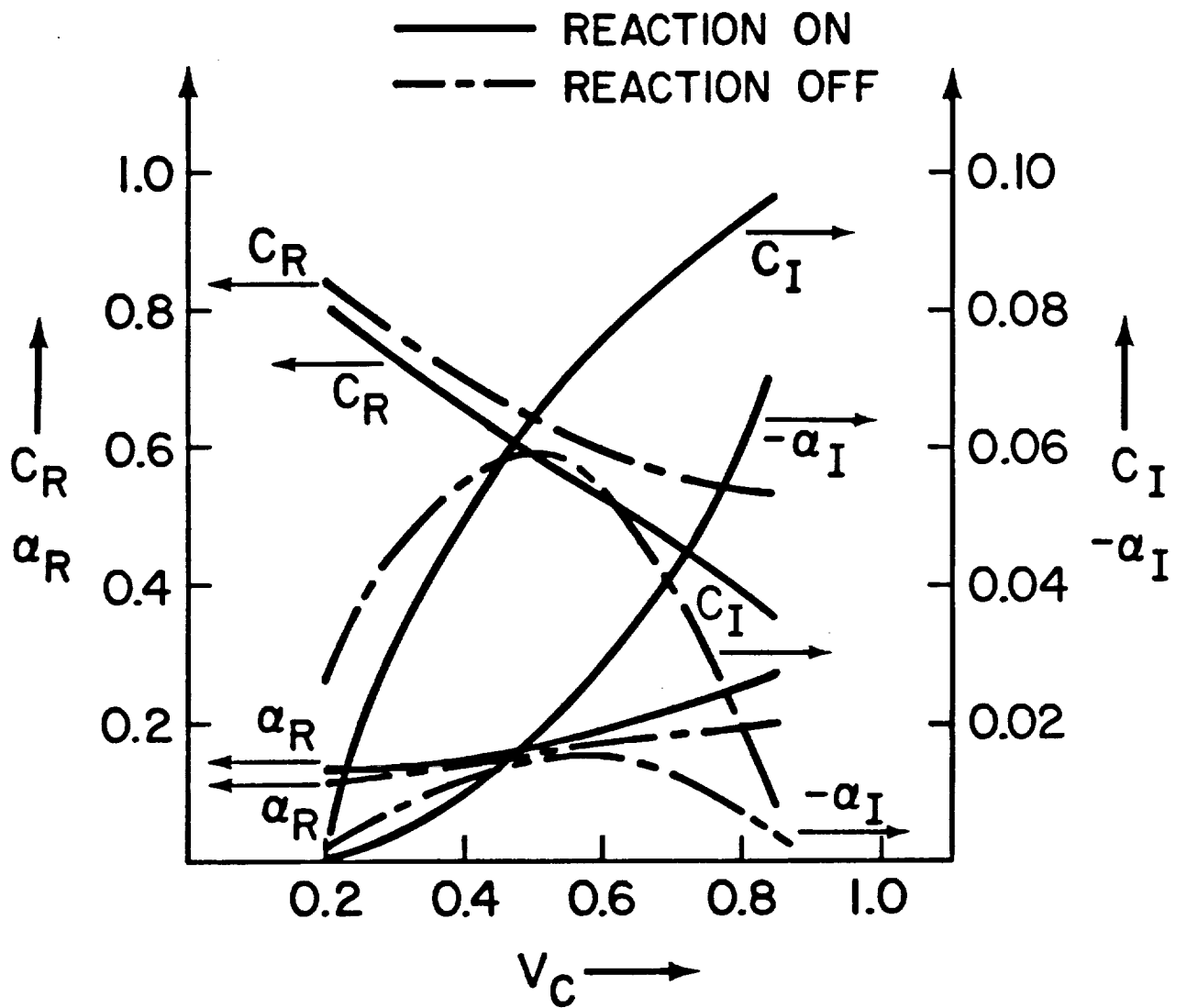


Figure 9 The eigenvalues for symmetrical oscillations as a function of wake velocity defect.

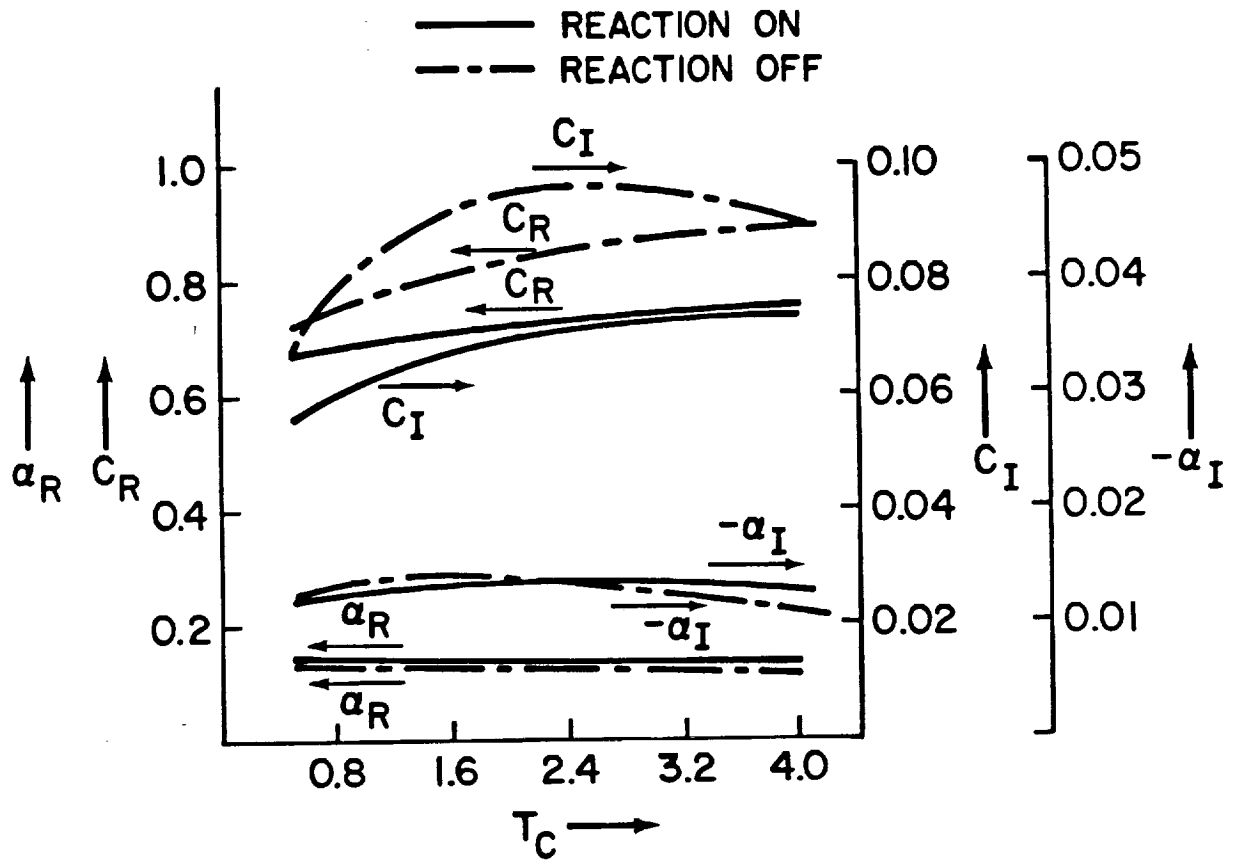


Figure 10 The eigenvalues for symmetrical oscillations as a function of wake temperature excess.

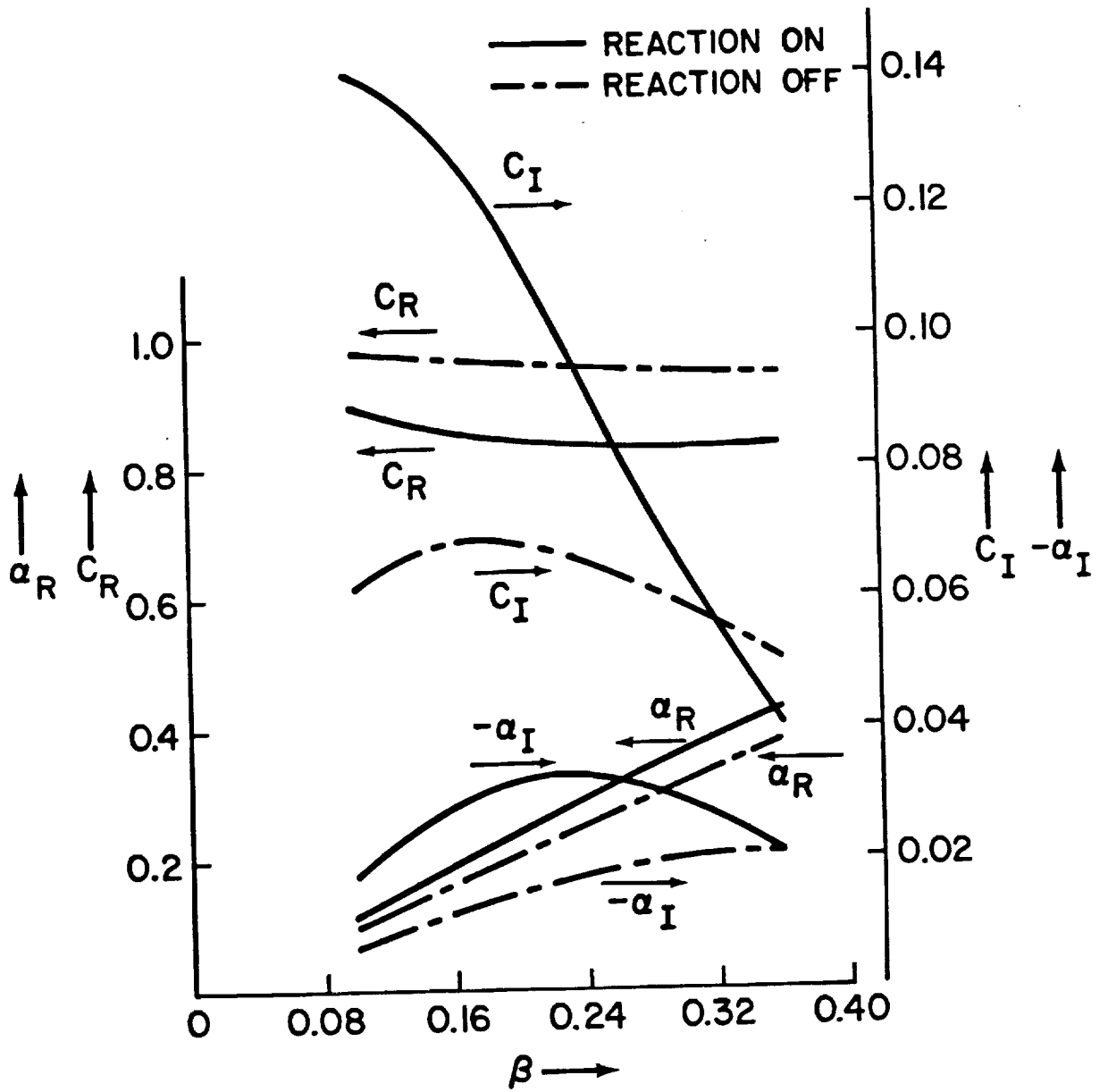


Figure 11 The eigenvalues for anti-symmetrical oscillations as a function of wave frequency.

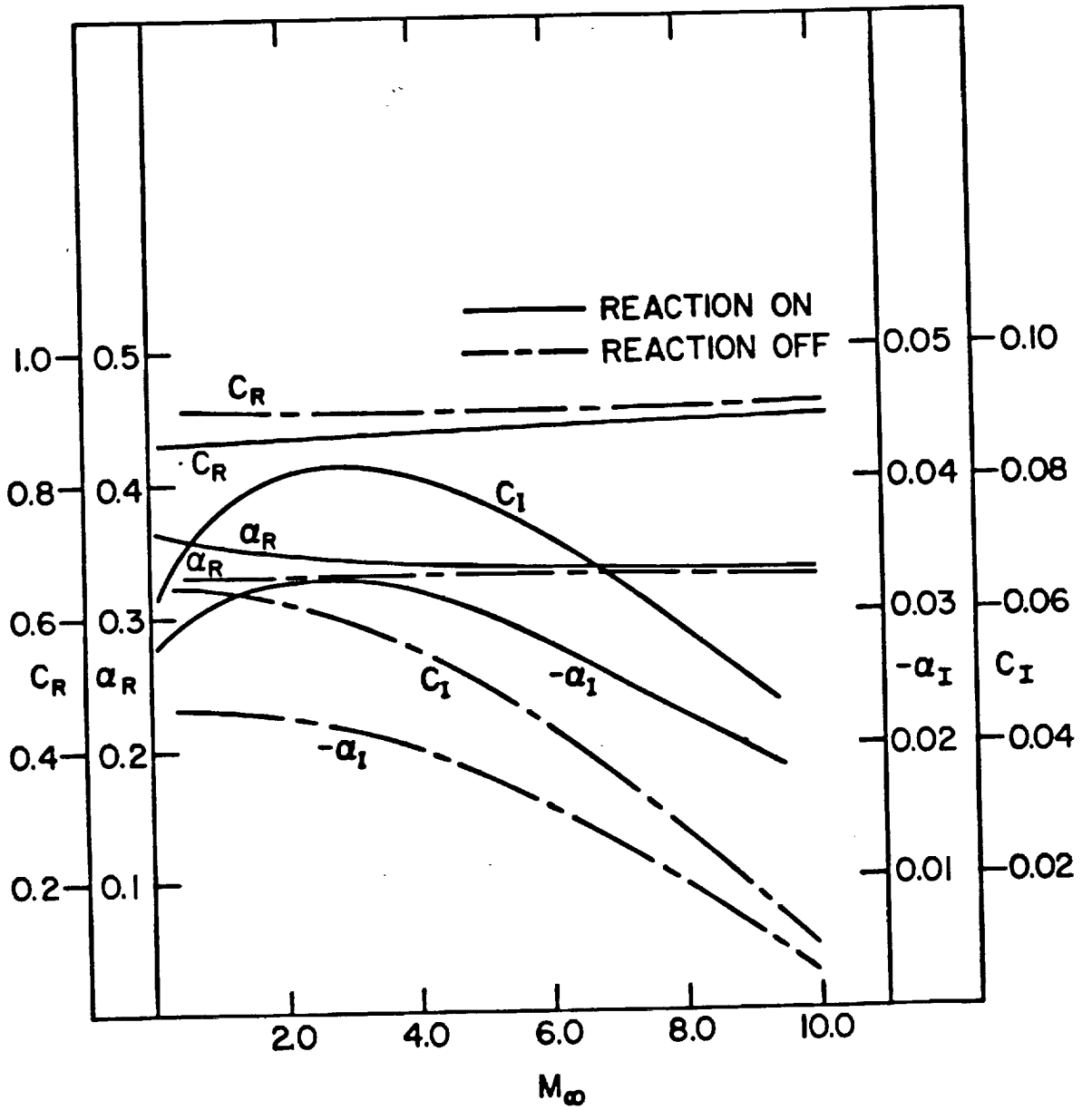


Figure 12 The eigenvalues for anti-symmetrical oscillations as a function of free stream Mach number.

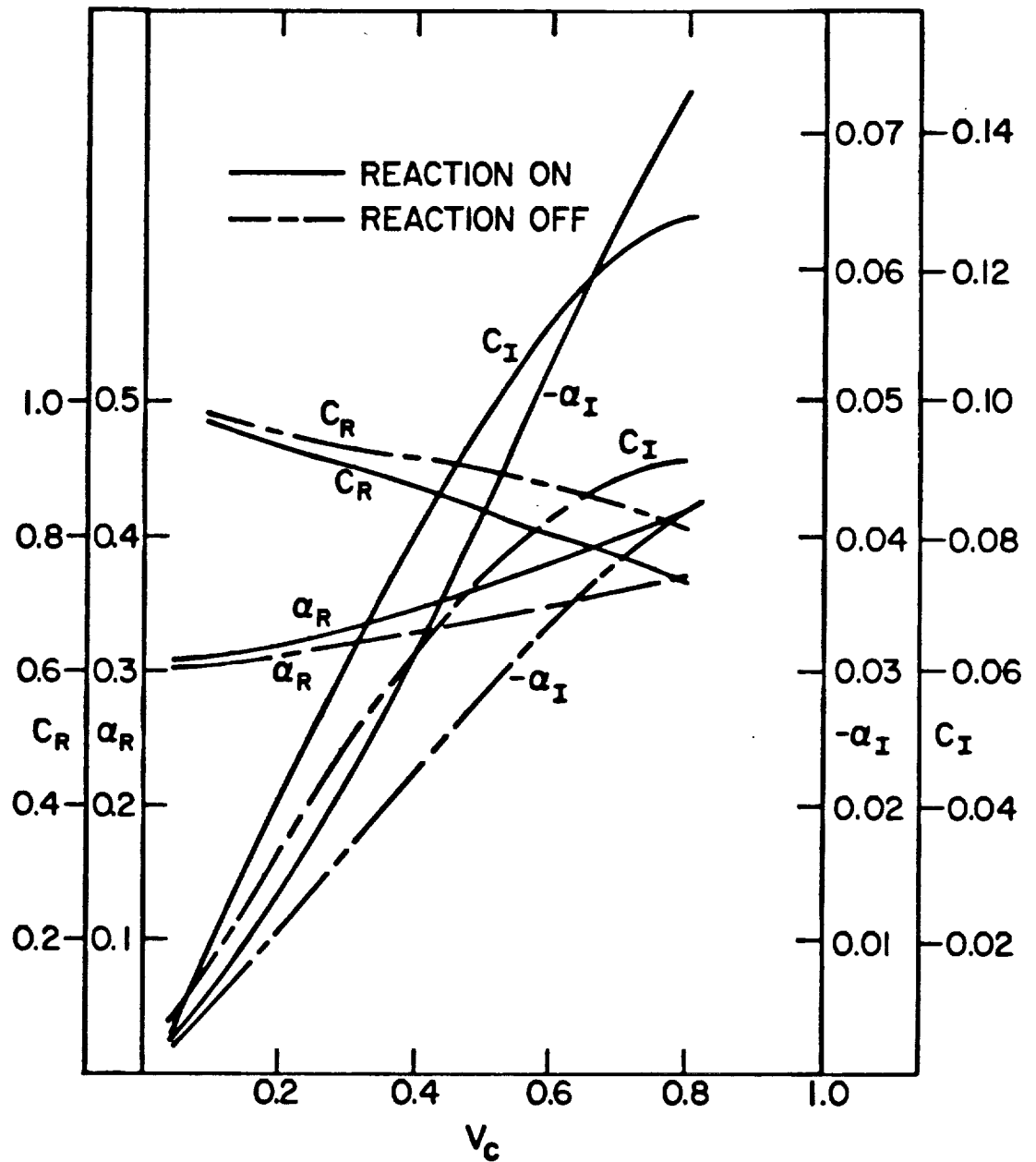


Figure 13 The eigenvalues for anti-symmetrical oscillations as a function of wake velocity defect.

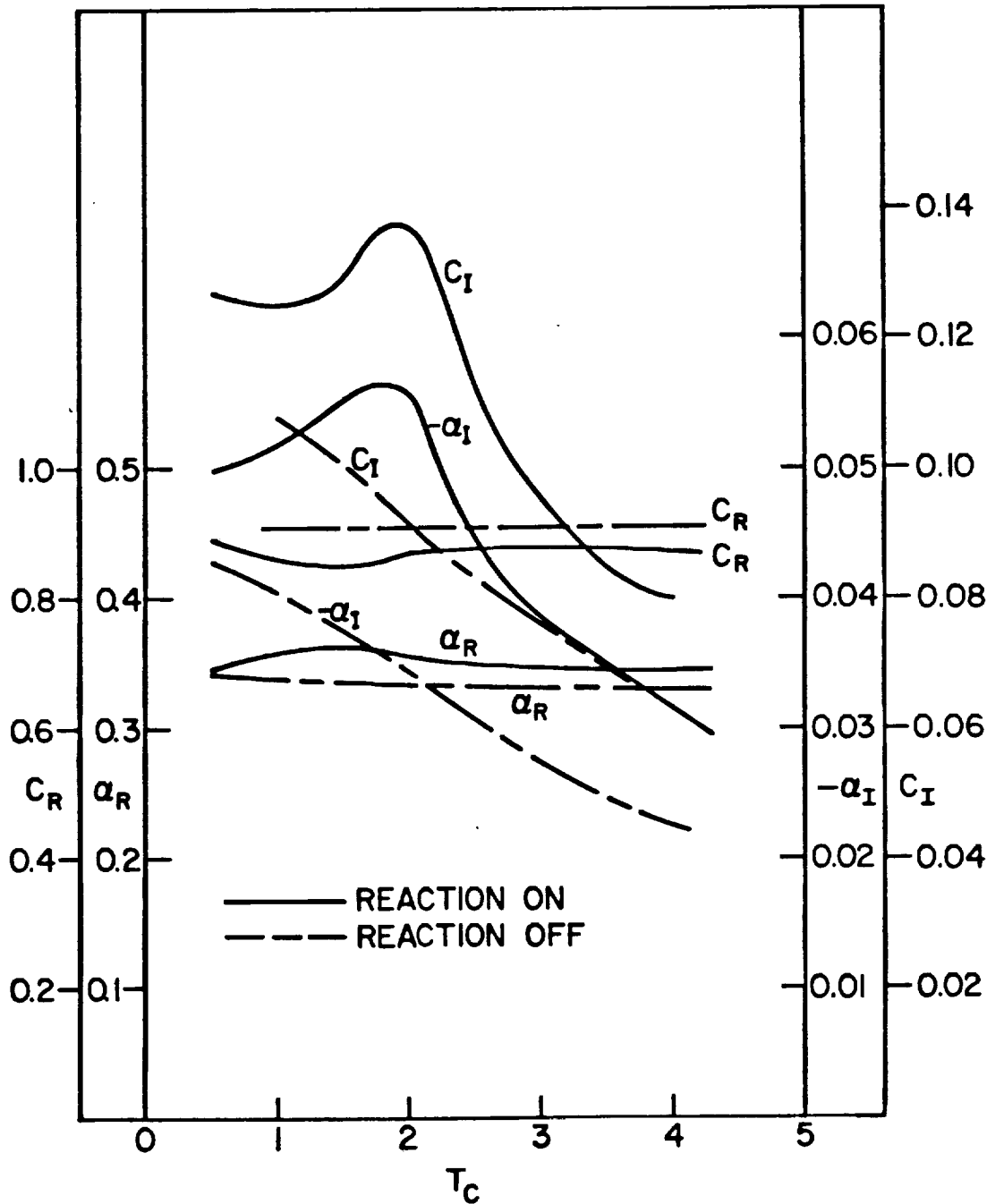


Figure 14 The eigenvalues for anti-symmetrical oscillations as a function of wake temperature excess.

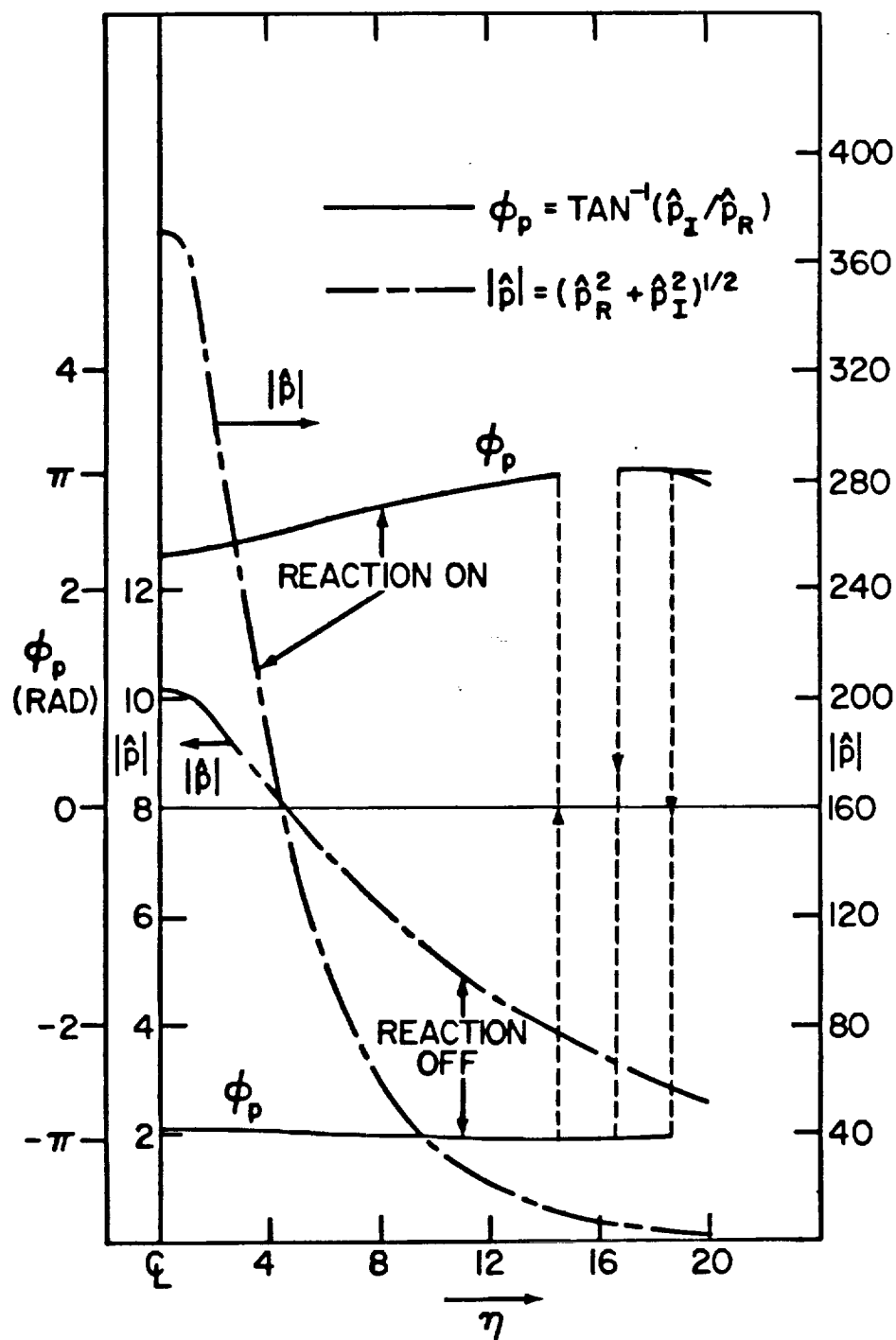


Figure 15 The characteristic variation of the pressure eigenfunction amplitude $|\hat{p}|$ and phase ϕ_p across the shear layer. For symmetrical oscillation, $\hat{p}'(0) = 0$ and $M_\infty = 2$, $\beta = 0.1$, $T_\infty = 1500^\circ\text{K}$.

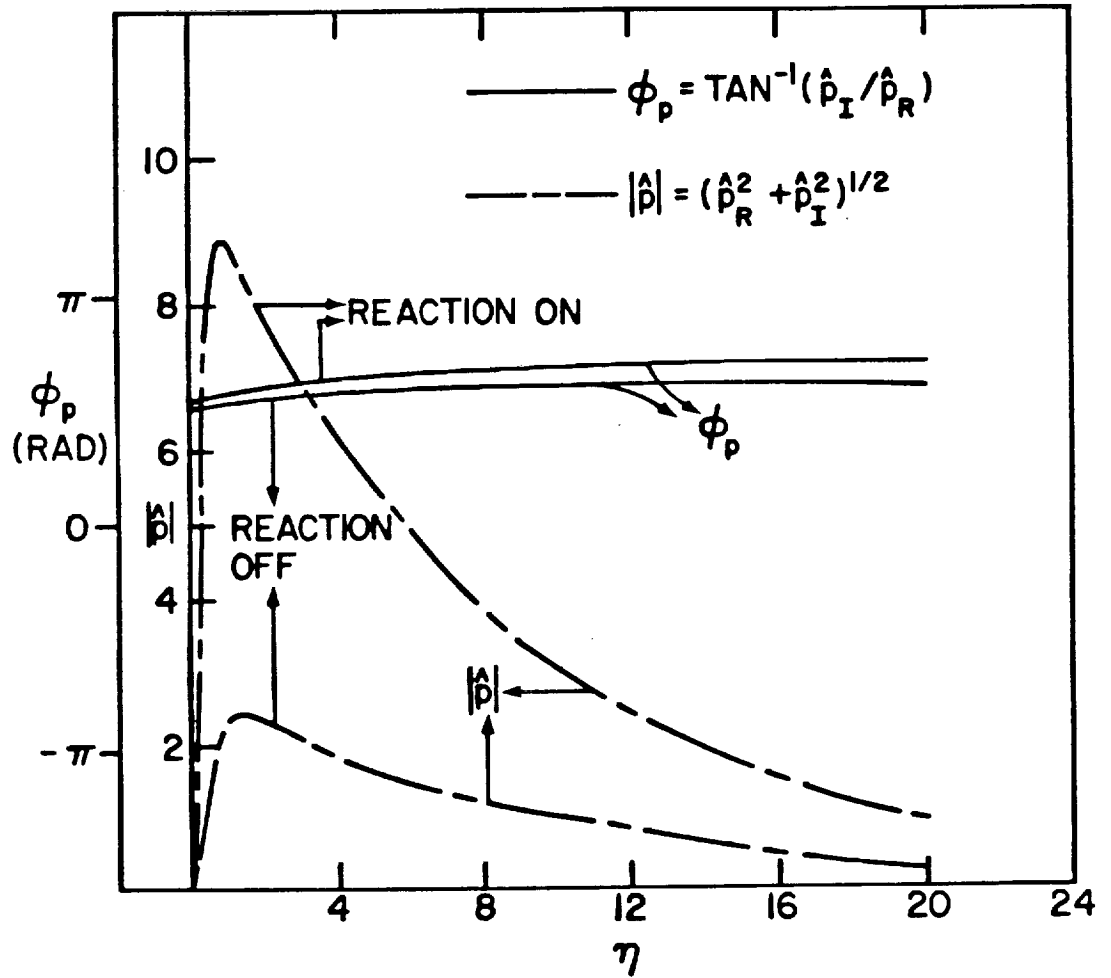


Figure 16 The characteristic variation of the pressure eigenfunction amplitude $|\hat{p}|$ and phase ϕ_p across the shear layer. For anti-symmetrical oscillation, $\hat{p}(0) = 0$ and $M_\infty = 2$, $\beta = 0.1$, $T_\infty = 1500^\circ\text{K}$.

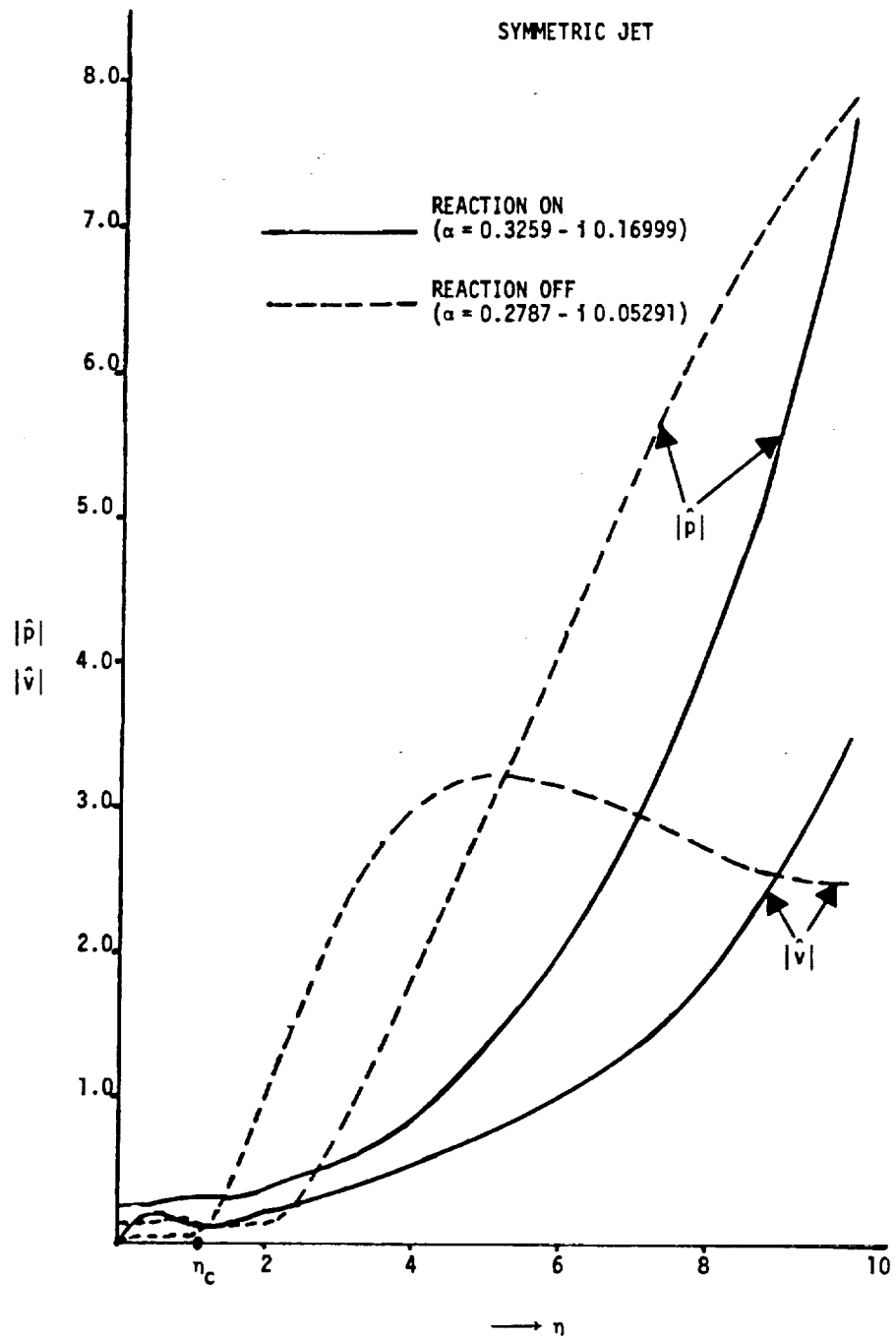


Figure 17 The characteristic variation of the amplitudes of pressure eigenfunction $|\hat{p}(\eta)|$ and vertical velocity eigenfunction $|\hat{v}(\eta)|$ across a symmetric jet. For symmetrical oscillations, $M_\infty = 2.0$, $T_\infty = 1500^\circ\text{K}$, $T_c = 3.0$ and $\beta = 0.1$.

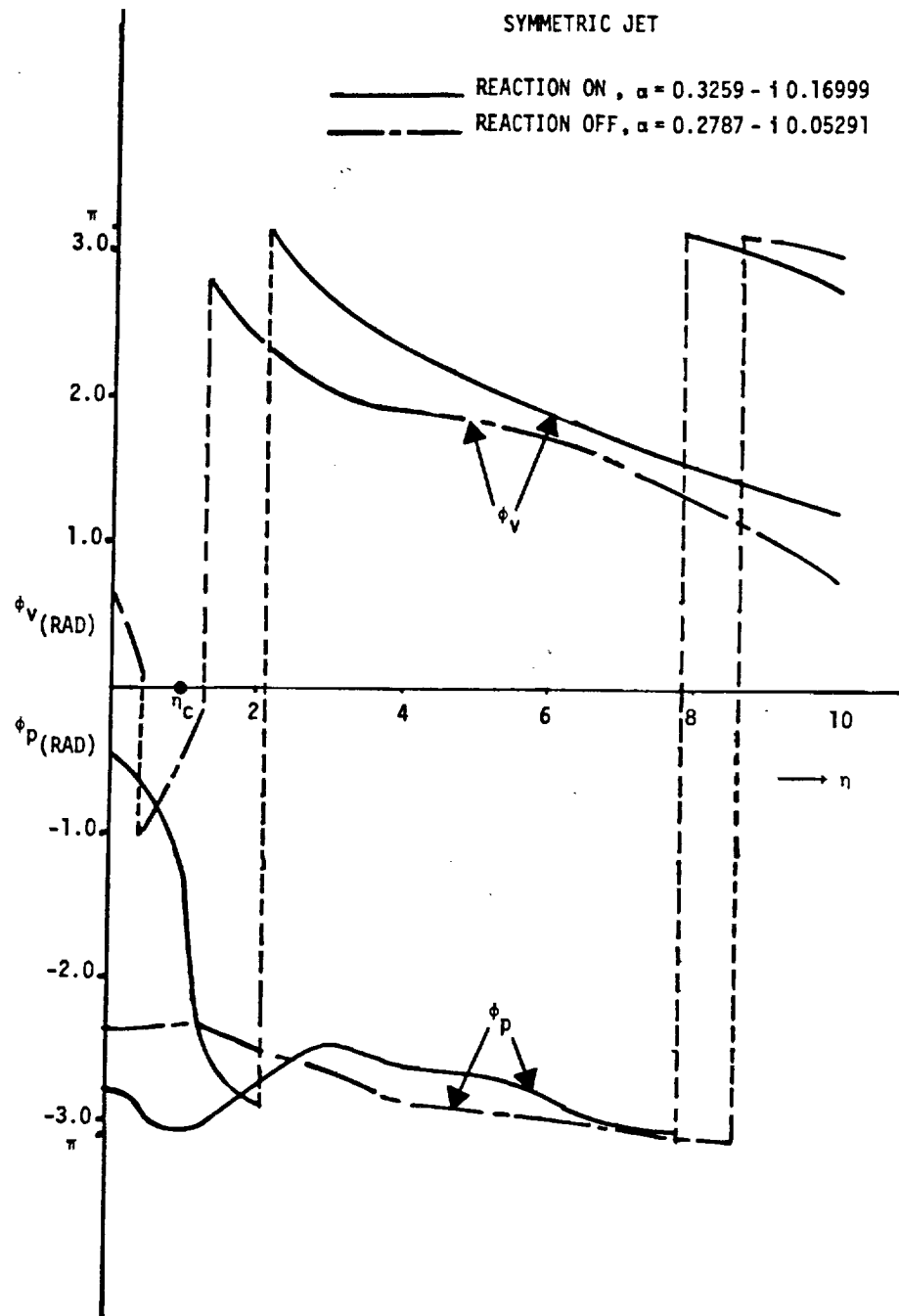


Figure 18 Phase changes of the pressure eigenfunction ϕ_p and vertical velocity eigenfunction ϕ_v across a symmetric jet. Test conditions same as in Figure 17.

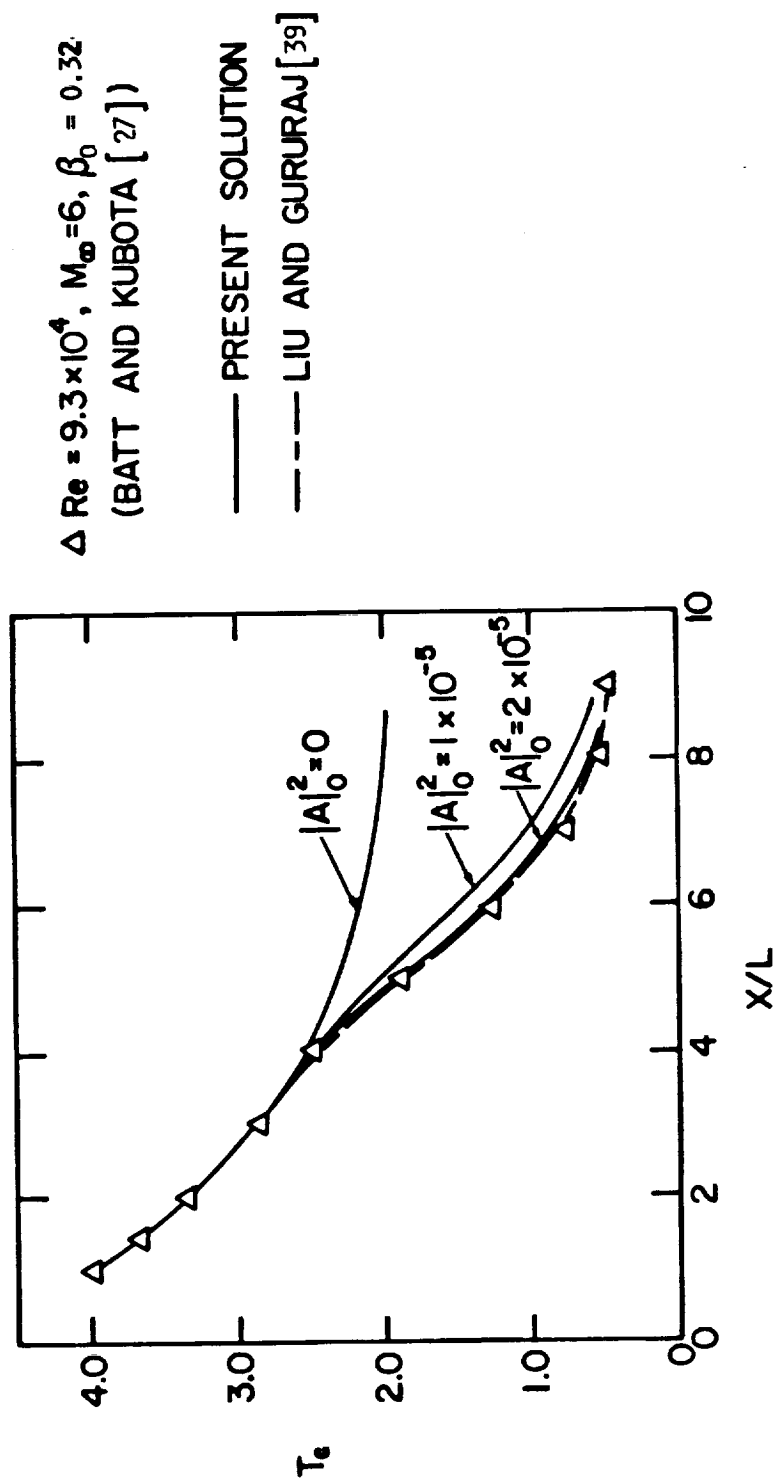


Figure 19 Variation of the centerline mean flow temperature excess for various initial amplitudes of the coherent structure. Laminar non reactive test case [39] for adiabatic flat plate wake at $M_\infty = 6, \text{Re}_L = 93,000, L = 2.54\text{cm}, x_0 = 1, V_{C_0} = 0.4, T_{C_0} = 4.0, (Y_{k_{C_0}} = 0.0; k = 1, 4), \beta_0 = 0.32.$

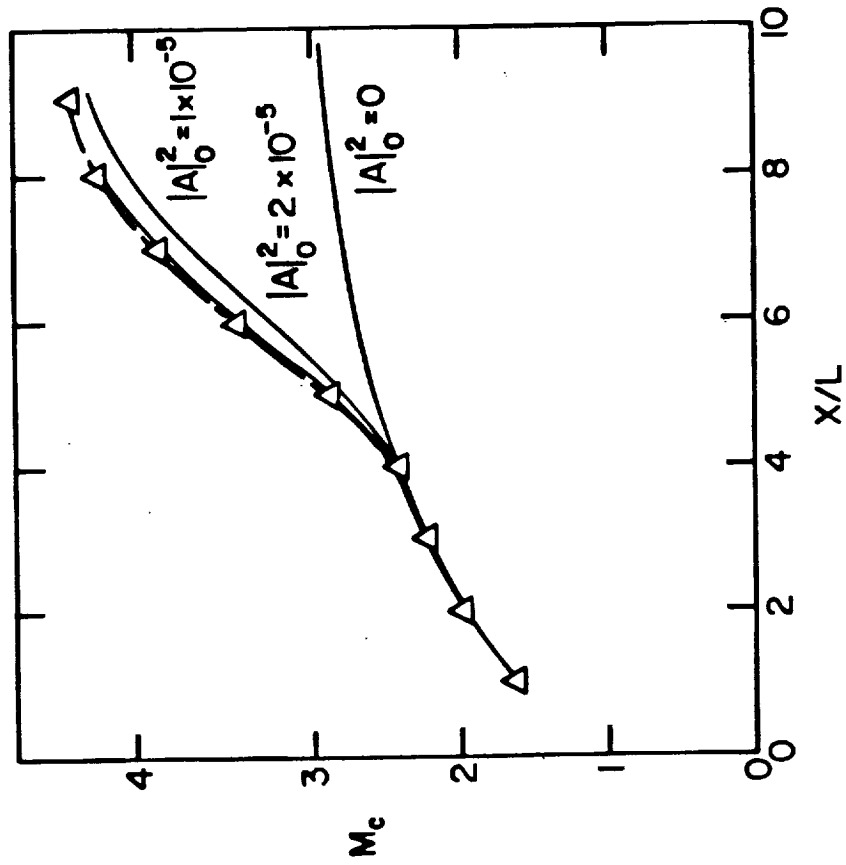


Figure 20 Variation of the centerline Mach number for various initial amplitudes of the coherent structure. Laminar non reactive case [39] for adiabatic flat plate wake at $M_\infty = 6$, $Re_L = 93,000$, $L = 2.54\text{cm}$, $x_0 = 1$, $V_{C_0} = 0.4$, $T_{C_0} = 4.0$, $(Y_{k_{C_0}} = 0.0, k = 1, 4)$, $\beta_0 = 0.32$

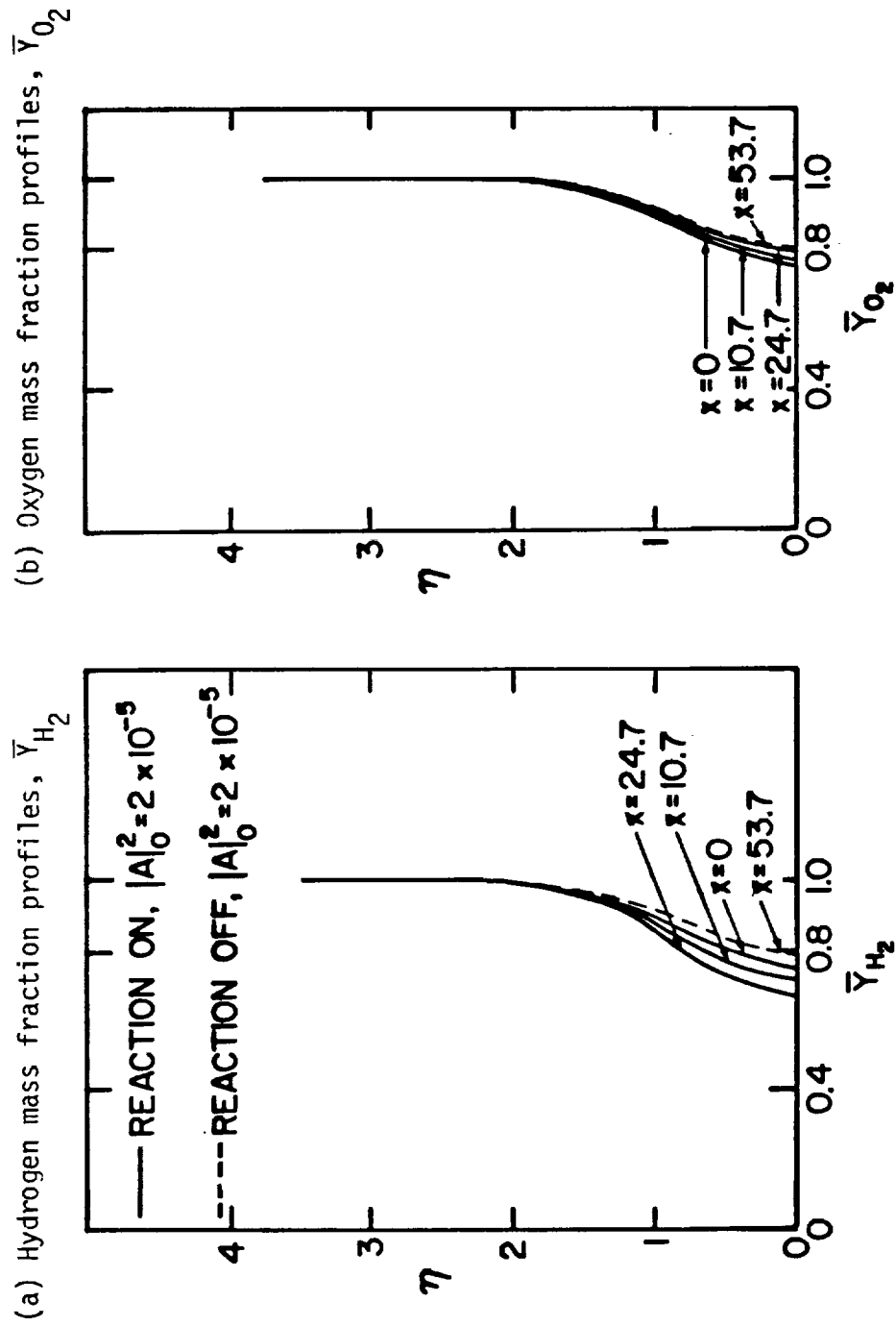


Figure 21 Mean flow specie mass fraction profiles across the wake at various axial locations for both non reactive and reactive cases. Laminar test case at $M_\infty = 2.0$, $T_\infty = 1200^\circ K$, ($Y_{k\infty} = 0.05, 0.90, 0.025, 0.025$), $L = 2.54cm$, $Re_L = 93,000$, $x_0 = 1.0$, $V_{c_0} = 0.4$, $T_{c_0} = 4.0$, $Y_{k\infty} = -0.25, -0.25, 3.0, 6.5$), $|A|_0^2 = 2 \times 10^{-5}$, $\beta = 0.3$

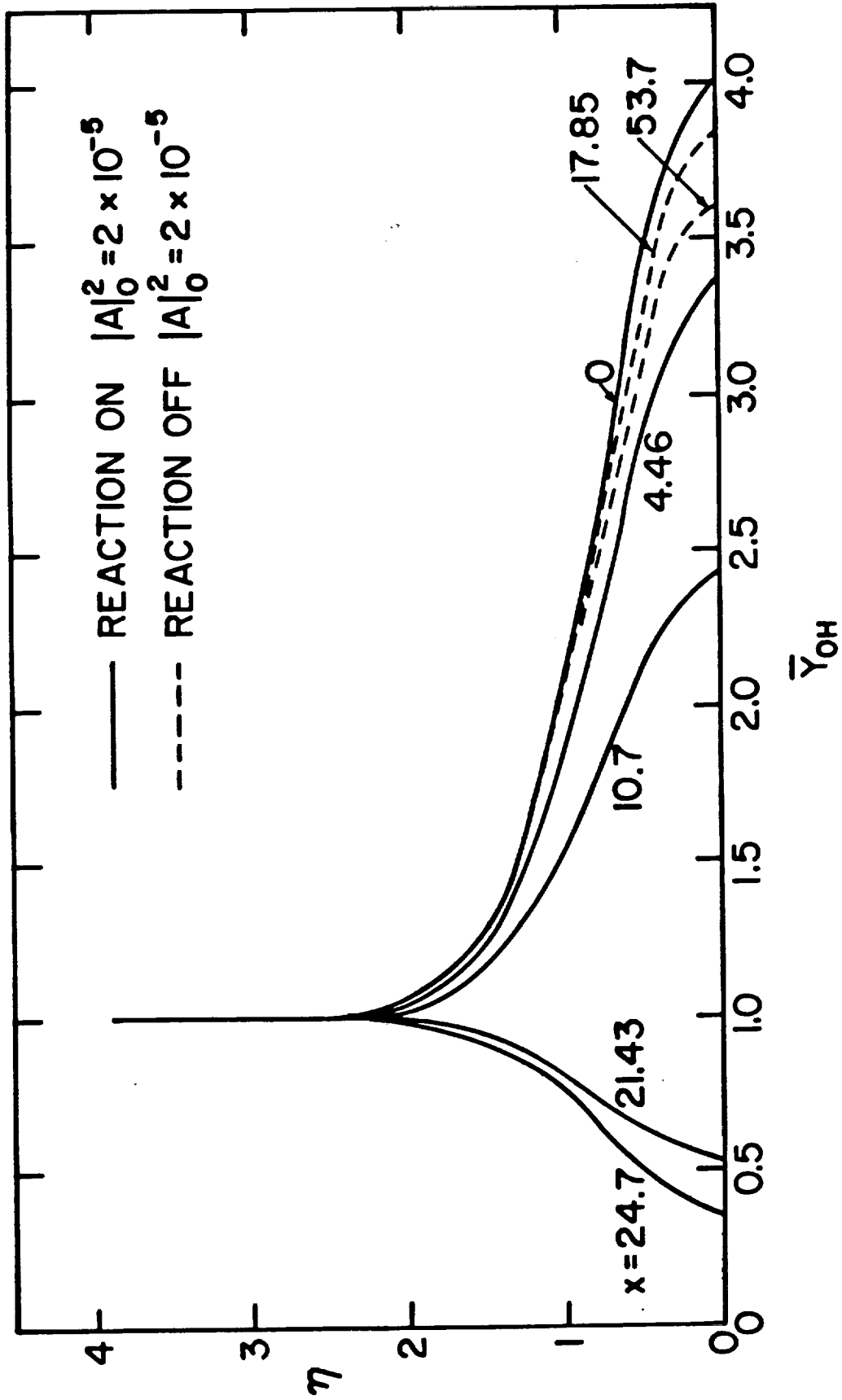


Figure 21c Hydroxyl mass fraction profiles, \bar{Y}_{OH} .

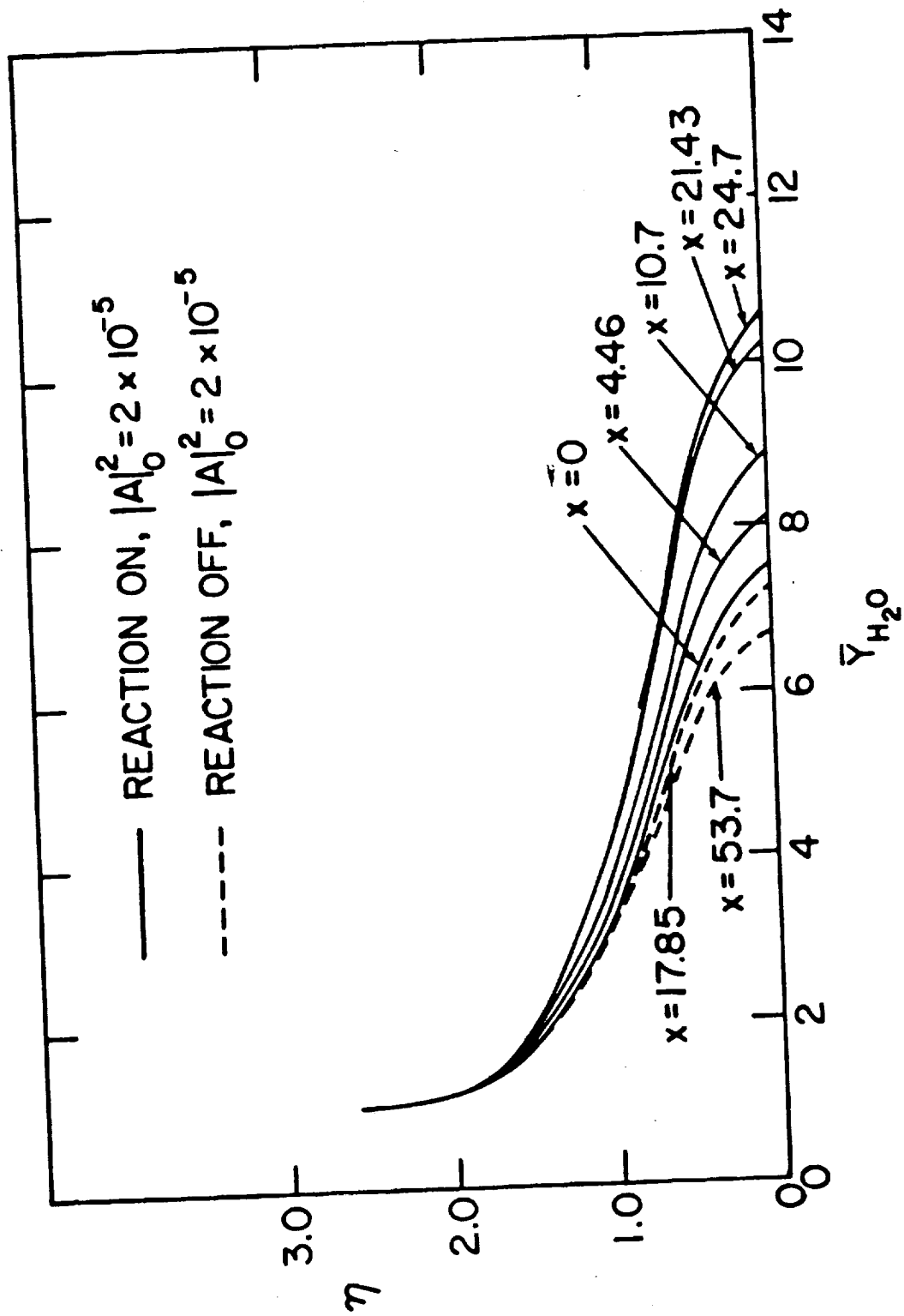


Figure 21d Water mass fraction profiles, \bar{Y}_{H_2O}

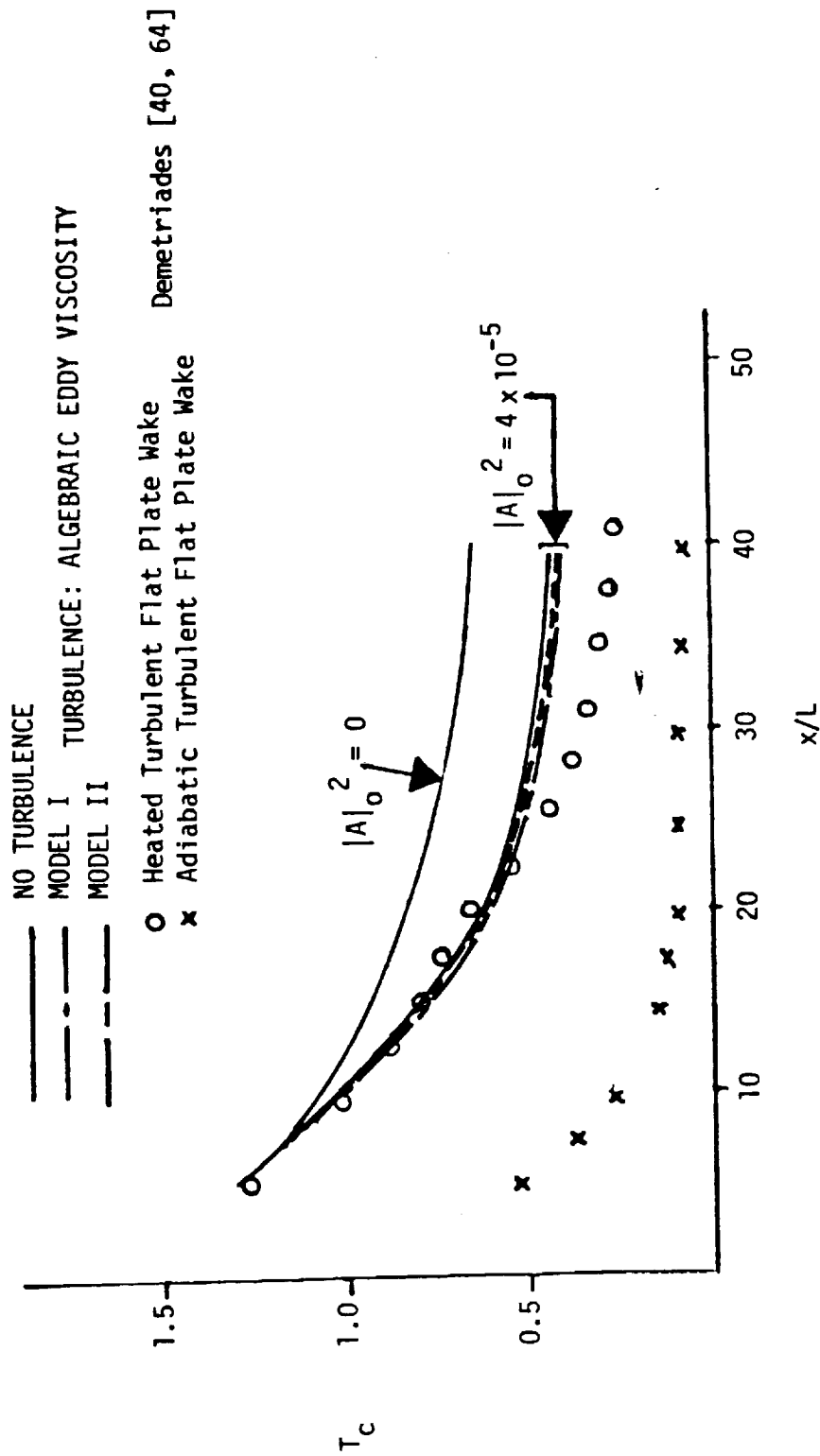


Figure 22 Decay of centerline mean flow temperature excess for non reactive turbulent wake behind flat plate at $U_\infty = 3.0$, $Re = 70,000/cm$, $\beta_0 = 0.3$, $C_D = 0.031$, $x_0 = 5.0$, $V_{C_0} = 0.23$, $T_{C_0} = 1.275$, $|A|_0^2 = 4 \times 10^{-5}$.

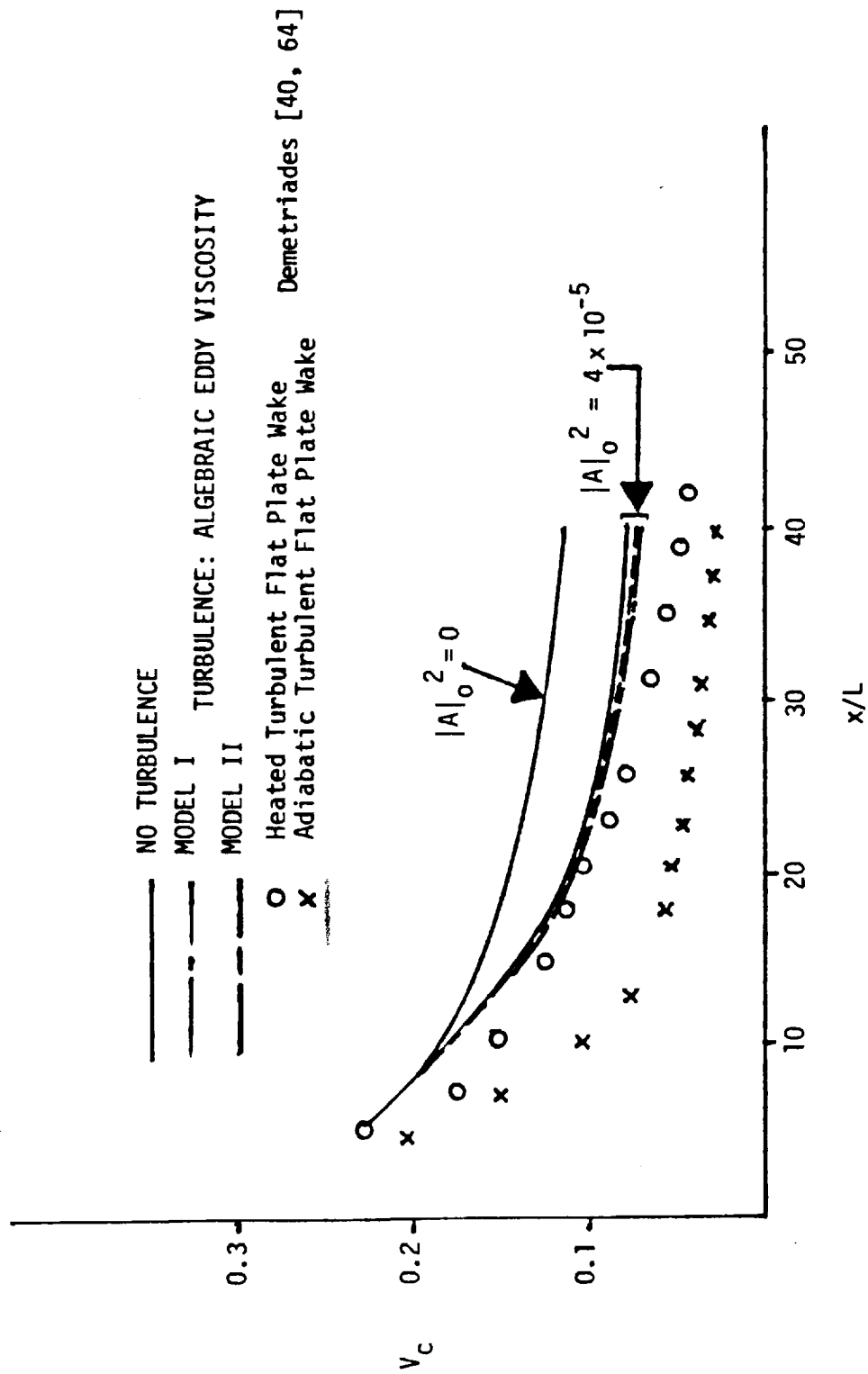


Figure 23 Decay of centerline mean flow velocity defect for non reactive turbulent wake behind flat plate at $M_\infty = 3.0$, $Re = 70,000/cm$, $\delta_0 = 0.3$, $C_D = 0.031$, $x_0 = 5.0$, $V_{c_0} = 0.23$, $T_{c_0} = 1.275$, $|A|_0^2 = 4 \times 10^{-5}$.

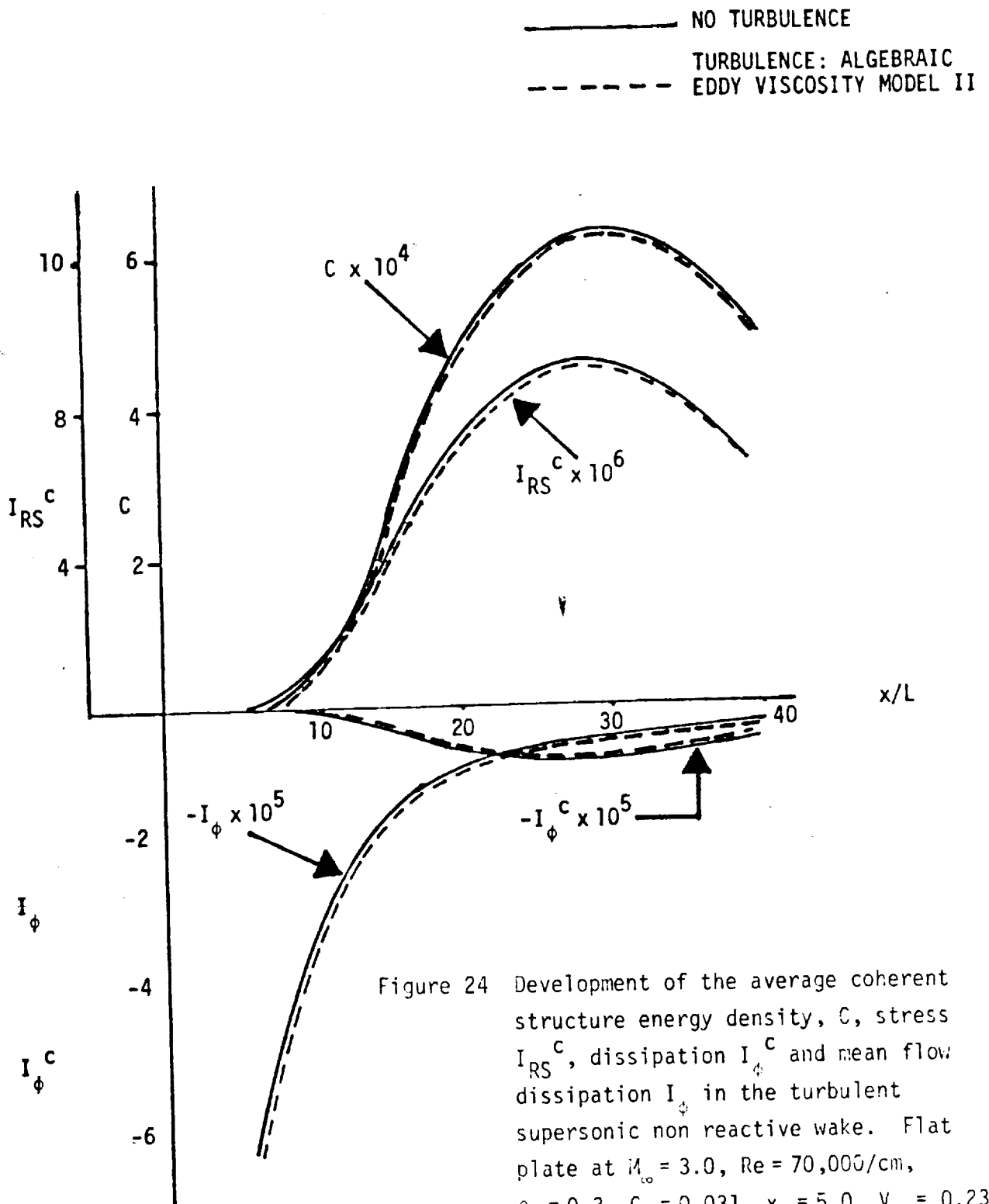


Figure 24 Development of the average coherent structure energy density, C , stress I_{RS}^C , dissipation I_ϕ^C and mean flow dissipation I_ϕ in the turbulent supersonic non reactive wake. Flat plate at $M_o = 3.0$, $Re = 70,000/cm$, $\beta_o = 0.3$, $C_D = 0.031$, $x_o = 5.0$, $V_{C_o} = 0.23$, $T_{C_o} = 1.275$, $|A|_o^2 = 4 \times 10^{-5}$.

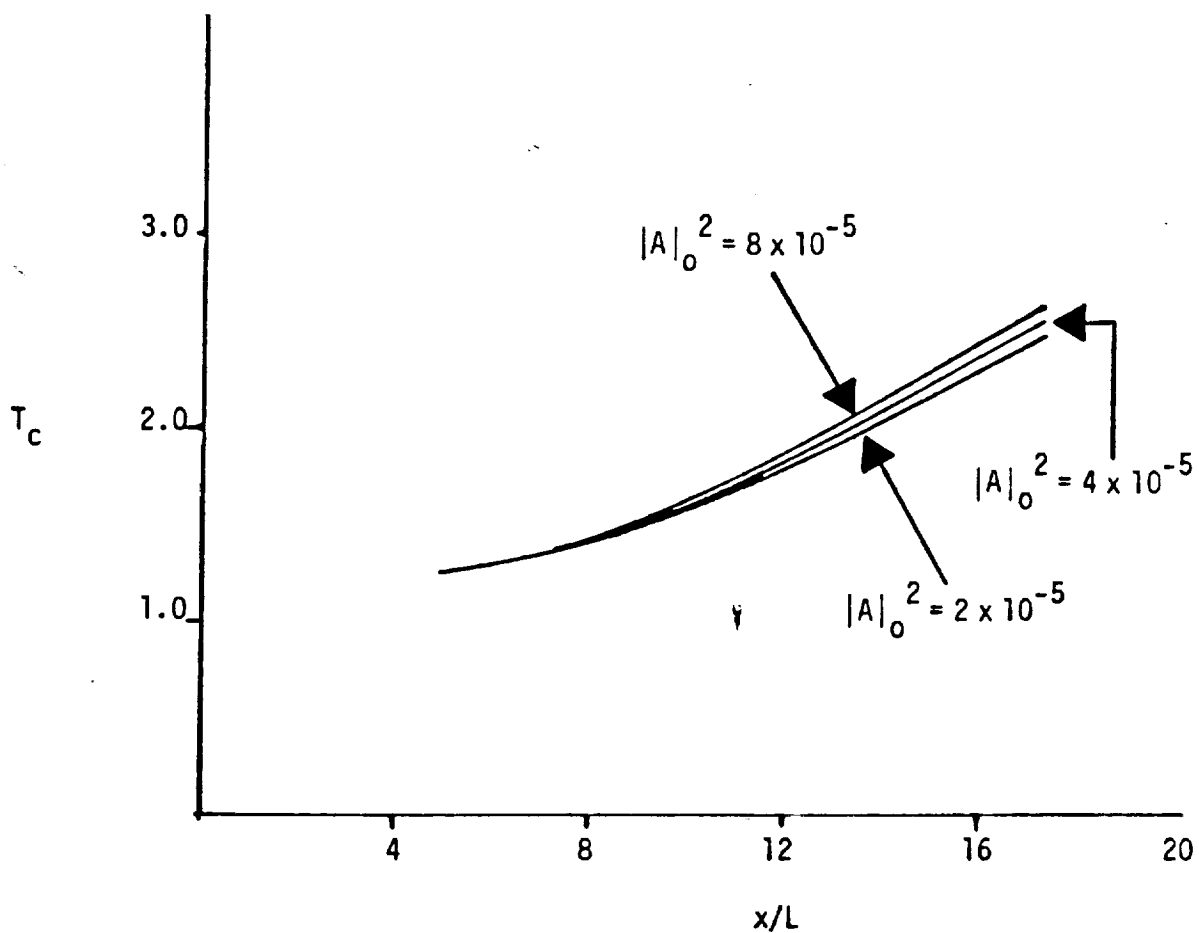


Figure 25 Growth of centerline mean flow temperature excess for various initial amplitudes of disturbance. Turbulent reactive test conditions: $M_\infty = 3.0$, $Re = 70,000/cm$, $T_\infty = 1500^\circ K$, $L = 0.3cm$, $\beta_0 = 0.2$, $x_0 = 5.0$, $V_{c_0} = 0.23$, $T_{c_0} = 1.275$, ($Y_{k_{c_0}} = 0.0$, $k = 1,4$).

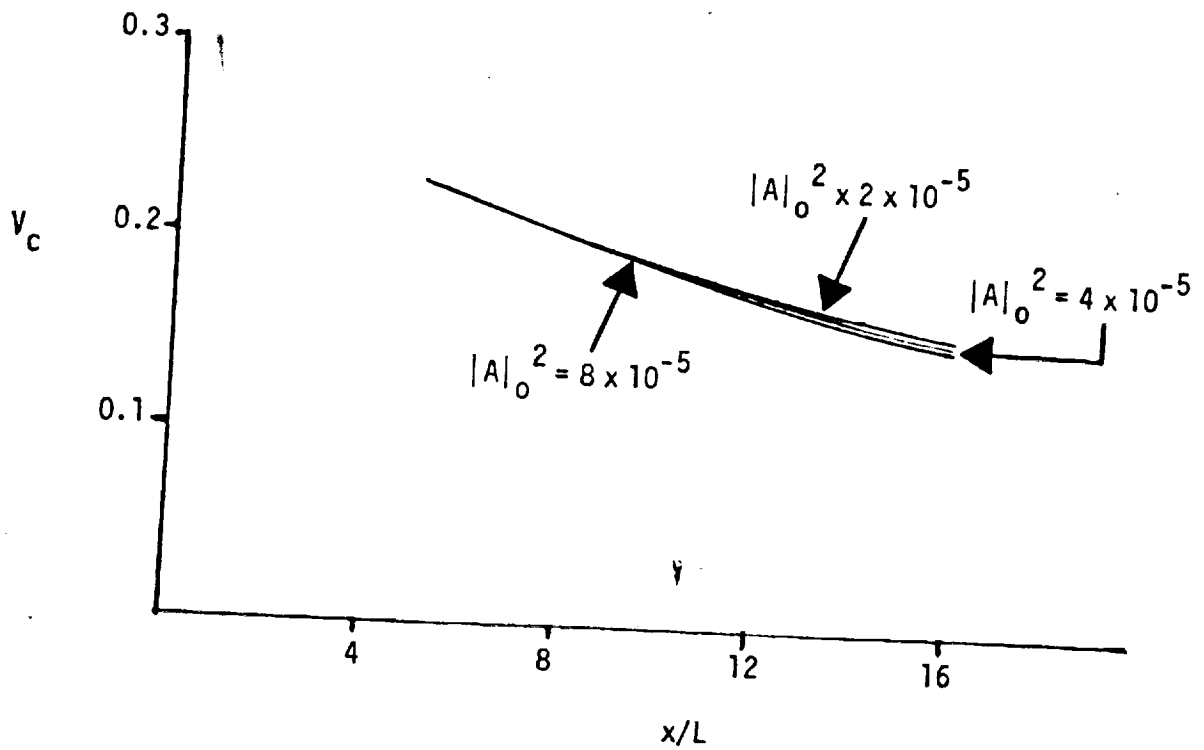
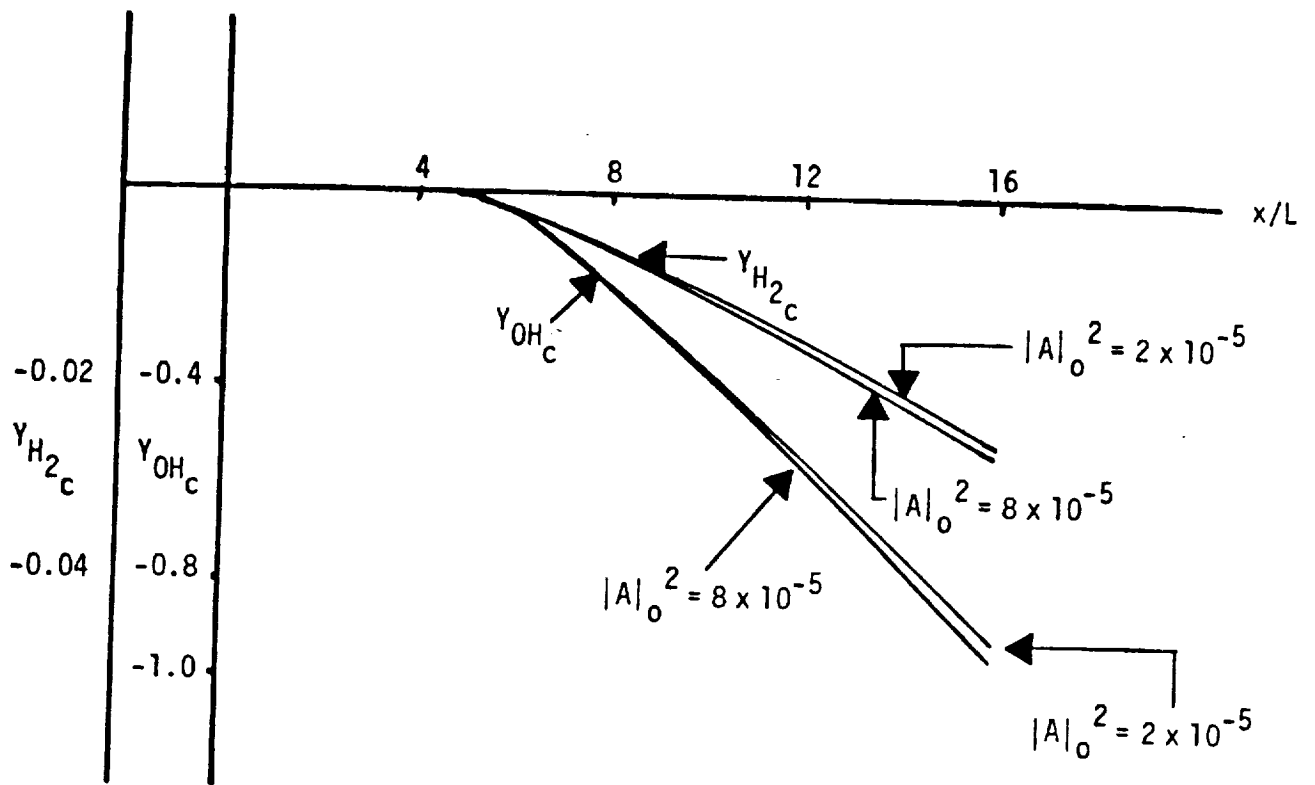
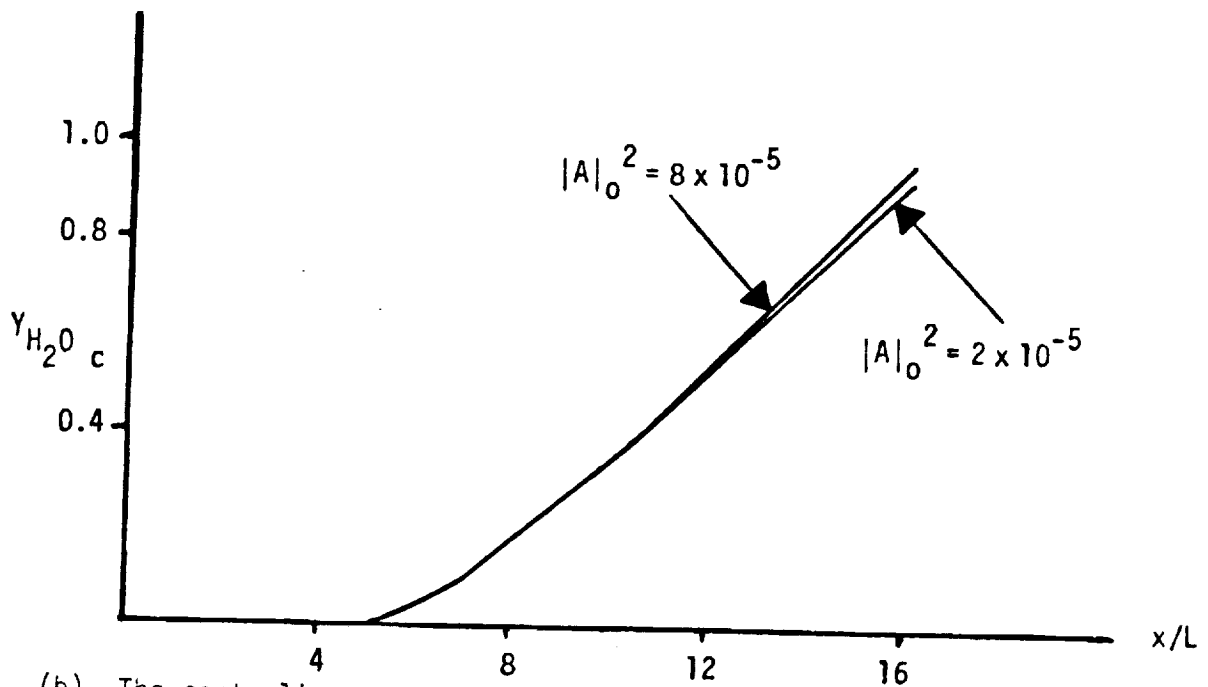


Figure 26 Decay of centerline mean flow velocity defect for various initial amplitudes of disturbance. Turbulent reactive test conditions as in Figure 25.



(a) The centerline mean flow hydrogen and hydroxyl mass fraction defects.



(b) The centerline mean flow water vapor mass fraction excess.

Figure 27 Development of the centerline mean flow specie mass fraction for various initial amplitudes of disturbance. Turbulent reactive test conditions as in Figure 25.

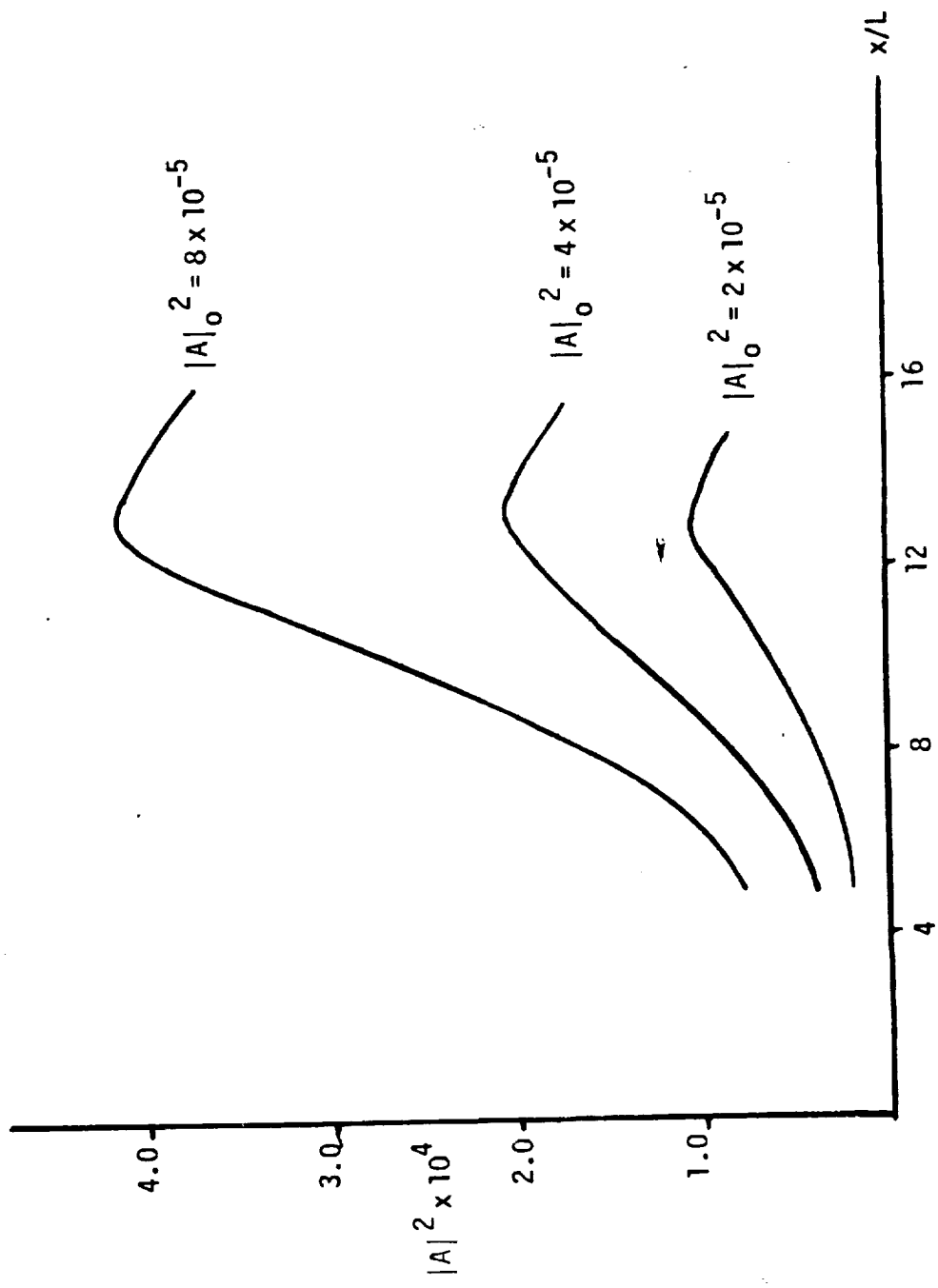


Figure 23 Growth and decay characteristics of the amplitude of coherent structure for various initial values. Turbulent reactive test conditions as in Figure 25.

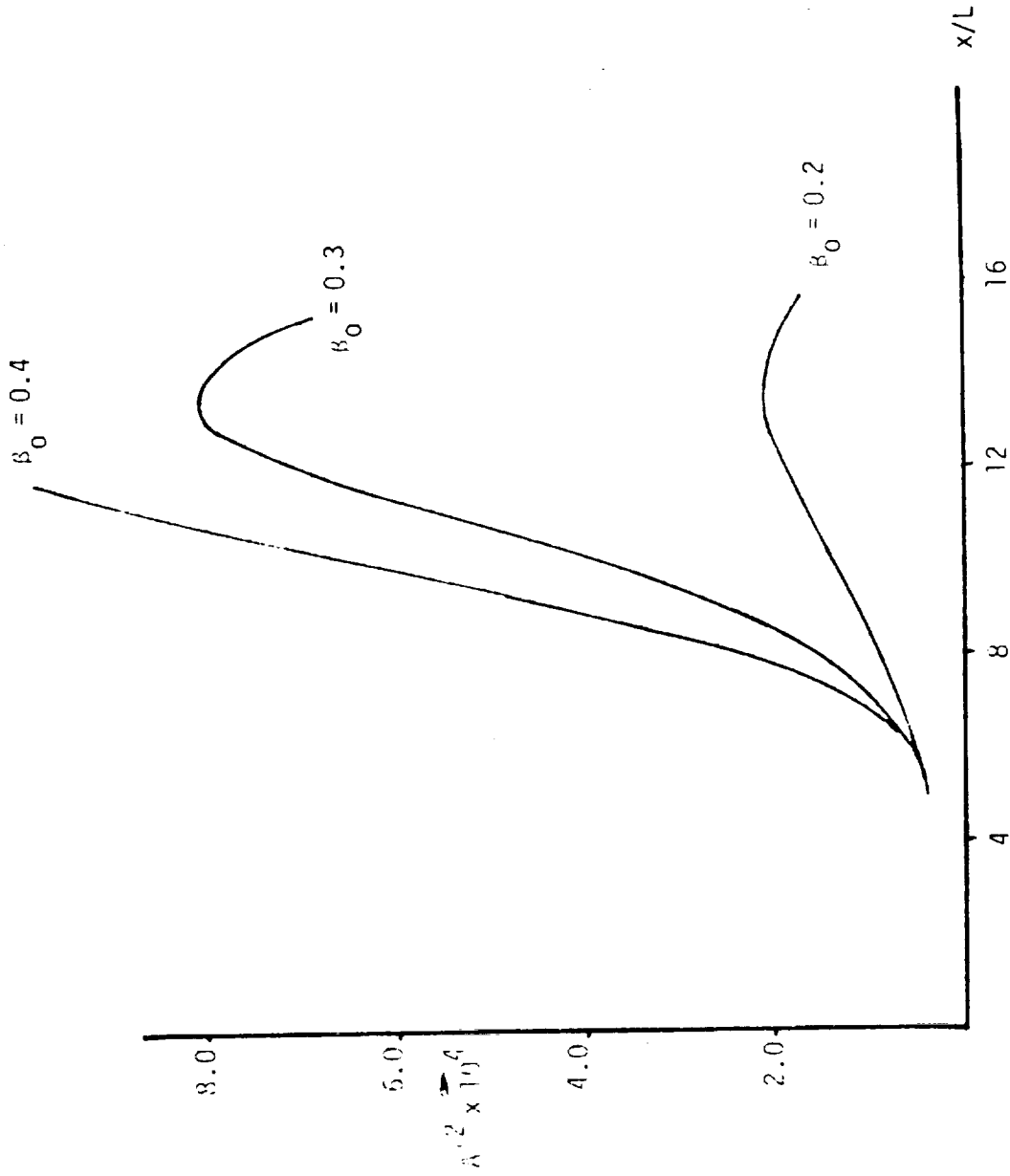


Figure 29 Growth and decay characteristics of the amplitude of coherent structure for various initial frequency of disturbance. Turbulent reactive test conditions: $M_\infty = 3.0$, $T_\infty = 1500^\circ\text{K}$, $L = 0.3\text{cm}$, $x_0 = 5.0$, $V_{c_0} = 0.25$, $T_{c_0} = 1.275$, $|A|_0^2 = 4 \times 10^{-5}$.

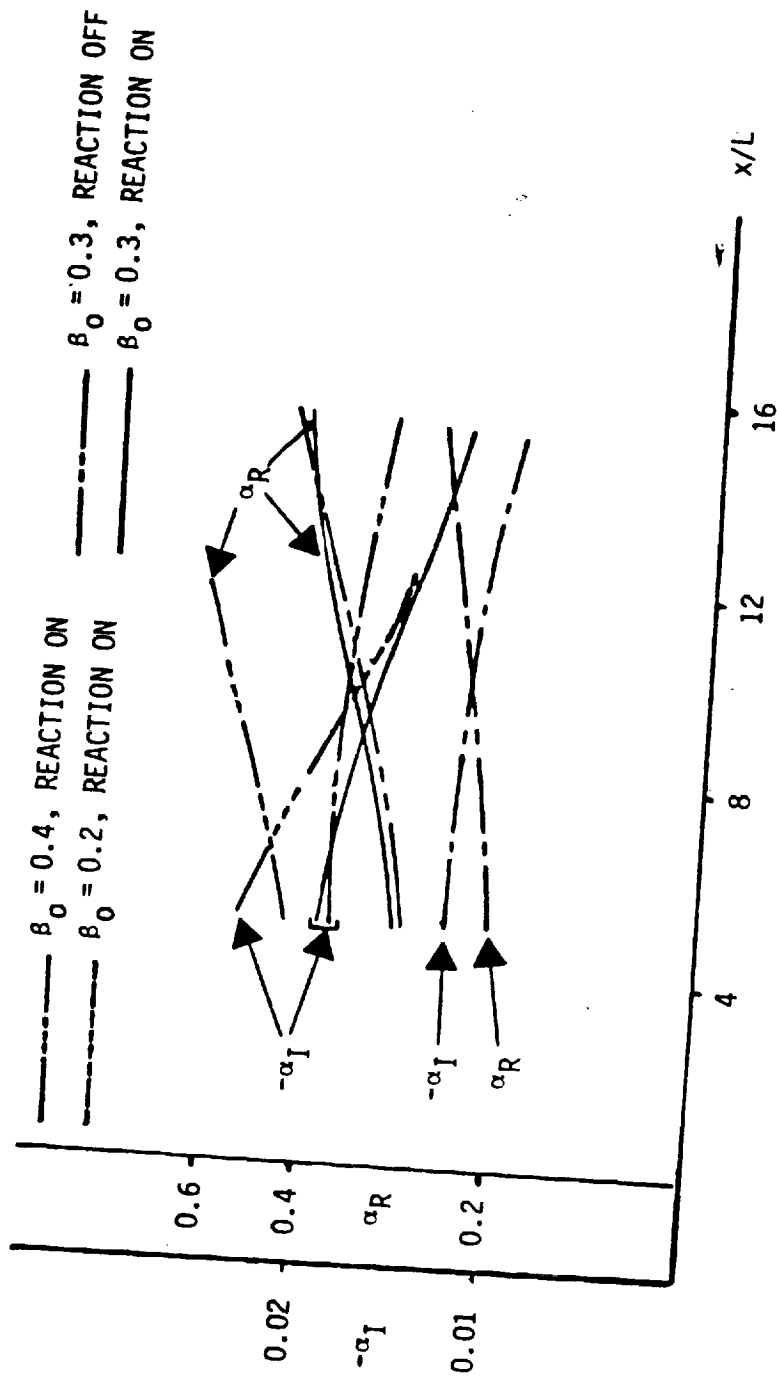


Figure 30 Characteristic variation of the eigenvalues of the local stability problem for various initial frequency of disturbance. Turbulent reactive test conditions as in Figure 25.

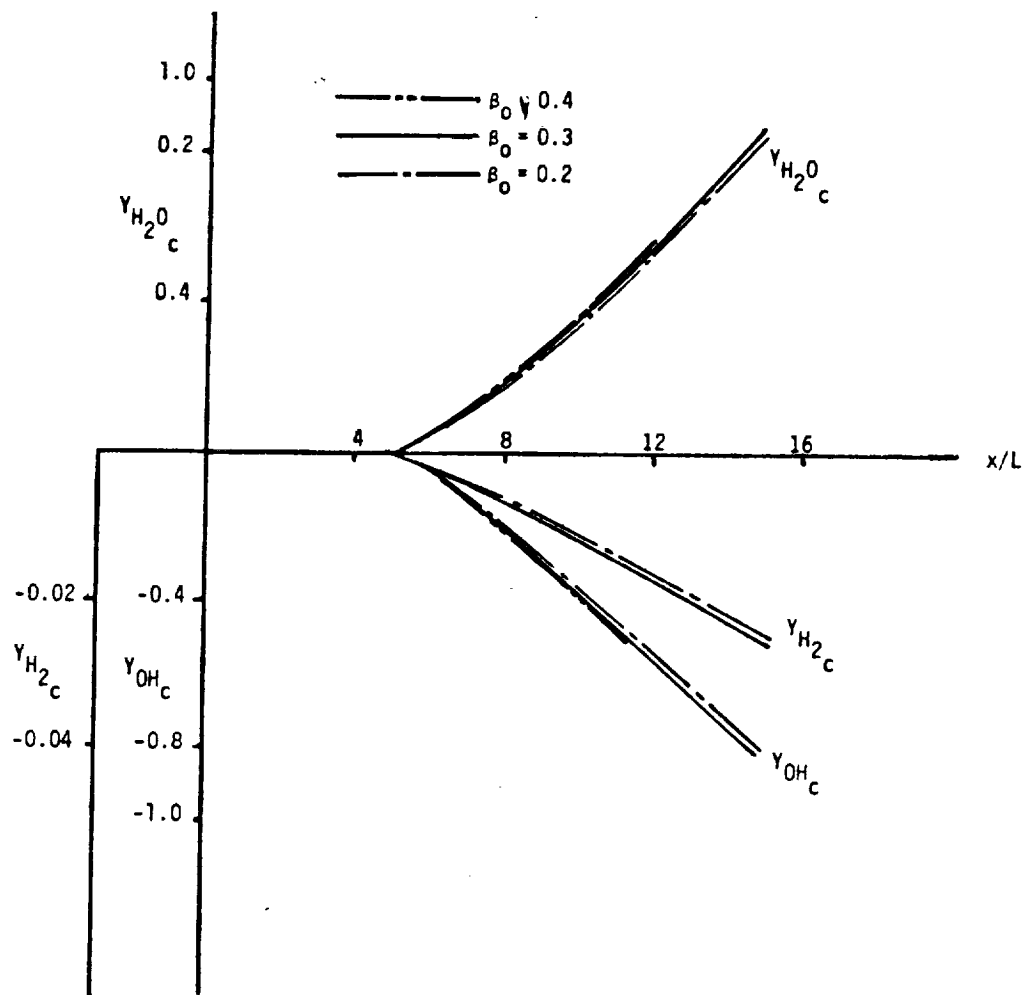


Figure 31 Development of centerline mean flow specie mass fractions for various initial frequency of disturbance. Turbulent reactive test conditions as in Figure 29.

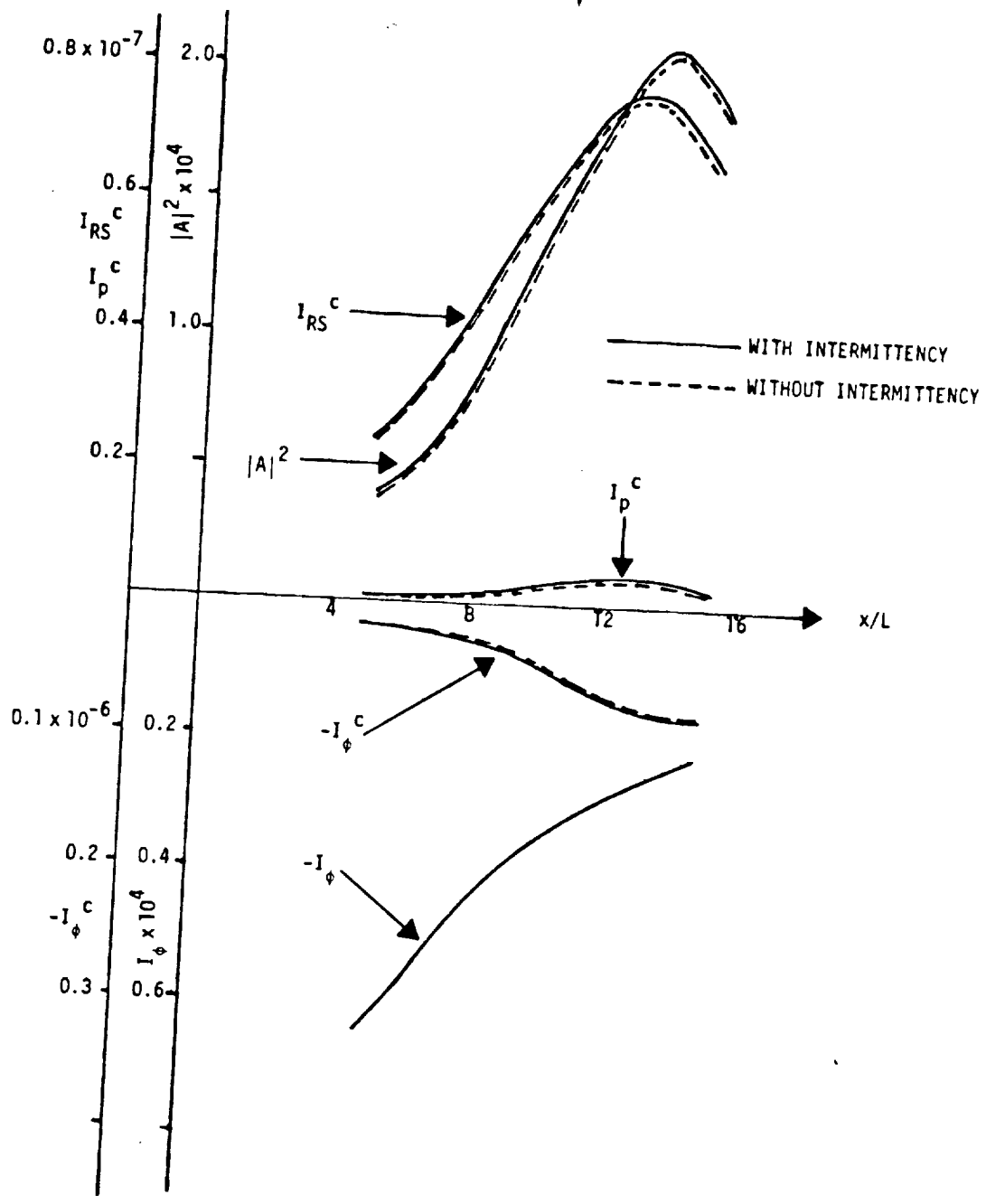


Figure 32 Development of the coherent structure energy transfer mechanism with and without intermittency. Turbulent reactive test conditions as in Figure 25.

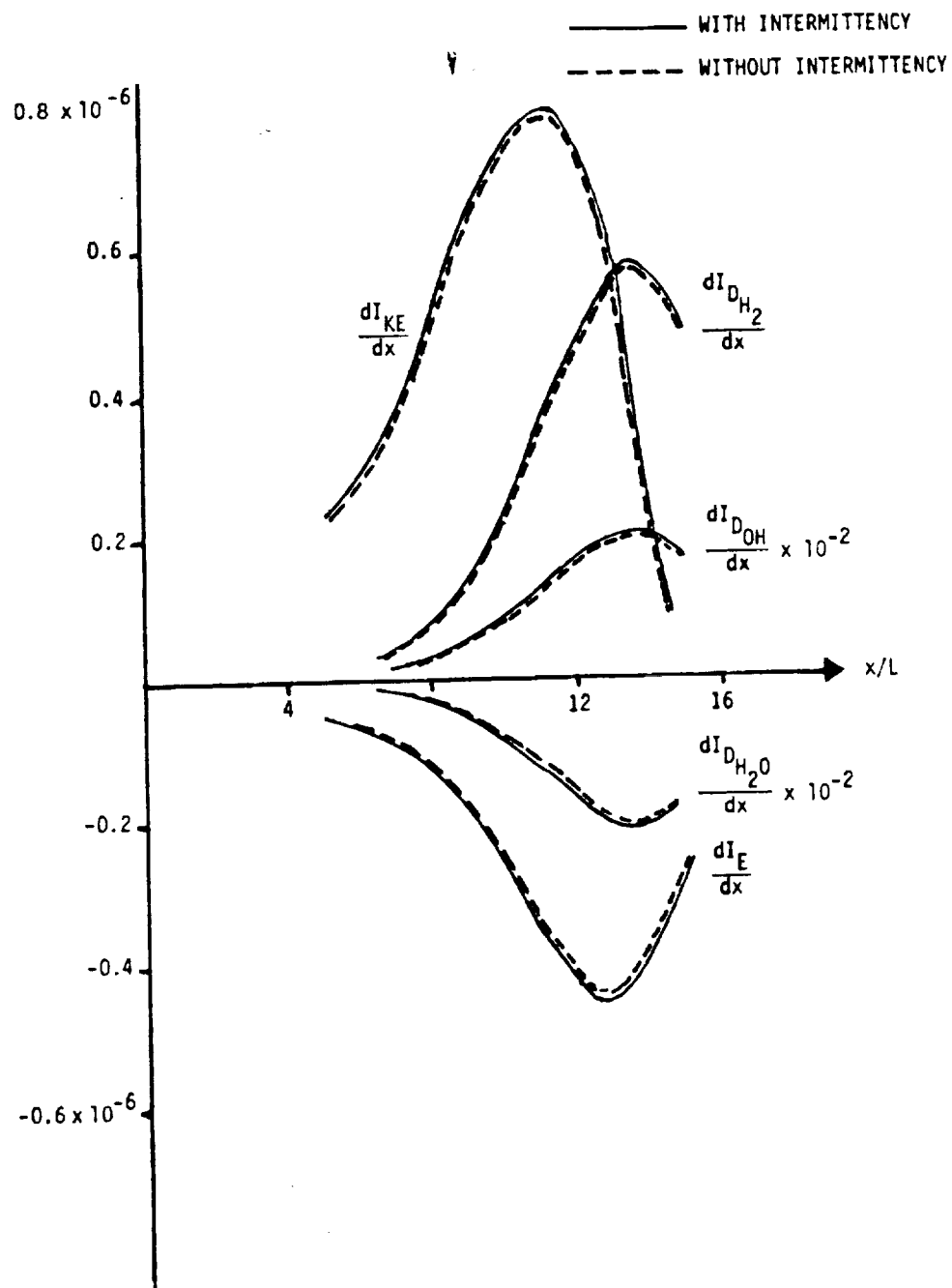


Figure 33 Contribution of the mean flow kinetic energy diffusion, I_{KE} , the total enthalpy diffusion, I_E and the specie diffusion, I_{D_K} , due to coherent structure motion. Intermittency effects in turbulent reactive wake with conditions as in Figure 25.

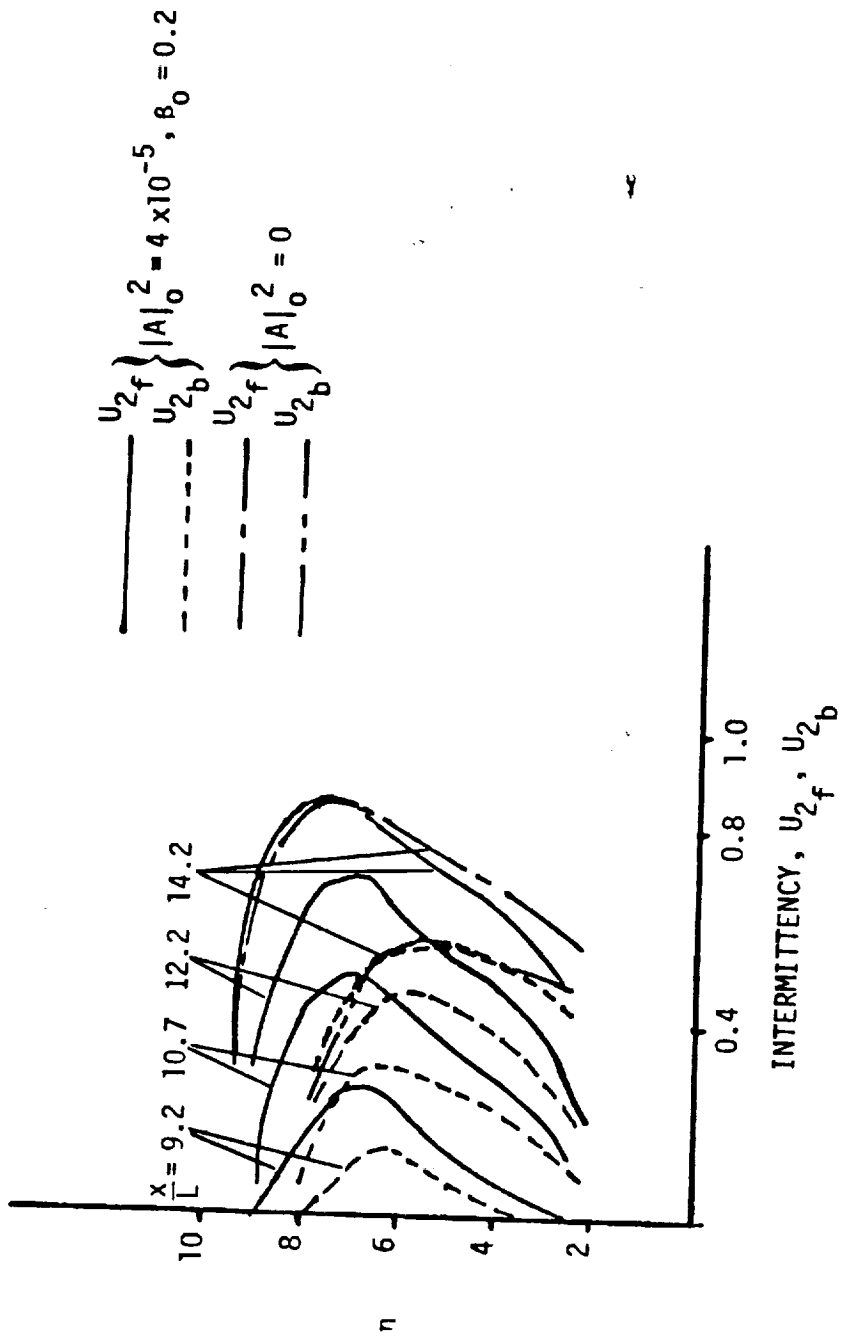


Figure 34 Variation across the shear layer of the intermittency factors for forward and backward rates at various streamwise locations in the reactive wake. Test conditions as in Figure 25.

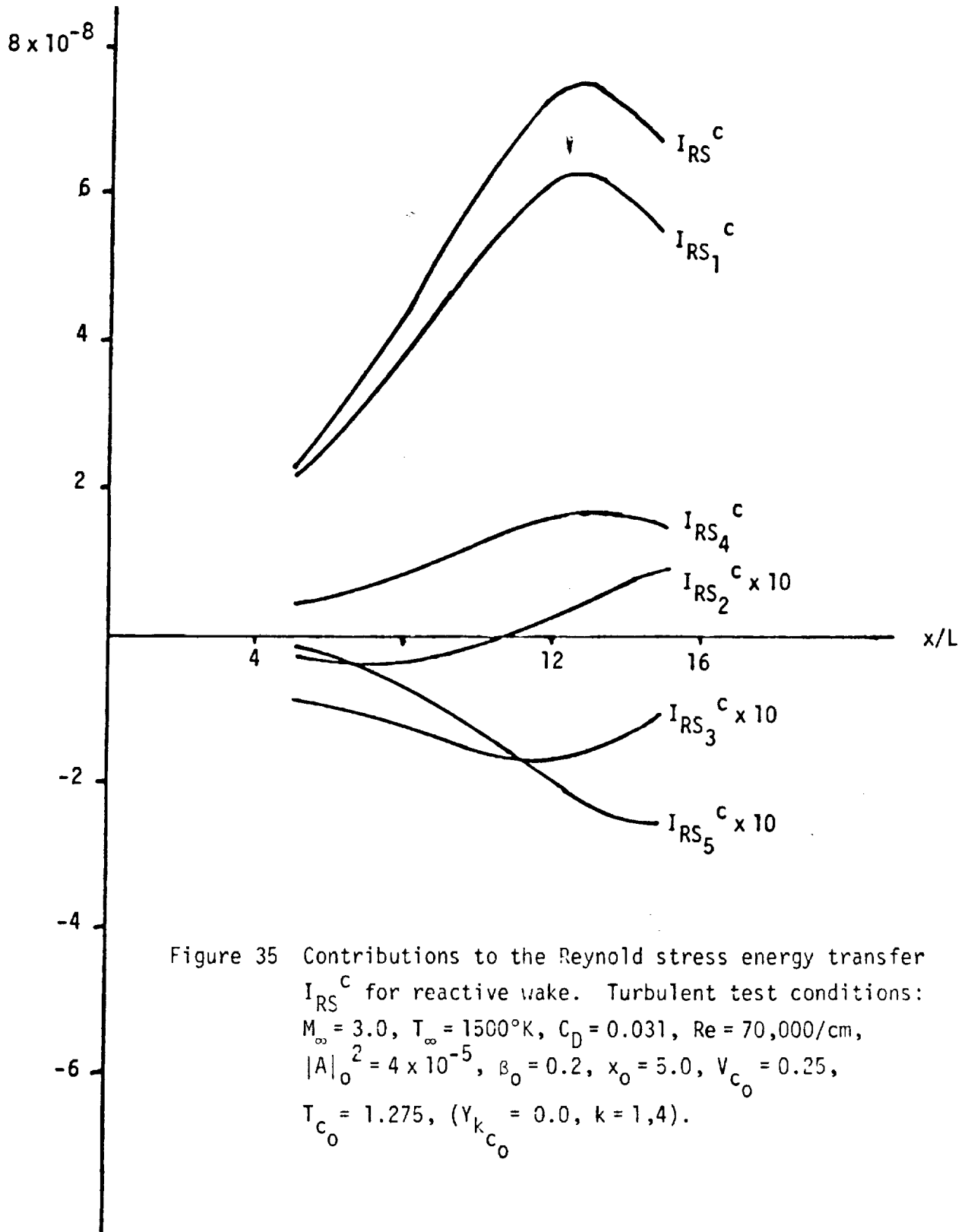


Figure 35 Contributions to the Reynold stress energy transfer I_{RS}^C for reactive wake. Turbulent test conditions:
 $M_\infty = 3.0$, $T_\infty = 1500^\circ\text{K}$, $C_D = 0.031$, $Re = 70,000/\text{cm}$,
 $|A|_0^2 = 4 \times 10^{-5}$, $\beta_0 = 0.2$, $x_0 = 5.0$, $V_{C_0} = 0.25$,
 $T_{C_0} = 1.275$, $(Y_{kC_0} = 0.0, k = 1,4)$.

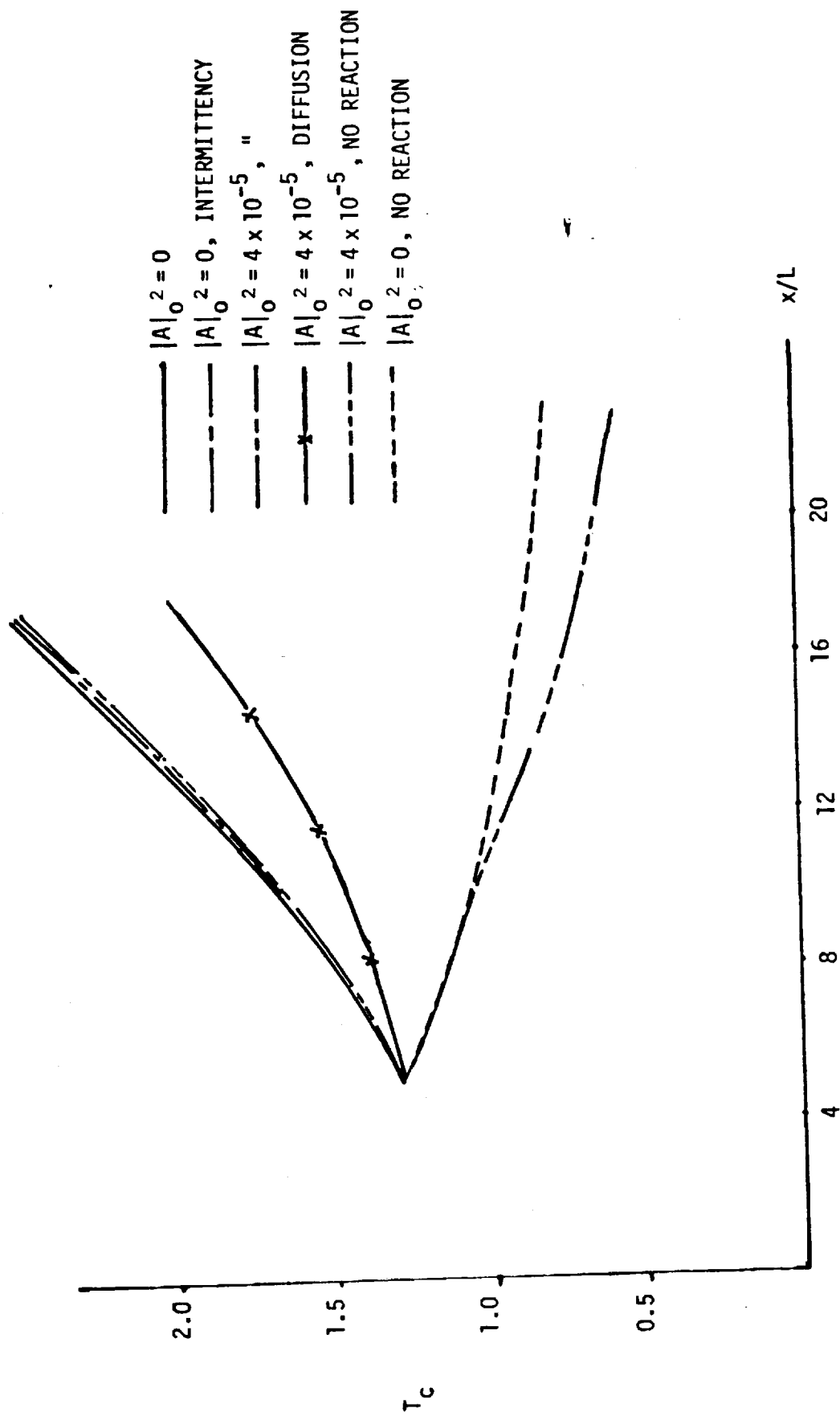


Figure 36 Development of the centerline mean flow temperature excess in turbulent reactive and non reactive wakes. Comparison of the effects of intermittency and diffusion for $|A|_0^2 = 0$ and 4×10^{-5} . Other conditions as in Figure 25.

———— $|A|_0^2 = 4 \times 10^{-5}$, REACTION
 - - - - $|A|_0^2 = 4 \times 10^{-5}$, NO REACTION
 x $|A|_0^2 = 4 \times 10^{-5}$, INTERMITTENCY, REACTION
 • $|A|_0^2 = 4 \times 10^{-5}$, DIFFUSION, REACTION

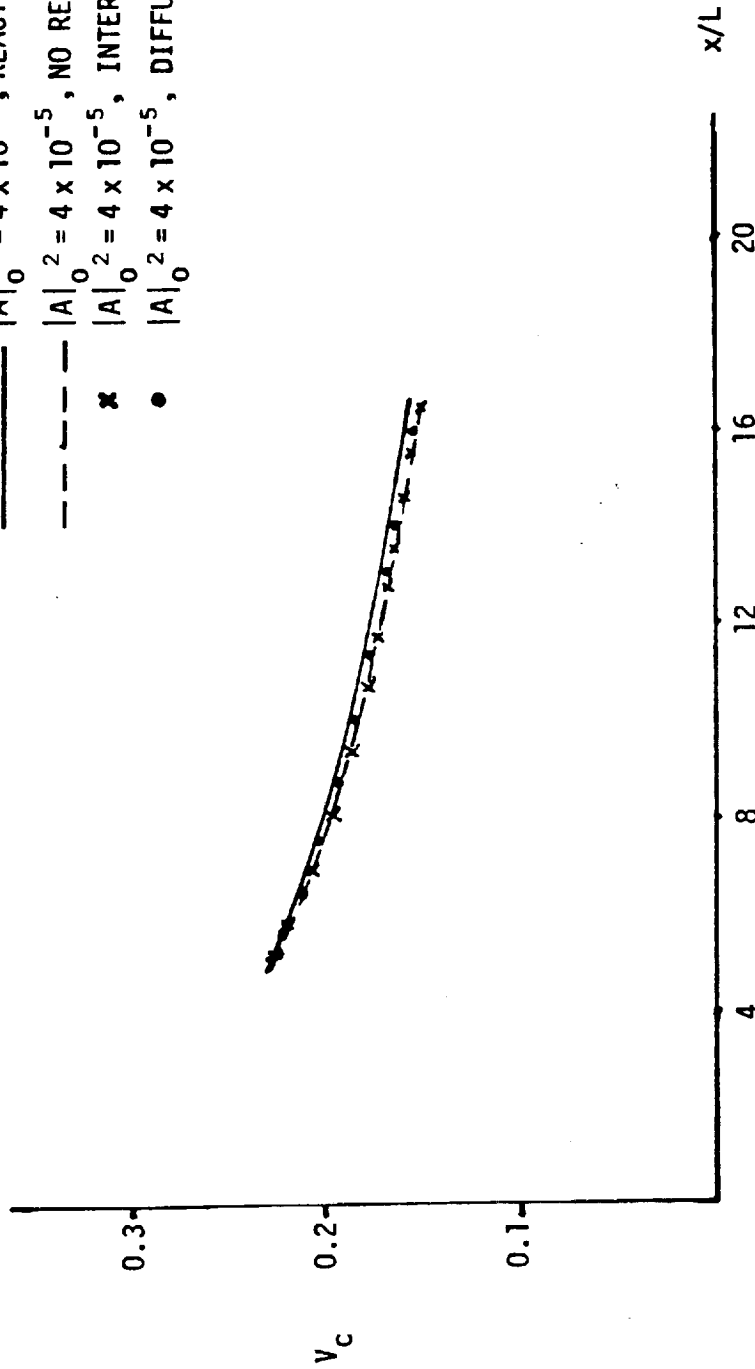


Figure 37 Decay of the centerline mean flow velocity defect in turbulent reactive and non reactive wakes. Comparison of the effects of intermittency and $|A|_0^2 = 4 \times 10^{-5}$. Other conditions as in Figure 25.

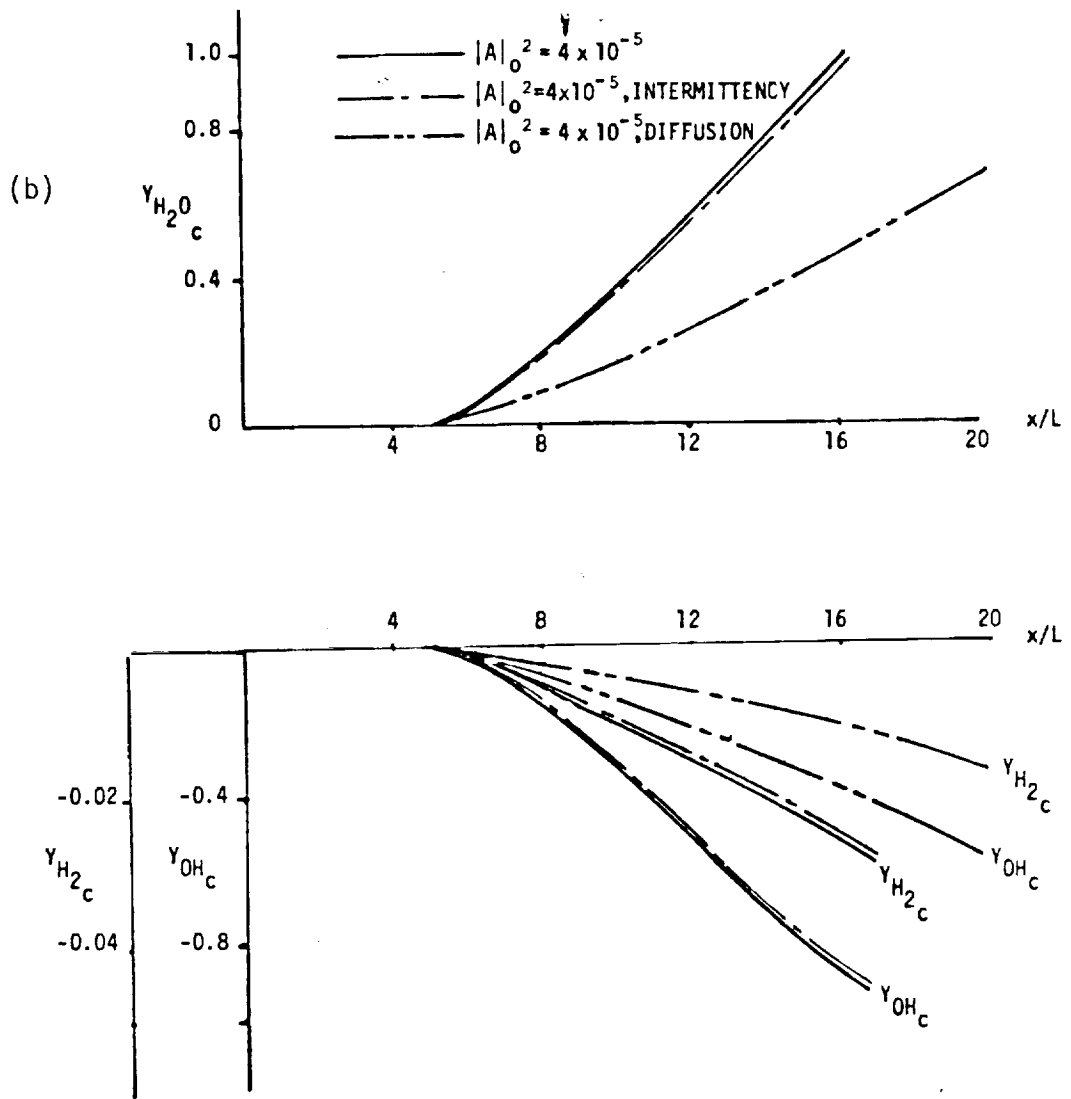


Figure 33 Development of the centerline mean flow specie mass fractions in turbulent reactive wakes. Effects of intermittency and diffusion for $|A|_0^2 = 4 \times 10^{-5}$. Test conditions as in Figure 25.

- (a) The hydrogen and hydroxyl mass fraction defects.
 (b) The water vapor mass fraction excess.

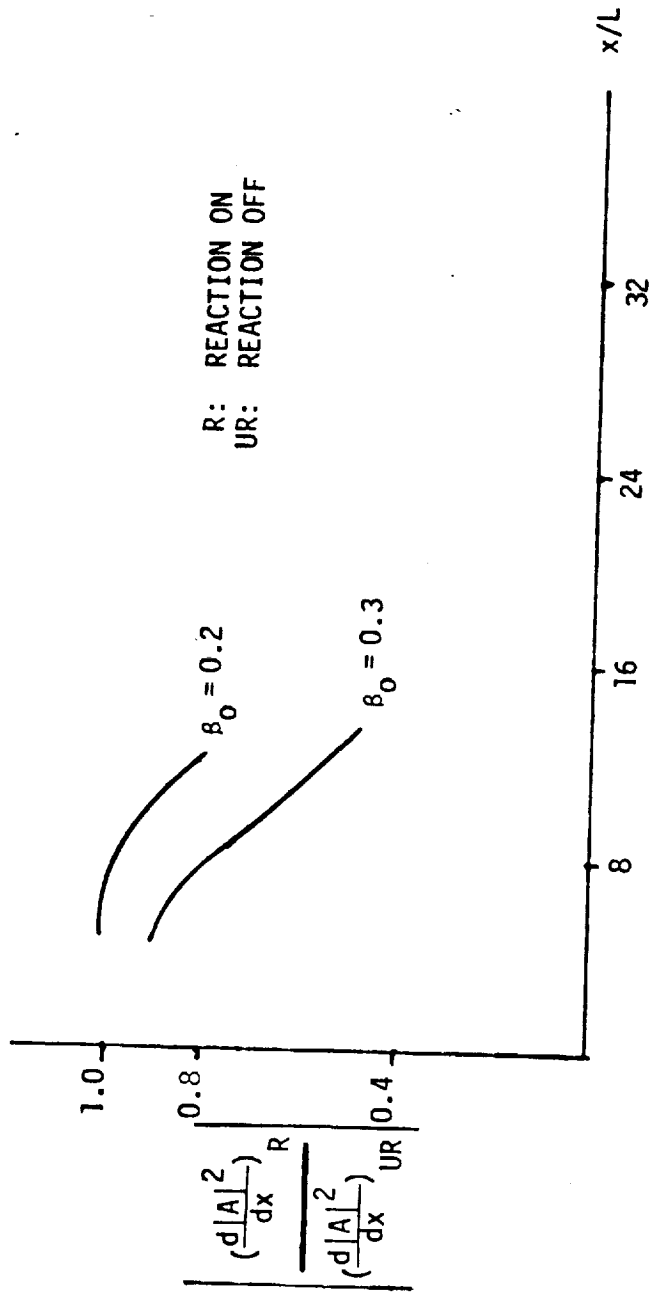


Figure 39 The streamwise development of the ratio between the reactive and non reactive disturbance amplitude growth rates for different initial frequency. Conditions as in Figure 25.

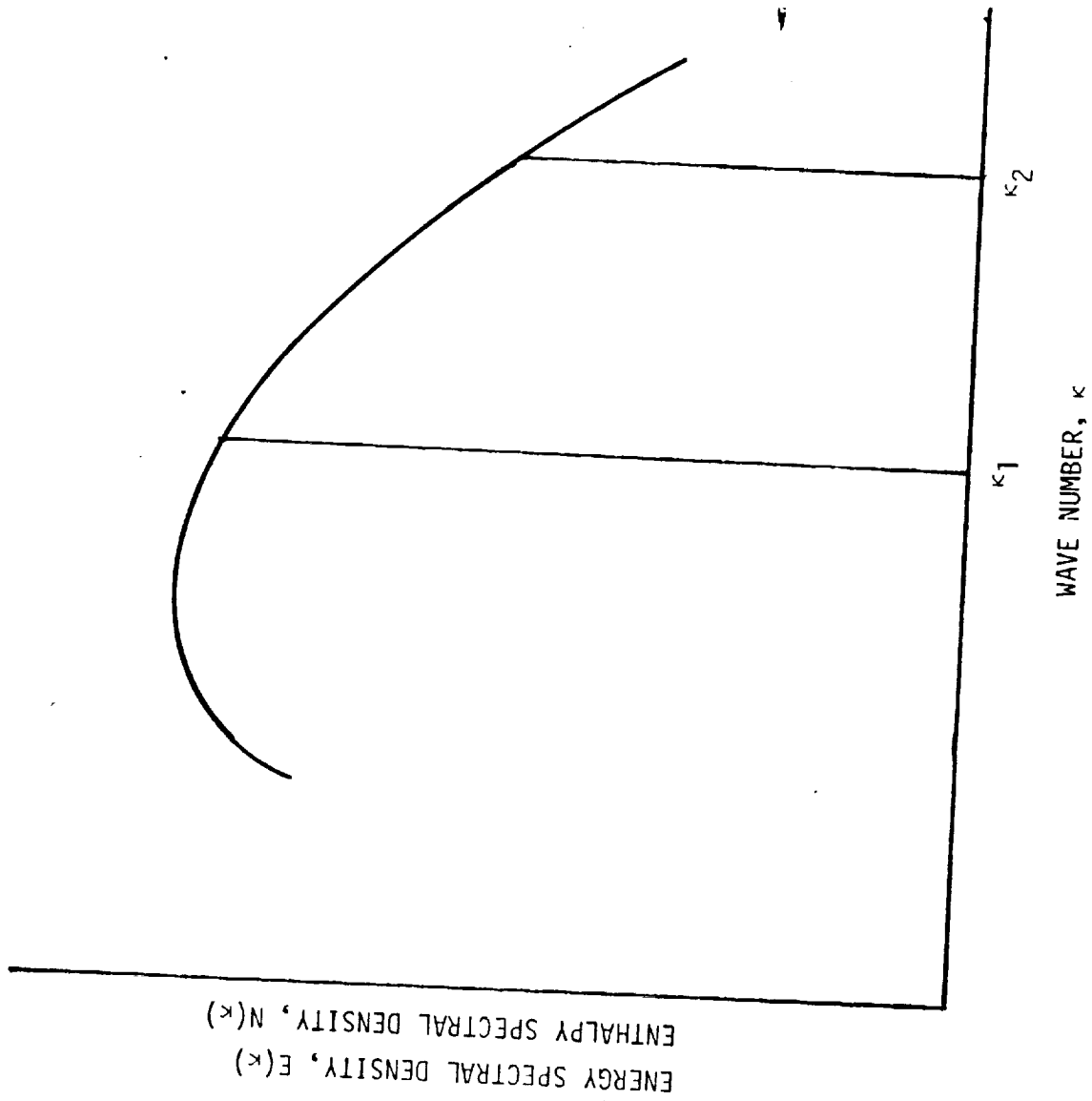


Figure 40 The spectral dependence of the turbulent kinetic energy, $E(k)$ and turbulent total enthalpy $N(k)$.

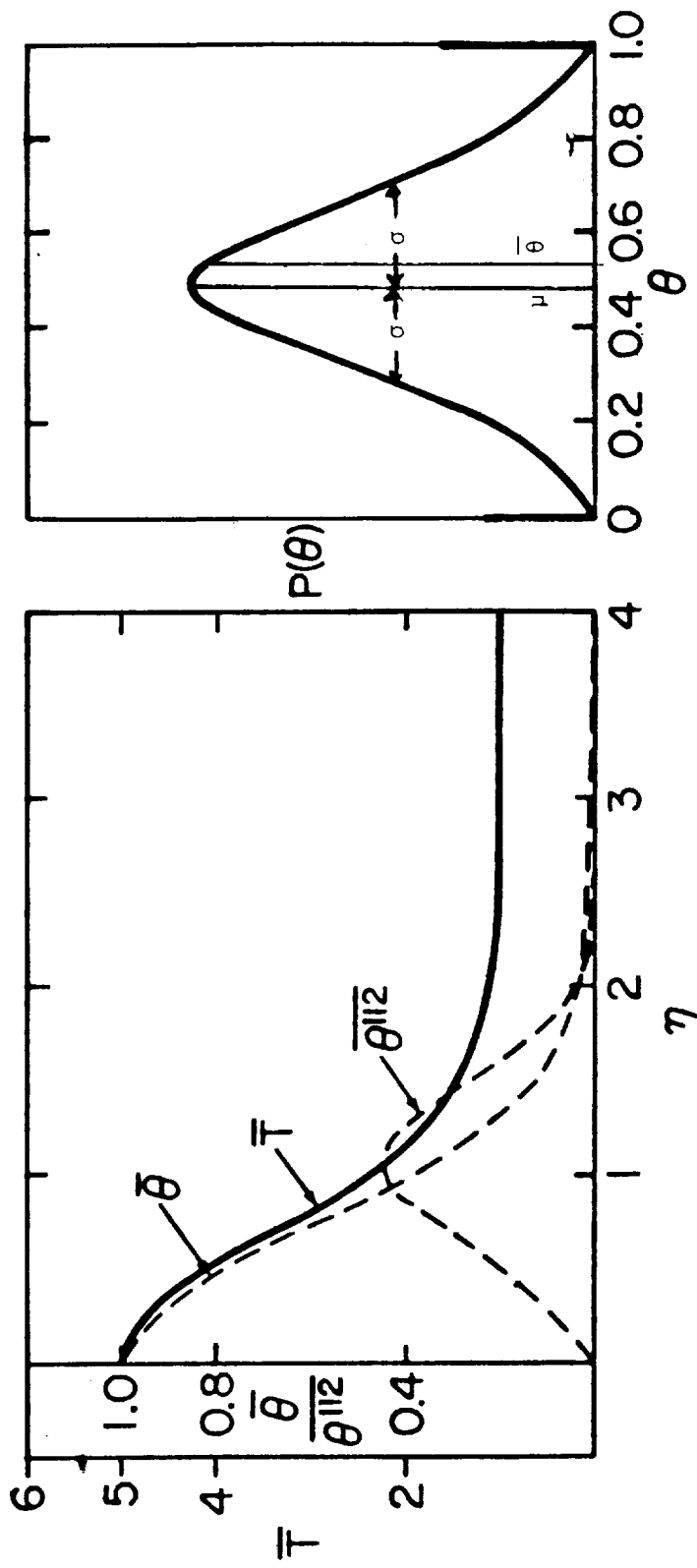


Figure 41a The variation across the shear layer of the mean flow temperature, \bar{T} normalized temperature $\overline{\theta^2}$ and normalized temperature fluctuation $\frac{\overline{\theta^2}}{\theta_{112}^2}$.

Figure 41b The clipped Gaussian probability distribution for normalized temperature, $P(\theta)$.

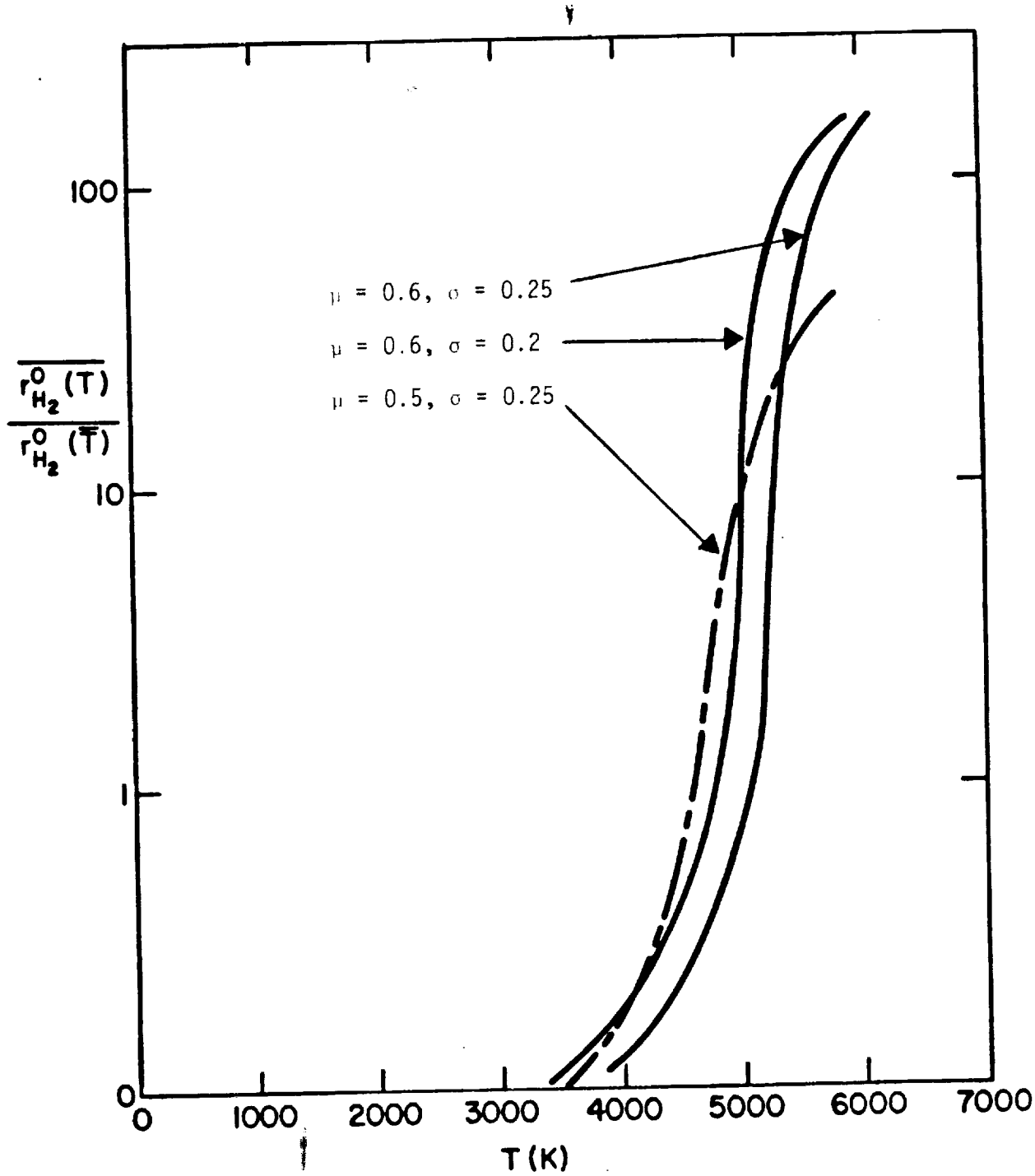


Figure 42 The effect of temperature fluctuation on the mean production rate of hydrogen as a function of temperature.

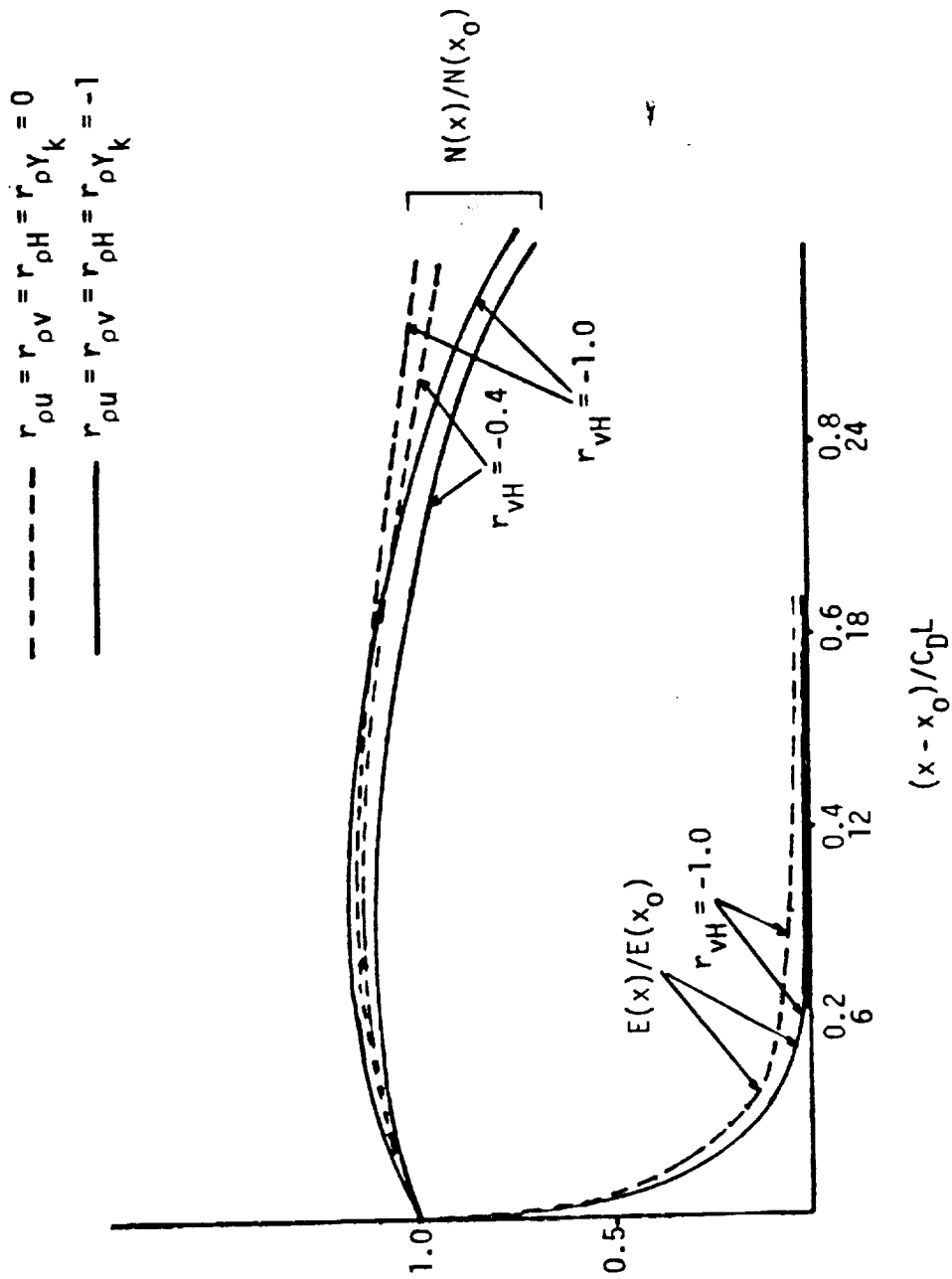


Figure 43 The effect of variation of the correlation coefficients on the streamwise development turbulent kinetic energy and turbulent total enthalpy fluctuation.

$$\text{---} \quad r_{\rho u} = r_{\rho v} = r_{\rho H} = r_{vH} = r_{vY_k} = -1, \quad \sigma(x)/\sigma(x_0)$$

$$\text{---} \quad r_{\rho u} = r_{\rho v} = r_{\rho H} = r_{vH} = r_{vY_k} = -1, \quad E(x)/E(x_0)$$

$$\text{---} \quad r_{\rho u} = r_{\rho v} = r_{\rho H} = r_{vH} = r_{vY_k} = -1, \quad N(x)/N(x_0)$$

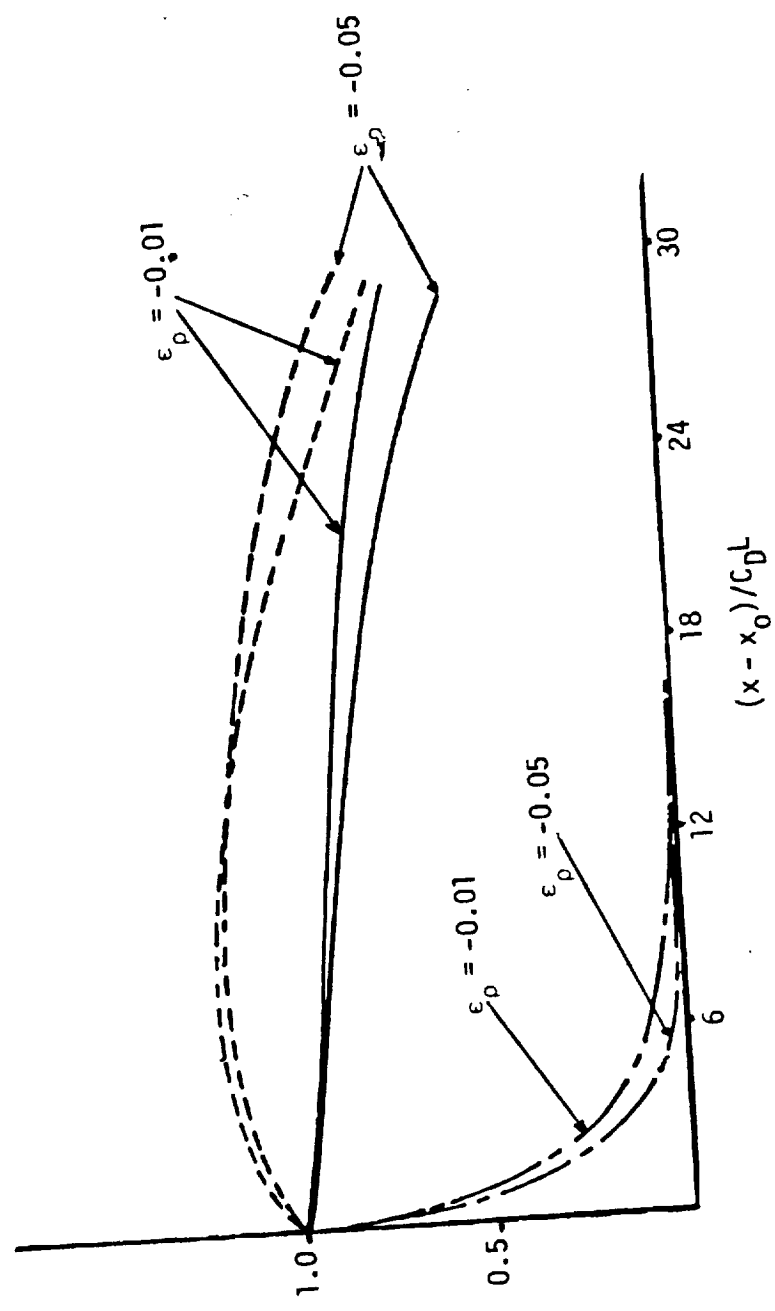


Figure 44 The effect of variation of density strain rate constant on the streamwise development of turbulent mass density fluctuation, turbulent kinetic energy and turbulent total enthalpy fluctuation.